Progetto S3 – Scenari di scuotimento in aree di interesse prioritario e/o strategico

Responsabili: Francesca Pacor (INGV-MI) e Marco Mucciarelli (Unibas)

TASK 6 – GUBBIO - DELIVERABLE D21

GEOLOGICAL MODEL OF THE GUBBIO BASIN (ITALY) FOR THE CHARACTERISATION OF LOCAL SEISMIC RESPONSE

A cura di

UR1 – *E. Fiorini, F. Pacor, D. Bindi*
UR2 – *A. Rovelli, F. Cara, G. Di Giulio, G. Milana, G. Monachesi*
UR3 – *D. Nieto, G. Bohm*
UR4 – *D. Albarello, V. D'Amico, M. Picozzi*
UR6 – *M. Mucciarelli*
UR11 – *G. Scarascia Mugnozzq, S. Rivellino,*
Università di Urbino – M. Menichetti
GFZ- Potsdam- S. Parolai, S. Richwalski, I. Orpsal

July 2007

INDEX

INTRODUCTION

Within the framework of the project S3 "Ground shaking scenarios for some strategic areas in Italy-Task6" the town of Gubbio has been selected as a test site to compute ground motion taking into account finite fault and site effects.

Gubbio is located in central Italy, on the northern slopes of one of the many valleys characterising the central Appennines. The historical settlement is located on a rocky slope, while new developments extend on the Quaternary fluvio-lacustrine deposits filling the basin. The Gubbio basin was chosen as a test site for a number of reasons: its geomorphological setting is very common in central and southern Italy, the area is characterised by frequent near events of moderate magnitude (Mmax 6) and large amplifications were observed there for the Colfiorito seismic sequence of the 1997/98.

In order to understand the mechanisms controlling the 3D seismic response of the basin, a subsurface model has been constructed.
The reconstruction of the model has been done using data coming from different surveys (figure A). Several active and passive seismic measurements have been carried out in the plain, also favoured by the intense seismic activity typical of the area. These investigations mainly consisted of monitoring activities of 4 temporary transects of seismometric stations, operating between June 2005 and May 2006 and described in detail in PS3-Deliverables D22-D23. Two transects have been positioned perpendicularly to the valley axes (GFZ and Ge2 Transects), one parallel (INGV transect) and one near Gubbio (Ge1 transect). More than 300 local and regional earthquakes have been recorded, with maximum magnitude equal to 4. A 2D array was run as well from June to September 2006, to better understand the generation of surface waves. All data are collected in a GIS (Progetto S3 Deliverable D23)

Parallel to these activities, ambient noise data have been collected in the field for 90 sites, using the single station technique for the estimation of the fundamental resonance frequencies. Furthermore, 4 noise measurements with a seismic array have been collected to build an S-wave velocity profile of soft sediments, considered representative for the whole plain. The geometry of the basin below 500 m of depth has been investigated through the acquisition of an active seismic line 4.5 km long, in correspondence of one of the transects.
This has been used to perform a tomography of arrival times which allowed to recognise the position and shape of the reflecting horizons. As a final step the first 30 metres of deposits have been characterised over a 30 km^2 area, using both stratigraphic investigations provided by the Gubbio Municipality and data collected from in-situ surveys and lab tests.

In this deliverable we describe the input data for the 3D model of the Gubbio basin and we outline the steps performed to define the geometry, the layers and their seismic properties on the base of the experimental data collected during the project and of the available geological information.

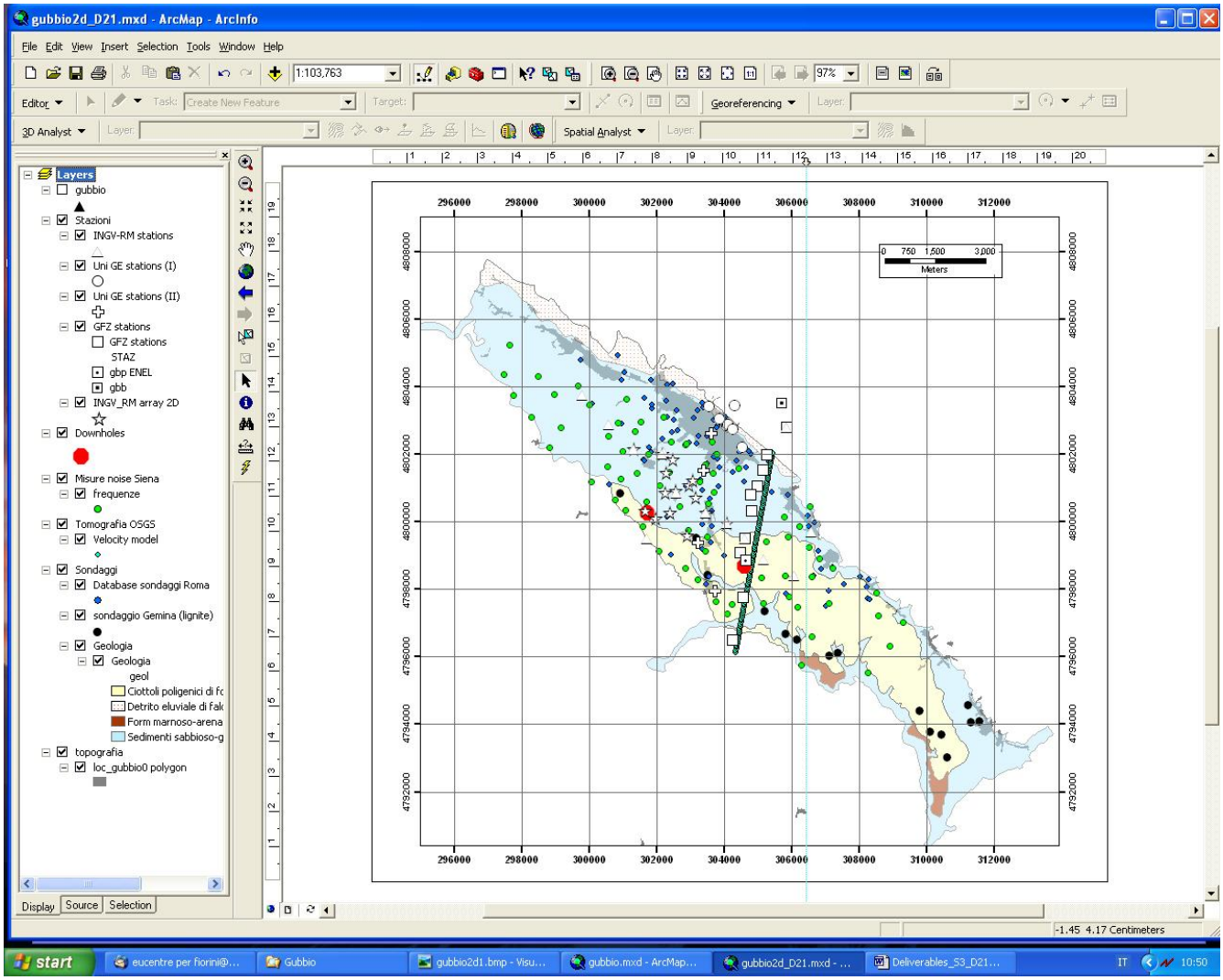

Figure A - Data collection in the Gubbio basin.

AKNOWLEDGMENT

We are very grateful for the collaboration and support given to us during the survey measurements and the data collection by:
Dr. S. Stocchi (DPC-Comune di Gubbio)
Dr. Pelicci (Comune di Gubbio)
and the people of Gubbio town

1. GEOLOGICAL AND STRUCTURAL DATA

In the Umbria Preappenines in Central Italy, the Gubbio normal fault and its continental basin represent one of the main geological features. The fault trace, NW-SE trending, is observable in the field for more than 30 km with at least three segments kinematically linked that give a general geometry south westward concave (figure 5.1). The fault has a throw of more than 1500 m with a total extension of 15 % and affect the SW limb of a rootless NE verging anticline (Menichetti & Pialli, 1986). The fault activity presumably starts in the Late Pliocene, while the continental basin sedimentation is recorded from the Pleistocene (De Feyter et al., 1990; Menichetti & Minelli 1991; Menichetti, 1992).
The basin related to the fault growth is asymmetric, oriented NW-SE, 20 km long and 6 km wide and infilled by sediments with fluvio-palu-lacustrine facies of the Pleistocene age. The depocenter of the basin, which was estimated about 400 m deep, is situated very close to the master fault plane and the sedimentary facies gently dipping to NE reflect the evolution of the hanging-wall fault plane (Menichetti, 1992).
The fault plane is composite and the total throw is distributed in several splays outcropping in the mountain slopes and corresponding with several morphological steps in the piedmont part of the valley. The inclination of the fault scarp varies from 70° to 40°, related to the cohesion and angles of internal friction of the calcareous and marls rocks of the stratigraphic succession. Others extensional structures are present in the SW part of the Gubbio area, where are known SW dipping faults with throw of hundreds of meters. Antithetic NE dipping faults, outcropping both in the calcareous anticline and in the hangingwall, have a limited extension with respect to the master fault plane

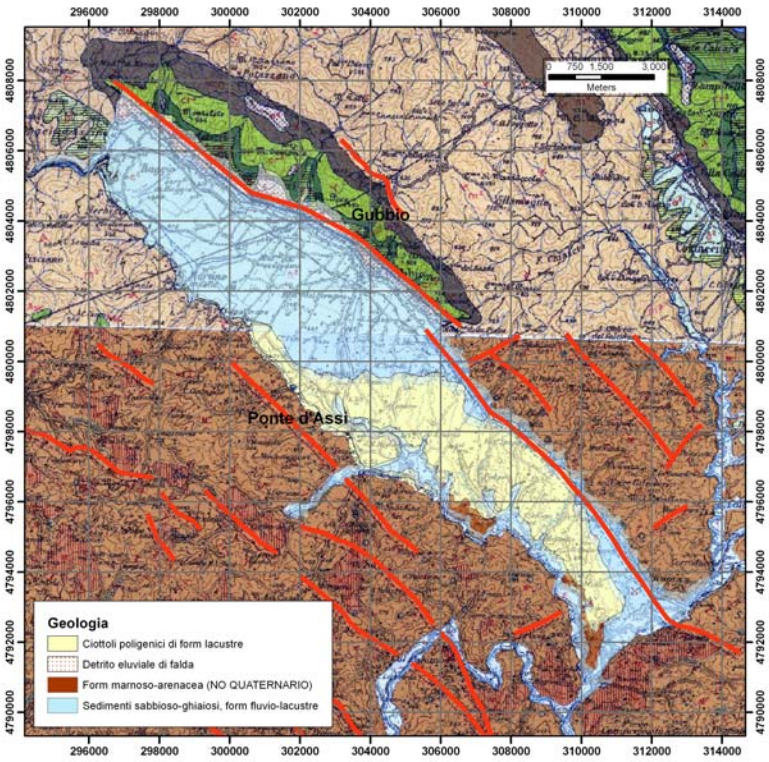

Figure 1.1 - Geological map from 1:100.000 sheet (116 and 123 of the geological map of Italy) with the main faults of the area. In green the calcareous outcrops

2. GEOTECHNICAL DATA

The activities carried out by Rome University consisted in the reconstruction of the engineering-geological model of the Gubbio basin area with the final aim of assessing the earthquake-induced deformation effects in first 50 b.g.l..

In the period July 2005- May 2007, activities were based on both collection of previously produced documents and reports and specific site and laboratory investigations.

In particular, the following activities were carried out.

1. Superficial geological survey (scale 1:10.000) for the definition of the geological setting.
2. Collection of subsurface stratigraphic data derived from site investigations (CPT, SPT, VES, boreholes) contained in technical reports hosted in the Gubbio Municipality files, as well as in private consulting companies and National Agencies (ANAS). Further, it was fundamental to collect and organize the stratigraphic data derived from about 60 borehole drilled on behalf of the Gubbio Municipality in the period September 2005 – April 2006.

The overall collected data were organized in a database (see fig. 2.1 for indication) purposely implemented. Specific attention was paid to the stratigraphy of the investigation, reported both as meters b.g.l. and elevation in meters a.s.l. of the introduced engineering geological units, defined in view of the subsurface units modelling.

As for that, three engineering geological or lithotechnical units were defined:
a) gravels and gravelly-sands,
b) silt and sandy silts,
c) clay and clayey silts.
In total, information coming from about 100 verticals, allowed the building of a preliminary engineering geological model. The soil mass of the investigated area in the Gubbio basin was scanned through layers at 5 m equidistance, between elevations 400 and 500 m a.s.l. For each layer, the extension of each engineering geological unit was contoured. As for the laboratory investigations, they were performed on both soil and rock samples at the geotechnical lab of the Dep. Earth Sciences.
On remoulded soil samples (fig. 2.2) the physical characterization was made (grain size, solid unit weight volume, Atterberg limits); the samples were collected during the different phases of borehole drilling. According to the plasticity chart, they belong to CH (high plasticity clays) and MH (high plasticity silts). On rock samples, apart from the unit weight volume, Point Load test was performed to get the Uniaxial Compressive Strength and the Tensile strength (fig 2.3).
On the basis of the laboratory and site investigations and referring to the previously mentioned layer, it was possible to define the engineering geological units distribution down to the maximum depth of -50 m b.g.l.; hence, engineering geological sections were derived both parallel and perpendicular to the Gubbio basin longitudinal axis and described in paragraph 2.2.

Document n°	Author/Year	Locality	Investigation	Coordinates	Elevation m a.l.s..	Depth b.l.g. (m)	Groundwater depth b.l.g. (m)	Stratigraphy	Lab tests
1	Pelicci/1993	Coppiolo	6 penetrometer 3 sond a distruzione	2322220 4801252 2322269 4801246	448	7.1 3 – 5 – 1.5	0,9	Indirect	CF,G,L,Tr, Td,Ed
2	Pelicci/1993	Historical centre	3 penetrometer 1 sond a distruzione	2323749 4802683 2323725 4802634	494	9 – 11.1 – 9.9 5	>20 (indirect)	Indirect	
3	Menichetti/1999	Historical centre	1 penetrometer 1 sond a distruzione	2323628 4802851	497	10.5 20	15	Indirect	
4	Menichetti/1999	Historical centre	1 penetrometer 1 sond a distruzione	2323538 4803228	500	10.5 20	15	Indirect	
5	Pelicci/1993	Mad. di Mezzopiano	1 penetrometer (400m distante)	2320900 4802730	445	9.6		Indirect	
6	Pelicci/1993	Mad. del Ponte	2 penetrometer	2322431 4803905	565	5.1	35-40 (indirect)	Indirect	
7	Pelicci/1993	Historical centre	2 penetrometer	2323143 4803121	495	8.4 – 7.2	>20 (indirect)	Indirect	
8	Pelicci/1992	Vigne	2 penetrometer	2323298 4803351	543	6.6 – 5.7		Indirect	
9	Pelicci/1991	Piaggiola	3 penetrometer	2323674 4801839	469	8.1 – 9.6 – 7.5	>10 (indirect)	Indirect	
10	Pelicci/1992	Frate Lupo	3 penetrometer	2324376 4801901	478	8.4 – 7.5 – 6.6	3	Indirect	

Fig. 2.1 - Database sample created to archive data (for test lab: CF physical characterization , G size distribution, L Atterberg limits, Tr triaxial test, Td shear test, Ed oedometric test).

REHOLE	Depth (m b. l. g.)	γ_s (kN/m^3)	LL (%)	LP (%)	IP (%)
Chiesa Cipolleto	15-18	26.6	56.5	28.56	27.94
Chiesa Cipolleto	27-30	27.5	53	31.3	21.7
Via Perugina	12-15	26.1	57.1	28.35	28.75
Fornace P.Assi	12-13	27.5	66.7	36.04	30.66
laghetto S.Erasmo	-	25.3	77	29.98	47

Fig. 2.2 - Table of main geotechnical parameters belonging to clay and clayey silts unit. Data come from some samples obtained during the execution of the boreholes for Seismic Microzonation of Gubbio.

LITHOLOGICAL UNIT	γ (kN/m^3)	Estimation of uniaxial compressive strength (MPa)	Estimation of tensile strength (MPa)
Scaglia Rossa	25.8	58.26-72.83	3.64
Scaglia Bianca	25.5	84.36-105.44	5.27
Marne a Fucoidi	23.9	53.6-67	3.35

Fig. 2.3 - Main parameters from rock samples.

2.1 DOWN-HOLE

Two down-hole measurements up to a maximum depth of 57 m were performed within the Gubbio plain. A sparker borehole source has been used to generate P and SH waves (Cardarelli, 2007).
The first borehole, funded by the Project DCP-S6, (S1, Fig. 2.1.1) was drilled near the site that recorded the Colfiorito 1997 M 5.9 earthquake and was 57 m deep (Sant'Erasmo area). The second borehole (S2, Figure 2.1.1), 44 m deep, was drilled in the Gubbio plain near the area where a 2D array of seismic stations has been deployed (La Torraccia area).

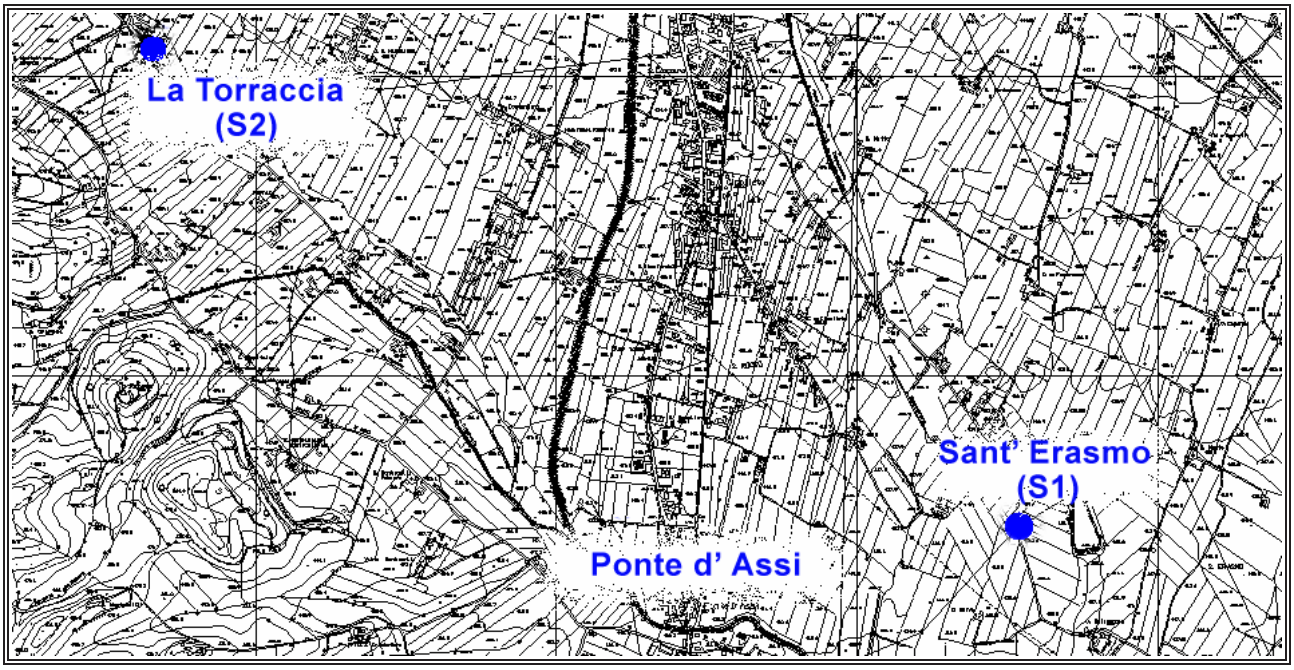

Figure 2.1.1 - Location of the S1 and S2 boreholes

During the drilling, geotechnical characterization of the soil core was done to determine moisture content, natural unit weight volume and pocket penetrometer strength. Moreover, undisturbed samples were collected for laboratory test; and casing was put in each borehole for successive in hole geophysical investigations.
Such investigations and the lab tests allowed to better define from a mechanical point of view the previously introduced engineering geological units and to assign them Vs values.

To characterize limy-clayey soils, some geotechnical tests were performed on samples collected at significant depth during the drilling. We obtained the following results:

- values of pocket penetrometric resistance ranging from 0.6 to 275 kPa for S1 and from 0.75 to 450 kPa for S2. In particular, for S1 mean values of about 200 kPa are present in the first 11 m consisting of clayey silt whereas values of about 100 kPa prevail for clays from 17 to 35 m and 50-60 m; for S2 we find mean values of about 200 kPa with a maximum peak of 450 kPa at 3.3 m.
- Unit weight volume ranging from 17.4 kN/m3 to 19.6 kN/m3 for S1 and from 18 kN/m3 to 19.7 kN/m3 for S2, considering limy-clayey soils (Figure 2.1.1).
- Water content ranging from 13% to 27% for S1 an from 21% to 35% for S2 (Figure 2.1.2). For S1 we find maximum values of water content at 4 m and between 14 to 28 m. They are probably related to capillarity linked to the groundwater table fluctuation in the sandy and gravely levels. For S2, peak values of about 35% are found between 14 and 16 m and at 29 m, whereas all silty-clayey soils of the area have mean values of about 25%.

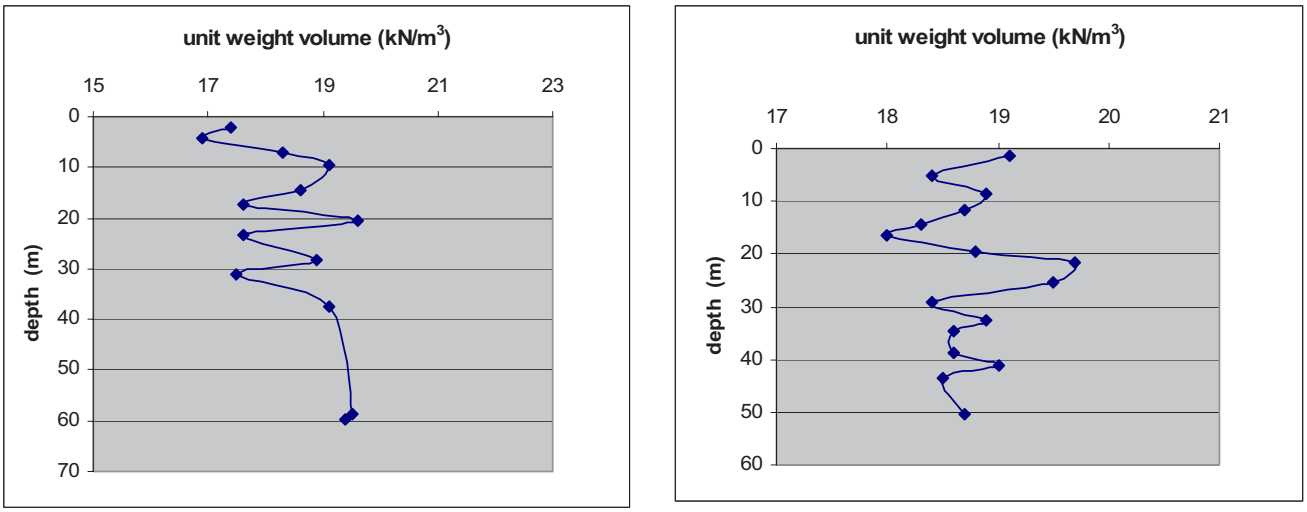

a) **b)**

Figure 2.1.1 – Natural unit weight volume vs depth in the S1 **a)** and S2 **b)** boreholes.

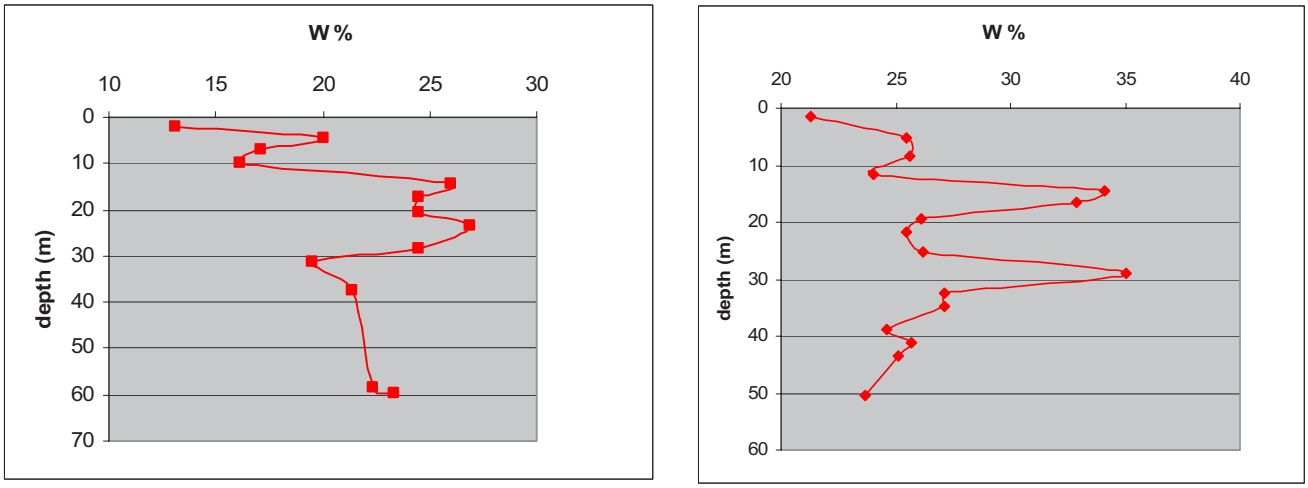

a) **b)**

Figure 2.1.2 - Natural water content vs depth in the S1 **a)** and S2 **b)** boreholes.

Lab tests were performed to define grain size distribution and plasticity index (PI) for limy-clayey soils sampled at different depth. For S1 site, PI is about 49% for the first 10 m and decreases to 25%-37% from 20 m until 60 m. These soils were classified as inorganic clay of high plasticity (CH) using Plasticity Chart (USCS classification).

For S2 PI is 42%-46% for the first 15 m then it decreases to 12%-19% from 20 to 50 m b.g.l. These soils were classified as CH until 15 m, inorganic clay of medium-low plasticity (CL) from 20 to 30 m and inorganic silt of low plasticity (ML-OL) from 43 to 50 m (Table 2.1.1).

Table 2.1.1 - Unit weight volume of solid phase and Atterberg limits vs depth for soils. All the soils belong to clay and silty clay lithotechnical Unit.

Depth (m)	γ_s (kN/m^3)	L.P.	L.L.	P.I.	Soil classification
2.2	26.2	31%	80%	49%	CH
7.5	26.7	29.5%	77.5%	48%	CH
20.5	27.2	25.9%	50.9%	25%	CH
28.3	27.3	17.9%	55.5%	37.6%	CH
59.8	27.2	25.7%	58.5%	32.8%	CH

a) S1 borehole

Depth (m)	γ_s (kN/m^3)	L.P.	L.L.	P.I.	Soil classification
5.3	26.1	29.1%	75.5%	46.4%	CH
14.5	26	31.4%	74.2%	42.8%	CH
21.6	26,8	22.4%	41%	18.6%	CL
31.5	27.6	23.9%	37.9%	14%	CL
43.6	27	29.4%	48.6%	19.2%	ML-OL
50.5	27.1	28.6%	41%	12.2%	ML-OL

b) S2 borehole

The down-hole measurements in the two boreholes indicate velocities spanning from 800 to 2200 m/s and from 150 to 750 m/s for Vp and Vs, respectively (Figure 2.1.4 and Figure 2.1.5). In particular both down-holes indicate a velocity contrast at about 50 m of depth, with shear velocity values that vary from 350-380 m/s to 600-750 m/s (Cardarelli, 2007).

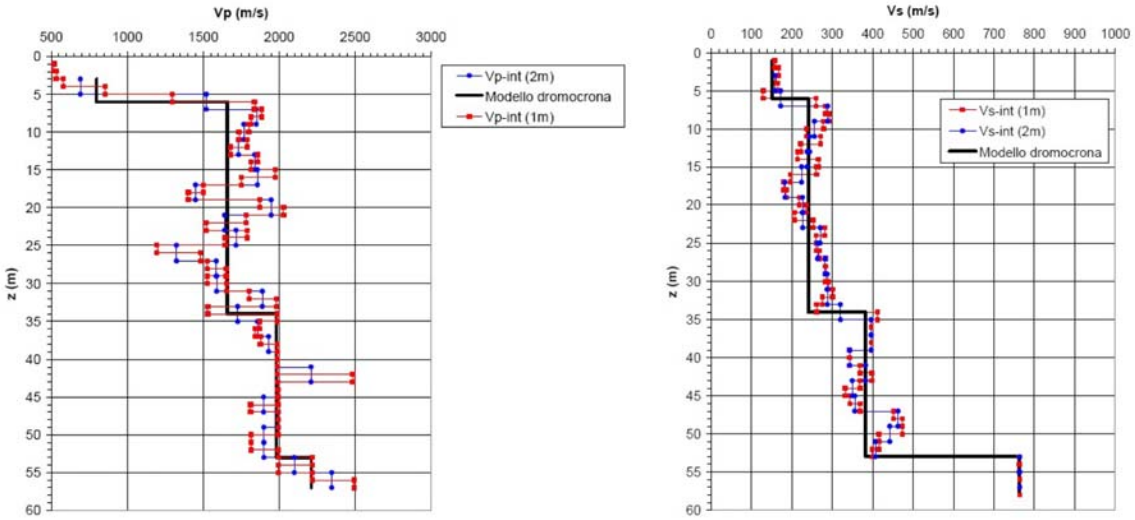

Figure 2.1.4 – Vp and Vs profiles for down-hole S1.

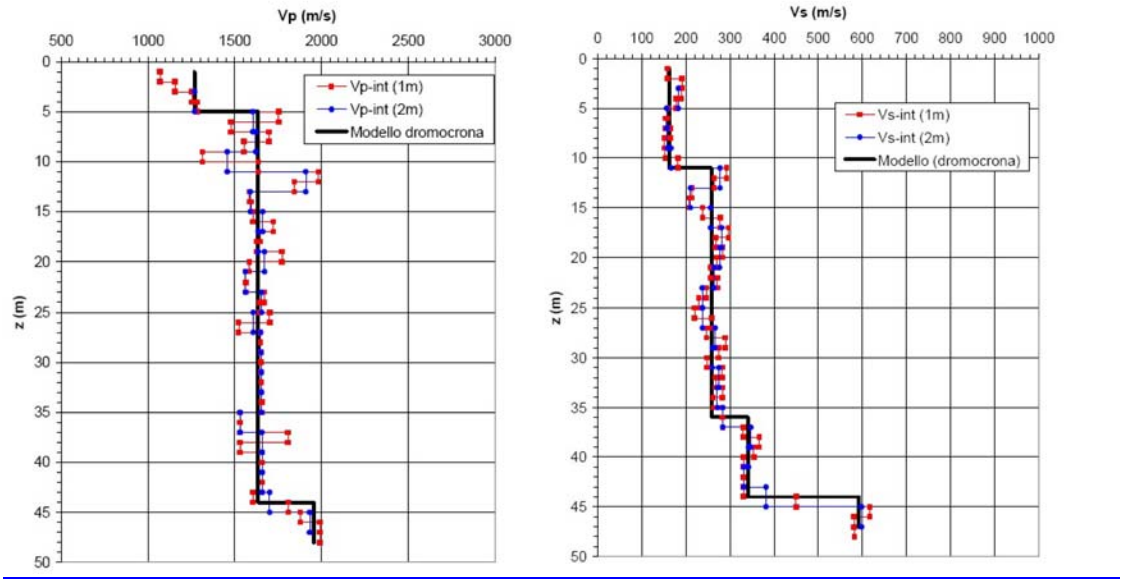

Figure 2.1.5 – Vp and Vs profiles for down-hole S2.

2.2 ENGINEERING GEOLOGICAL MODEL UP TO 30M

Three main lithotechnical units were defined in the subsurface of Gubbio Basin:

- gravel breccias or gravelly sands,
- sandy silts and clays
- limy clays.

By correlating the units present at different elevation for each borehole, we reconstructed the spatial distribution of these units, up to a maximum depth of 30m b.g.l.. Contouring at different depths (Figure. 2.2.1) shows that well-thickened breccia/gravels or gravelly sands with some layered clayey levels are present until the elevation of 450 m a.s.l. (Figures 2.2.2 and 2.2.3).

These soils, mainly composed of limy grains, belong to debris fans, close to the eastern edge of the basin where breccia prevail, while moving towards the centre of the basin they belong to alluvial fans.

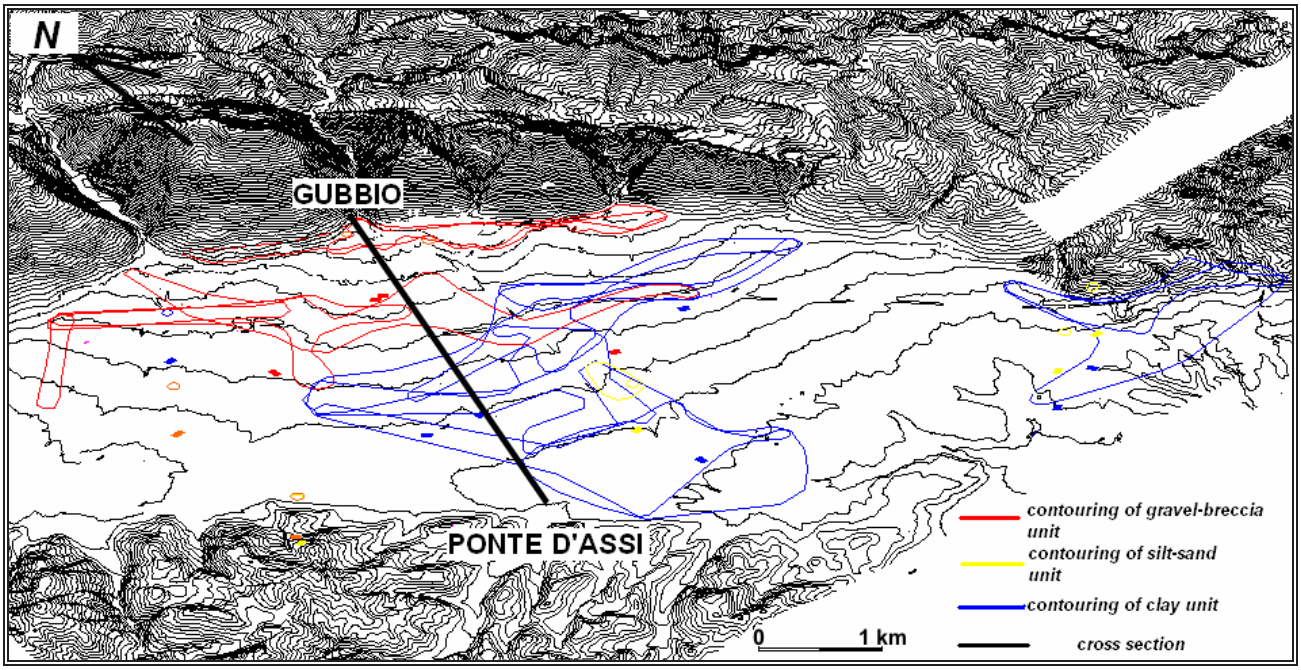

Figure 2.2.1 – Example of contouring of the lithotecnical units at different depth below ground level.

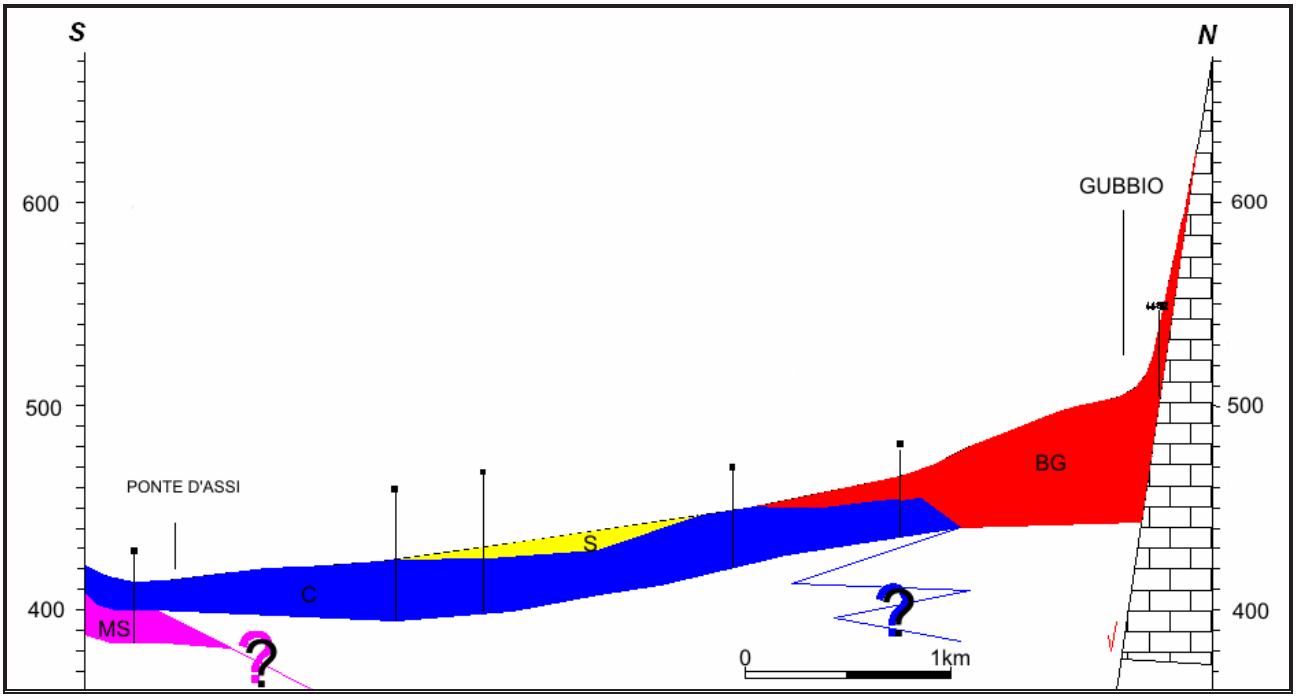

Figure 2.2.2 – Cross section through Gubbio Basin: BG breccia/gravel and sandy gravel; S sandy silt; C clay and clayey silt; MS marls and sandstones (Marnoso-Arenacea Formation).

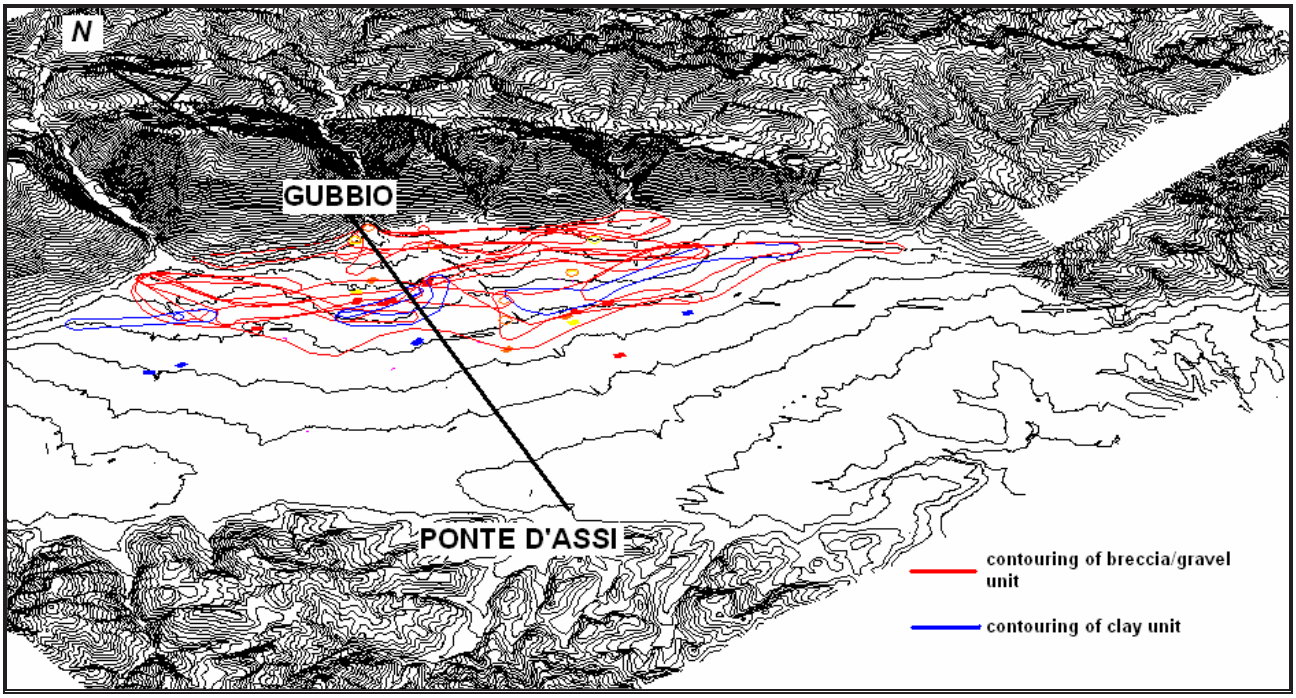

Figure 2.2.3 – Contouring lines from 500 to 450 m a.s.l.

Starting from 445 m a.s.l. (Figure 2.2.4) clayey soils of lacustrine origin prevail, especially in the central and south-western area, whereas lenses of sands and gravels are mainly present near the river Soanda also at great depth, as observed in the two boreholes.

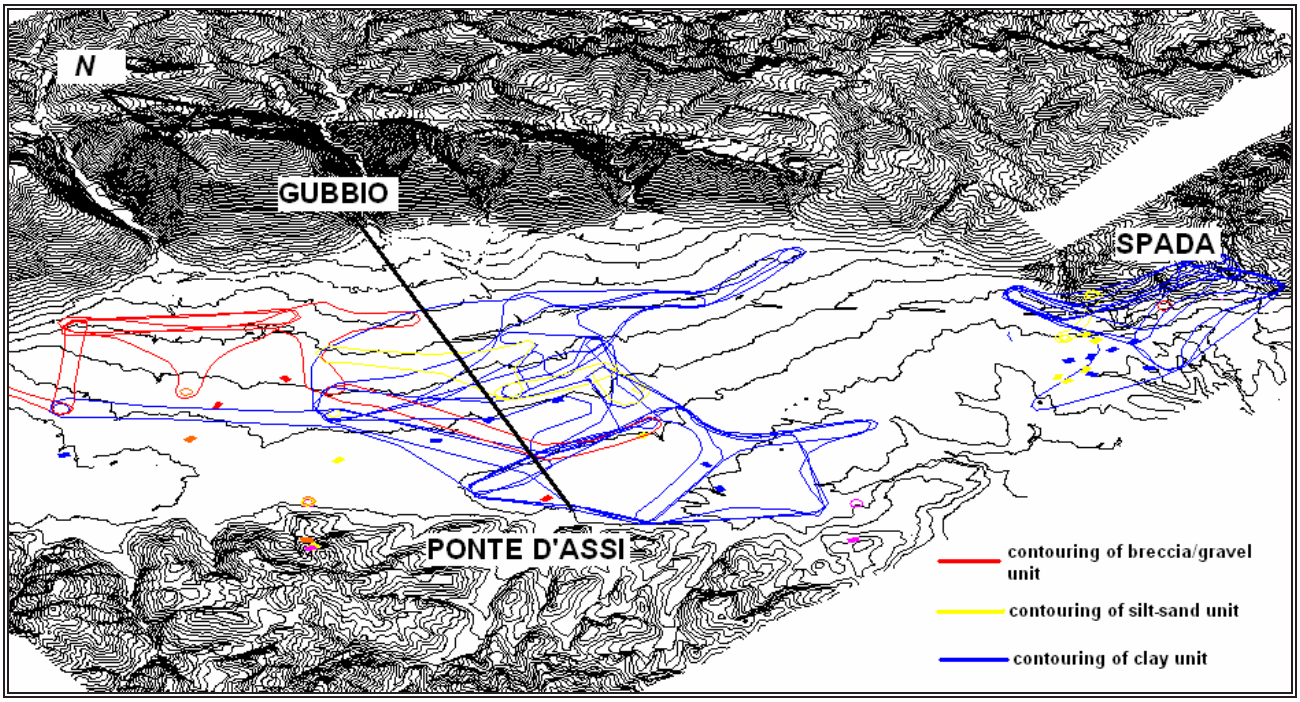

Figure 2.2.4 – Contouring lines from 445 to 400 m a.s.l. .

The investigations and the lab tests described in the previous paragraphs allowed to better define from a mechanical point of view the previously introduced engineering geological units and to assign them Vs values (fig. 2.2.5 and 2.2.6).

As for geotechnical parameters of the different lithotechnical units some values of angle of shear resistance (ϕ) and cohesion (c) can be given using data from site and lab tests obtained from investigations performed in the area including those coming from the boreholes S1 and S2 (Table 2.2.1).

Table 2.2.1 - Geotechnical parameters of the different lithotechnical units

LITHOTECHNICAL UNIT	γ (kN/m³)	ϕ (°)	c (kN/m²)
Breccia/Gravel or sandy gravel	17.5-18	30-35	
Sandy silt	17-18	26-32	
Clay and silty clay	17-20	14-22	15-70

Based on all these acquired data, the geotechnical parameters listed in Table.2.2.1, were given to the engineering geological units and consequently three representative schematic soil columns referred to the first 50 m b.g.l. were obtained in terms of lithological characters and geotechnical parameters (Table 2.2.2).

Layer	Litotech. Unit	Vs	γ	H	σv	IP	D
		m/s	*KN/m³*	*m*	KN/m²		%
I	Silty clay	200	17,9	12,3	110,1	48,5	5
II	Silty sand	220	18,1	5,5	-	-	5
III	Silty clay	250	185	20	330,3	29,8	5
IV	Sand/gravel	380	18	14,7	-	-	5
V	Gravel	760	18	6	-	-	-

a)

Layer	Litotech. Unit	Vs	γ	H	σv	IP	D
		m/s	*KN/m³*	*m*	KN/m²		%
I	Clayey silt	160	18,7	13	121,5	46,4	5
II	Gravel	280	18	3,1	-	-	5
III	silty clay	250	18,8	21,4	335,3	16	5
IV	silty clay	320	18,8	8	467,4	16	5
V	sand/gravel	600	18	4,5	-	-	-

b)

Layer	Litotech. unit	Vs	γ	H	σv	IP	D
		m/s	*KN/m³*	*m*	KN/m²		%
I	Gravel	280	18	15	-	-	5
II	silty clay	250	18,5	5	242,7	50	5
III	Gravel	280	18	10	-	-	5
IV	silty clay	320	18,8	30	481,2	15	5
V	silty clay	500	19	-	-	-	-

c)

Table 2.2.2 – Synthetic stratigraphies belonging to S1 (a) S2 (b) and S3 (c).

Two of them are representative of the stratigraphic sequence deployed in the borehole S1 and S2 and are thought to be located in coincidence of the two boreholes, while the third one is considered representative of the engineering geological sequence close to Gubbio centre (labelled S3) and is located close to Gubbio downtown.

3. NOISE MEASUREMENTS

3.1 ESTIMATES OF THE RESONANCE FREQUENCIES

It is widely accepted that maxima of the function H/V describing the ratios between average spectral amplitudes of horizontal (H) and vertical (V) noise field components corresponds to resonance frequencies f_0 of the sedimentary cover (see, e.g., Lachet and Bard, 1994; Tokimatsu, 1997; Bard, 1999; Nakamura, 2000; Fäh et al., 2001; SESAME European project, 2005). On its turn, this parameter supplies information on the ratio between the average Vs velocity V_a in the sedimentary cover and its thickness H. In particular, as a first order approximation, it holds that $f_0 = V_a/4H$. This property has been widely used to infer thickness of recent sedimentary cover in several parts of the World (e.g., Yamanaka et al., 1994; Ibs-von Seht and Wohlenberg, 1999) from passive seismic measurements.
This approach has been adopted to provide a preliminary estimate of the subsurface geometry of the seismic bedrock in the Gubbio area. To this purpose, an extended survey of the seismic environmental noise field was performed.
Environmental noise measurements were acquired through an ultra-compact and ultra-light instrumental tool (TROMINO®: http://www.tromino.it) purposely developed for high resolution digital measurements of seismic noise. At each site, noise was registered during day time for 20 minutes at 128 Hz sampling rate. Data analysis was performed using the "Grilla®" software provided by Micromed (http://www.tromino.it/frameset-grilla.htm). Registered time series relative to each ground motion component was subdivided in non-overlapping time-windows of 20 s. For each of these, the signal was corrected for the base-line, padded with zeros and tapered with a Bartlett window; the relevant spectrogram was then smoothed through a triangular window with frequency dependent half-width (10% of central frequency) and the H/V ratio of horizontal to vertical spectral components (the former being the geometric mean of N-S and E-W components) was computed for each frequency. Lastly, spectral ratios relative to all the time-windows considered were averaged and a mean HVSR curve computed, along with the relevant 95% confidence interval.
Before interpreting the resulting curve in terms of site geo-structural features, we checked the possible occurrence of spurious H/V peaks (e.g., due to impulsive or strongly localized anthropic sources). To this purpose, we analyzed both the time-stability of spectral ratios over the recording length and their directionality: if non-stationary or strongly directional effects were identified, the relevant portions of recording were discarded. The peak frequency f_0 and amplitude A_0 (along with relevant uncertainties) were then computed by averaging all the frequency/amplitude values corresponding to the H/V maximum in each considered time-window (for details, see D'Amico et al., 2004). On this regard, only maxima inside the frequency range 0.1-20 Hz were taken into account.
The interpretation of the HVSR curve was then carried out conformably to international consensus criteria (see SESAME European project, 2005). According to these, firstly we verified the curve reliability (i.e. sufficient number of windows and significant cycles for a given f_0, acceptably low scattering between all windows over a given frequency range around f_0) and secondly we checked the "clarity" and reliability of the H/V peak (i.e. fulfillment of amplitude and stability criteria). Particular attention was devoted to identify

eventual peaks of industrial origin (sharp peaks on all single-component spectra, getting sharper with decreasing smoothing) or induced by low-frequency disturbances (wind blowing in case of near tall buildings, bad soil-sensor coupling, etc.) and to better resolve broad or multiple peaks (i.e. by varying the smoothing parameters). In all unclear situations, however, the measurement was repeated. In case of curves showing a single peak, f_0 was considered as the fundamental frequency f_r at the site. When another peak f_1 ($>f_0$) was present, this was interpreted as a further natural resonance frequency associated with a shallower impedance contrast at depth. In about 10% of measurements this secondary peak was present. However, since the main interest of the study was the determination of the total depth of the sedimentary cover, these secondary peaks have been disregarded. Those curves with none clear and statistically significant peak were considered "flat" and interpreted as indicative of subsurface structures devoid of any sharp contrast of impedance at depth.

In order to evaluate the repeatability of the H/V measurements, at 10 sites the noise measurements have been repeated in different meteorological conditions and using different instrumental tools. In particular, H/V noise measurements have been carried out on the sites where the GFZ seismic array operated. Comparison of the results obtained showed that major features of the H/V spectral ratios as a function of frequency at the sites considered are substantially independent from the instrumental apparatus used for the measurements and can be considered as repeatable measurement. Only in the case of low frequency resonance (<.5 Hz) a significant dependence on the regional meteo-climatic conditions have been found. In fact, during particularly quite meteorological conditions, low frequency maxima tend to disappear. To avoid this problem, all the measurements have been carried outwith perturbed weather conditions.

H/V measurements have been performed at 90 sites. After a careful re-examination of the results obtained, 10 measurements have been discarded due to the presence of a strong anthropic noise or due to a bad positioning of instrumentation. The position of measuring points where reliable estimates have been obtained are shown in figure 2.1. In about the 10% the H/V curves indicate the presence of a double maximum. In these cases, the one corresponding to the lowest frequency has been considered only.

The results in Figure 3.1 indicate a good geographical coherency of the results obtained. In fact lowest resonance frequencies have been obtained along the axis of the alluvial basin, with values lower than 0.5 Hz, while f_0 values tend to increase moving towards the boundaries of the plain. Along the northernmost part of the eastern border of the plain (including the Gubbio old centre), in correspondence of the Carbonatic outcrop, H/V measurements indicate the absence of resonance peaks. Just west to this "no resonance" belt, a sharp variation exists towards a zone characterized by low frequency resonance. Along the same northern border, south-eastward in correspondence of the flysch outcrop, the situation appears different, with a soft transition from relatively high to low frequency resonance frequencies moving towards the plain. A reversed situation has been found along the opposite border of the basin with a softer transition from high to low resonance frequencies to the northwest and with a sharpening of this transition to the Southeast. If one considers the results obtained along the median axis of the plain, one finds a progressive reduction of the resonance frequency moving from the centre of the basin towards the edges.

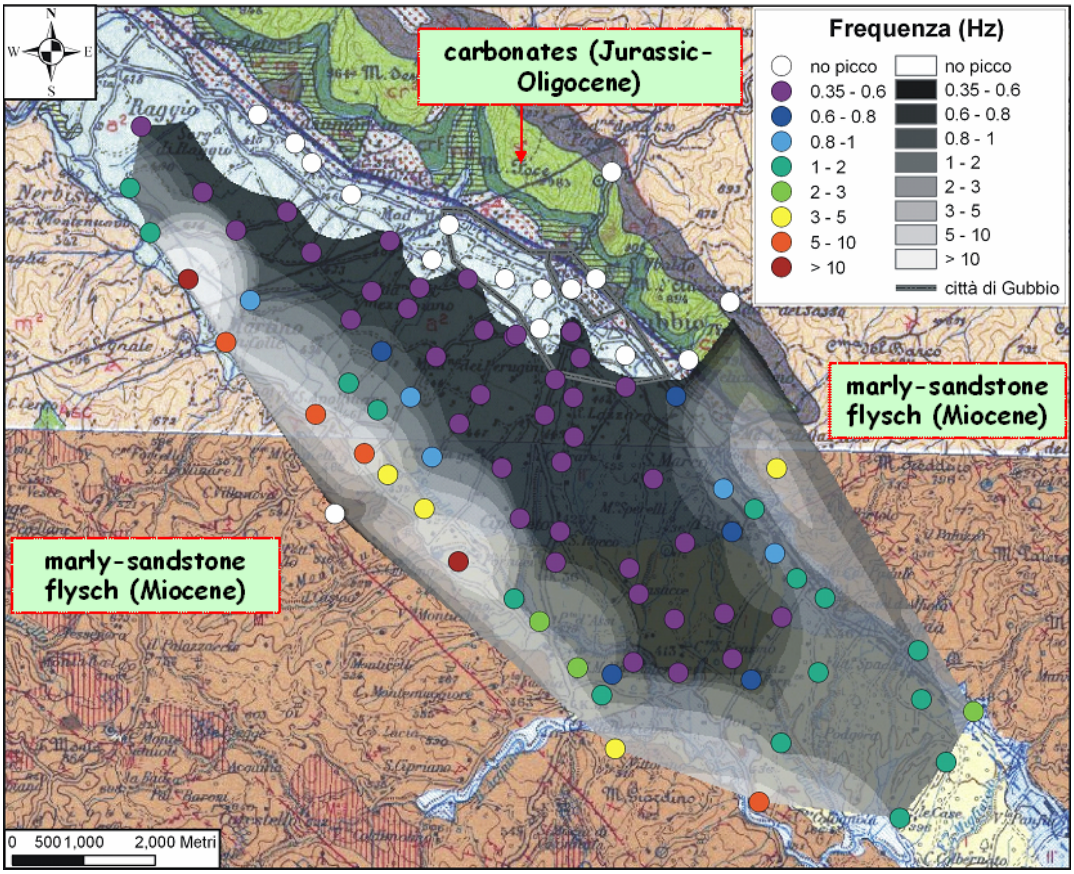

Figure 3.1 - Location of sites where H/V spectral ratio measurements have been carried on. Colours indicate the estimated value of the local fundamental resonance frequency. The is-frequency curves have been obtained by linear interpolation of measured sites. The contour is superimposed to the Geological map of the area.

A possible first order interpretation of these findings could be the following. The no-resonance belt could correspond to the area where carbonatic breccias and alluvial fans dominate the subsoil. These sediments are probably characterised by a relatively high Vs velocity with respect to clays and sand sediments characteristic of the alluvial basin. This could imply that no or low contrast exists in this area between seismic impedance of sediments and bedrock, making ineffective the trapping of seismic energy responsible for the resonance. The low values of f_0 obtained throughout the alluvial basin, indicate a relatively deep sedimentary cover (of the order of hundreds of meters). In the assumption of a constant velocity profile in the alluvial sedimentary cover, one can imagine a relatively flat bottom of the basin, whose horizontal dimensions are larger in the southernmost part of the basin and becomes narrower north-westward. In the north-westernmost part of the basin, the thickness of the alluvial cover decreases towards the opposite borders of the basin. However, while there is a progressive decrease in thickness going from the centre of the basin towards south-west, north-westward this decrease is sharp and roughly corresponds to the Gubbio fault trace. The reverse situation occurs in the south-easternmost part of the basin. All these features seem to exclude a cylindrical shape of the basin and stress the importance of the geological differences of the outcropping bedrock (carbonatic north-westward and marly-sandstone south-eastward) along the north-western boundary of the basin.

3.2 DISPERSION CURVES FROM SMALL ARRAY 2D

In order to check this hypothesis, estimates of the S-wave velocity profile in the shallow subsoil were experimentally deduced through noise recordings at arrays of sensors (e.g., Okada, 2003) conducted at 10 sites (Fig. 3.2.1). All the sites were investigated through arrays of sensors deployed in a 2D geometry (L- or cross-shape) with length of singular deployments from 50 up to 100 m depending on the space locally available. Seismic noise was recorded for 20 minutes at 128 Hz sampling rate by using 16 vertical geophones (4.5 Hz) and a digital acquisition system produced by Micromed (http://micromed-it.com/brainspy1.htm). Relevant Rayleigh-wave dispersion curves were then derived through the extended spatial autocorrelation (ESAC) technique (Ohori et al., 2002; Okada, 2003).

Five out of 10 of the sites considered have been located in correspondence of silt-sand or clay outcrops typical of the alluvial plain. In particular, one site corresponds to the S1 site (S. Erasmo in section 21) and one to the centre of the seismic array deployed by the INGV Team (Section 3.3). But in one case, well defined Rayleigh waves dispersion curves have been obtained at these sites (Figure 3.2.2).

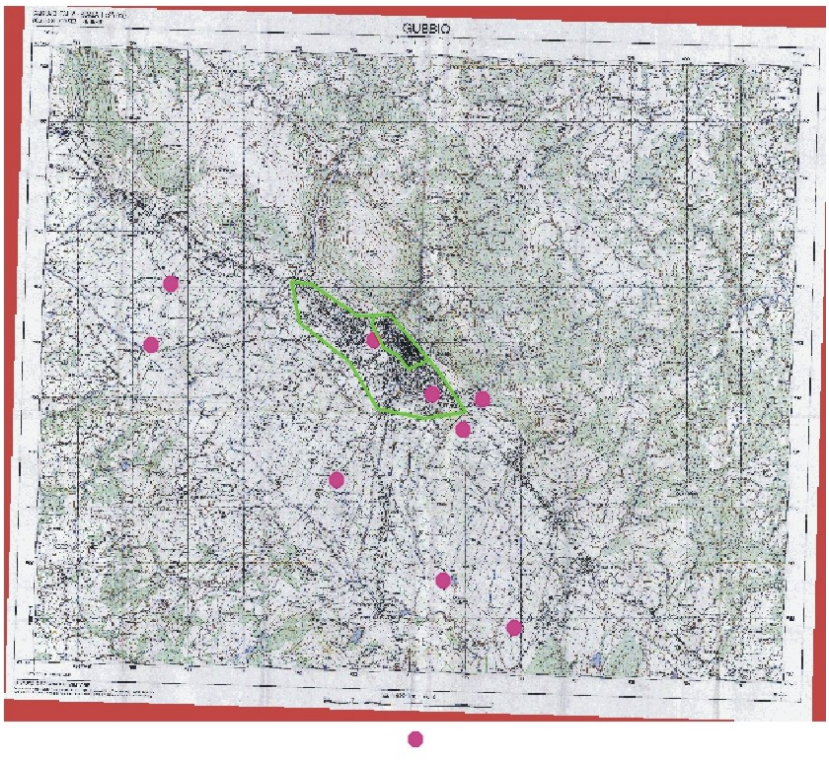

Fig. 3.2.1 - Location of noise measurements carried out by using array arrangements

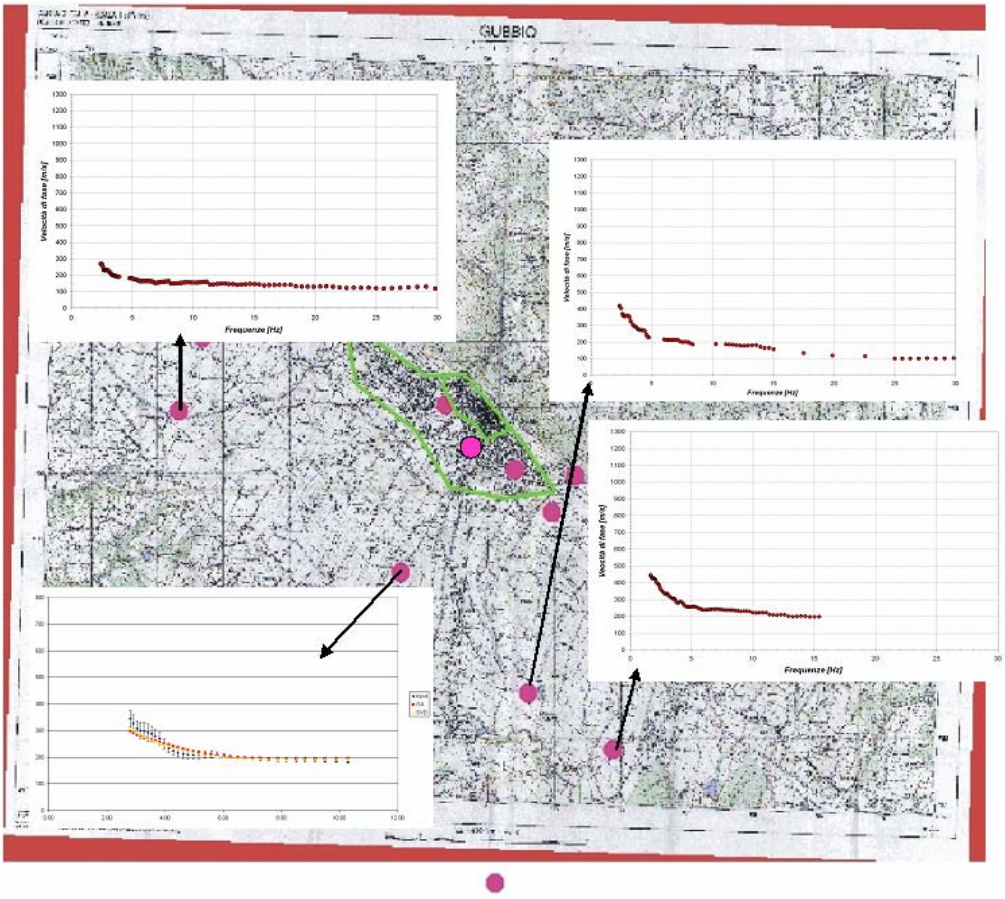

Figure 3.2.2 - Rayleigh dispersion curves obtained at the sites located in the alluvial plain.

As concerns the other sites, one has been located south of the plain where the presumed seismic bedrock outcrops while the others have been located along the north-eastern boundary of the plain where carbonatic breccias and alluvial fans dominate. The results obtained in these cases are shown in Figure 3.2.3.
The comparison between the results in the figures 3.2.2 and 3.2.3 shows a clear difference between the average phase velocities. These result generally higher on the outcropping bedrock and along the breccias and alluvial fans with respect to those in the alluvial plain. The analogy between the results obtained on the bedrock outcrop and those at the foothill in correspondence of the Gubbio downtown suggests that a similar average Vs values characterize these domains. This could explain the lack of resonance phenomena revealed by the H/V measurements (Section 2) due to the lack of any significant contrast of the seismic impedance of the sedimentary cover and bedrock.

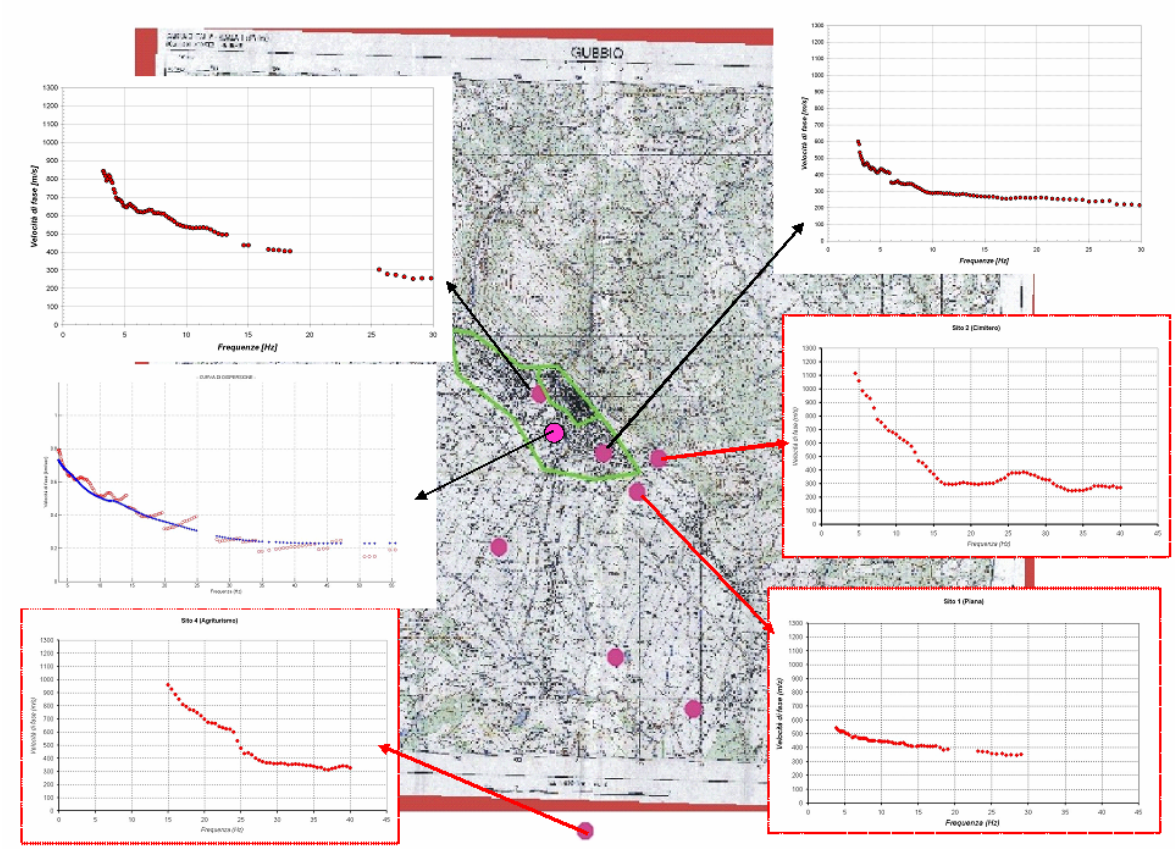

Figure 3.2.3 - Rayleigh dispersion curves obtained at the sites located on the outcropping bedrock and along the north-eastern border of the alluvial plain.

In order to better evaluate these differences in terms of shallow Vs profile, some dispersion curves have been inverted by using an SVD inversion procedure (Nelder and Mead, 1965).

The result obtained at three sites located in correspondence of clay formations are reported in figure 3.2.4. These indicate that a "typical" Vs profile seems to characterize the alluvial plain. This typical profile can be interpolated by using a "standard" profile in the form adopted by Ibs-von Seht and Wohlenberg (1999). This profile can be considered representative of the Clay units at least up to depths lower than 100 m.
The same inversion carried out by considering the dispersion curves obtained near the Gubbio downtown are shown in figure 3.2.5.
The comparison with the Vs profiles in figure 3.2.4 clearly shows that the last sites are characterised by a steeper velocity gradient and a marked heterogeneity at least as concerns the two sites considered.

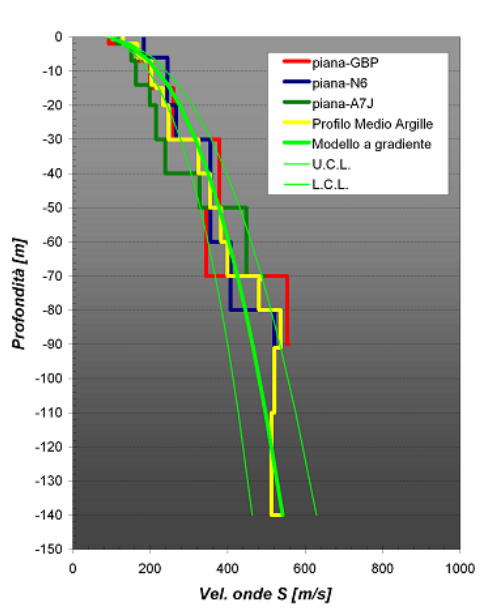

Figure 3.2.4 - Vs velocity profiles obtained at three sites located in correspondence of Clay units in the Gubbio Basin (red, blue and dark green). The yellow line indicates the average profile for the three sites. The Light green thick line indicates the interpolated standard profile in the form $Vs=101\ (1+z)^{0.33}$. The thin lines in light green indicate the 95% confidence interval for the standard profile.

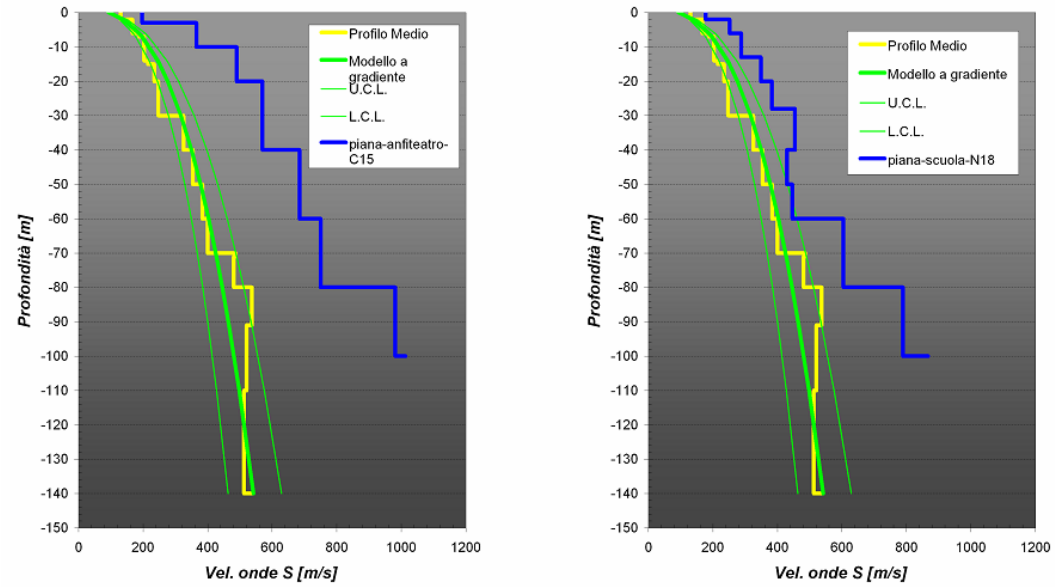

Figure 3.2.5. Vs velocity profiles obtained at two sites located in correspondence of the carbonatic debris and alluvial fans near the Gubbio downtown (Blue lines). These profiles have been compared with typical Vs profile for the clay units in figure 3.2.4.

3.2.1 Joint Inversion of dispersion and H/V curves at the S. Erasmo site (Siena)

The SVD inversion of Rayleigh waves dispersion curves does not allow to define the Vs profile at depths larger than 100 m. In order to evaluate if this depth is sufficient to parameterize the whole sedimentary cover, one can use the approach proposed by Ibs-von Seht and Wohlenberg (1999) consisting the combined use of the „standard" Vs profile determined above for the clay units and f0 estimates deduced by H/V measurements. In this way, one obtain depths that, at the centre of the basin reach more than 400 m. This implies that the Vs profiles determined by inverting the dispersion curves only are not sufficient for the correct parameterization of the Gubbio basin.

As shown by previous studies (Parolai et al., 2005; Picozzi et al., 2005), a possible strategy for retrieving consistent S-wave velocity profiles both in the sediments and in the bedrock is to perform a joint inversion of Rayleigh-wave dispersion and HVSR curves. Therefore, at each array recording site a HVSR measurement was contextually carried out. To perform the joint inversions, a combination of different inversion procedures (i.e. genetic algorithms and generalized least-squares methods) was chosen, since this can result a very effective strategy to manage the extreme non-linearity of the problem (Picozzi and Albarello, 2007). To this purpose, both the genetic and the generalized least-squares algorithm, respectively proposed by Yamanaka and Ishida (1996) and Arai and Tokimatsu (2005), were implemented in a MATLAB code (for details see the reference papers). The forward modeling of Rayleigh-wave phase velocities and HVSR curves was performed in the assumption of vertically heterogeneous 1D models using the modified Thomson-Haskell method proposed by Hermann (2002) and following the indications of Tokimatsu et alii (1992) and Arai and Tokimatsu (2004), respectively. Both these formulations assume that the noise wavefield is dominated by surface waves (at least as concerns its most coherent and statistically persistent component), include the presence of higher modes and consider both the Love and Rayleigh waves propagation in the H/V spectral ratios modeling.

Preliminarily to the inversion by genetic algorithms, a search area for the parameters to invert (i.e. S-wave velocity and thickness H of each layer) was defined. Moreover, though sensitivity analyses (e.g., Arai and Tokimatsu, 2004) showed that the dependence of Rayleigh-wave dispersion and HVSR curves on P-wave velocity is much smaller than that on VS and H, different VS /VP ratios were tested during the inversion. Then, 100 populations of models (each one of 50 individuals) were selected, tested and combined by a series of genetic operations (Parolai et al., 2005). Picozzi and Albarello (2007) showed that, though genetic algorithm allows to single out the hyper-volume of the parameters search area where the global minimum of the inversion problem lies, it could be unable to identify that model which completely reproduces both the available data sets. Therefore, the minimum misfit model of each inversion through genetic algorithm was used as starting guess of the linearized inversion with the generalized least-squares algorithm.

This approach has been adopted to invert the noise data registered both with the array and single station (H/V) configurations at the S1 borehole (S. Erasmo Fig. 2.1). The results obtained are shown in figure 3.2.6 and show the presence of a sharp transition at a depth of about 500 m from the surface. They also show that the Vs profile is characterized by a

relatively steep increase of the Vs values in the first tens of meters and by a progressive reduction of the velocity gradient with depth.

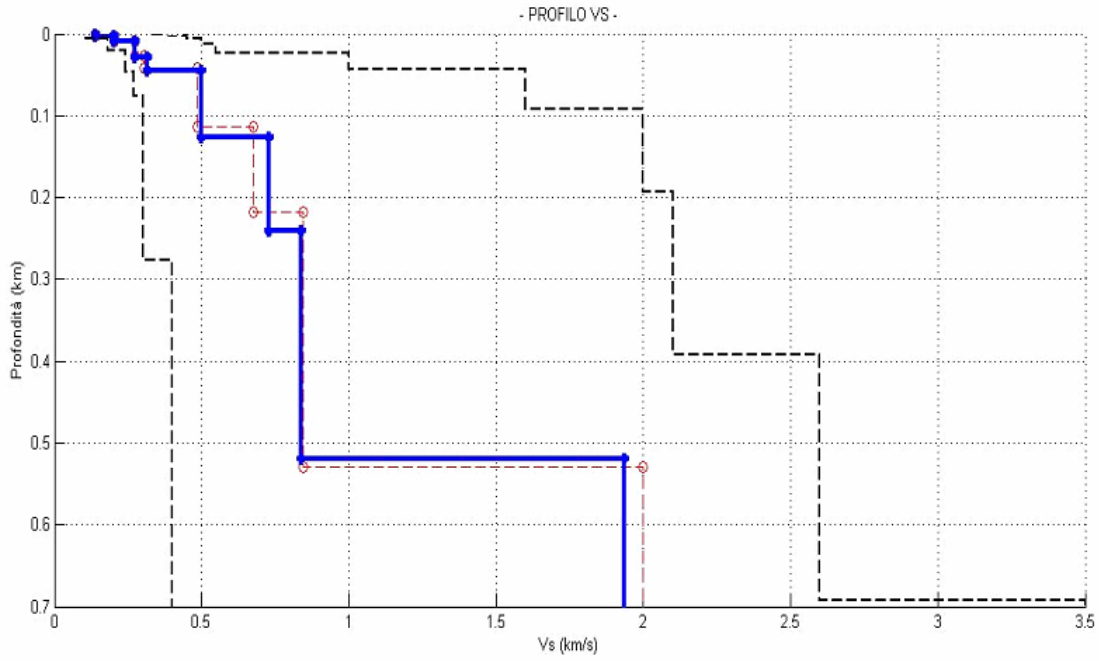

Figure 3.2.6 - Vs velocity profile obtained at the S1 station by the joint inversion of H/V and dispersion curves by using the Genetic Algorithm approach (see text). The blue lien indicate the best fitting curve while the dotted line indicates the search area for the minimization

3.3 DISPERSION CURVES FROM LARGE 2D ARRAY

A two-dimensional seismic array was deployed in the alluvial basin of Gubbio about 2 km south-west to the town (Figure 3.3.1).
It was composed of 15 seismological stations (table 3.3.1) with an average distance of about 500m and a maximum aperture of about 3500m (Fig. 3.3.1). The instrumentation consisted of 3-component 5sec receivers (Le3d-5s) connected to Marslite or Reftek130 digitizers.
The time synchronization has been provided by a GPS timing connected to each station. The seismological stations operated in continuous modality from June to September 2006 recording about 80 local earthquakes (1.0 <M< 3.7; 2km< epicentral distances <120km). Data analysis on a selected subset of about 40 good-quality earthquakes (horizontal site-to-reference spectral ratio technique, response spectra ratios) allowed to estimate the variation of the local seismic response for the target area (see Deliverable D22-D23).
Moreover, ambient noise has been processed in terms of horizontal-to-vertical spectral ratio (HVNSR) to compute the resonance frequency and, therefore, to check the homogeneity of the seismic response among stations of the array.

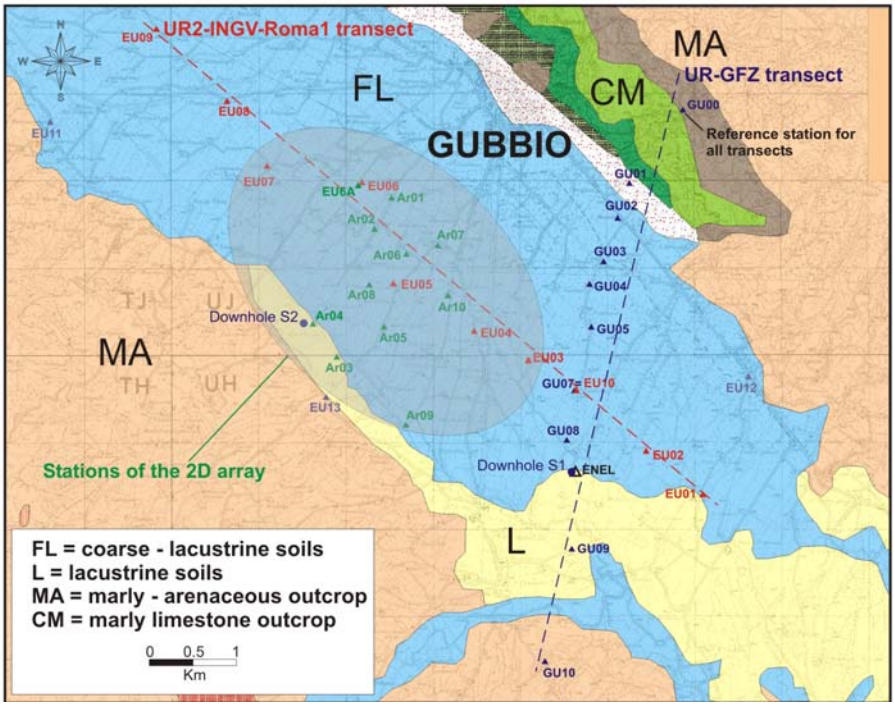

Figure 3.3.1 - Two dimensional seismic array of velocimetric station

Figure 3.3.2 shows that stations near the edge of the basin (AR03, AR04, AR05 and AR09) have a higher resonance frequency (0.7-1.1 Hz) than the ones of middle plain (about 0.4 Hz). However, HVNSRs of two other stations differ from the HVNSR of the central part of the array: EU07, that is the most north-western site, shows a resonance frequency of 0.7 Hz, whereas EU04 is affected by cultural noise due to its vicinity to an heavy traffic road.
For the remaining 9 stations having a consistent resonance frequency (about 0.4 Hz), we applied an array techniques based on ambient noise vibrations to derive a shear velocity profile at larger depth than the down-hole surveys.

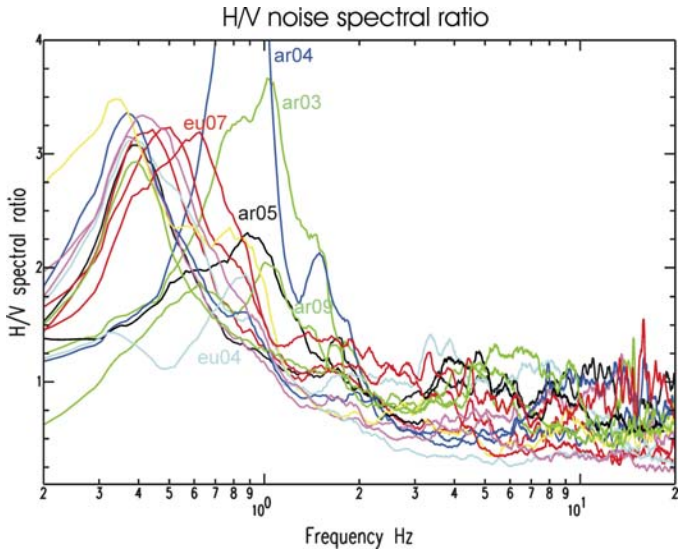

Figure 3.3.2 - HVNSR for the station of the array

Table 3.3.1 – Stations of the 2D seismic arrays – coordinates are in WGS84

Station ID	Location	Longitude	Latitude
EU03	Zampagli's home	12.58274°	43.32521°
EU04	Cipolleto school	12.57507°	43.32790°
EU05	Ferranti's home	12.56386°	43.33338°
EU6A	Procacci's home	12.55860°	43.34326°
EU07	Paciotti's home	12.54809°	43.34433°
AR01	Angeletti's home	12.56243°	43.34166°
AR02	Municipal slaughterhouse	12.55997°	43.33801°
AR03	Municipal kennels	12.55658°	43.32581°
AR04	Regional plants nursery	12.55280°	43.32790°
AR05	Church - S.Agostino	12.56181°	43.32756°
AR06	Casagrande's home	12.56867°	43.33494°
AR07	Paffi's home	12.56970°	43.33643°
AR08	Urbani's home	12.55974°	43.33287°
AR09	Ortoguidone camping	12.56819°	43.32163°
AR10	Tasso's home	12.57106°	43.33181°

The apparent phase velocities of the vertical component of the seismic noise have been measured using different array methods (FK, MSPAC and ReMi). The computation of the theoretical array transfer function allowed to determine the performance of our array (fig. 3.3.3). We retrieved a dispersion curve in the frequency band 0.6 - 1 Hz (Fig. 3.3.4)

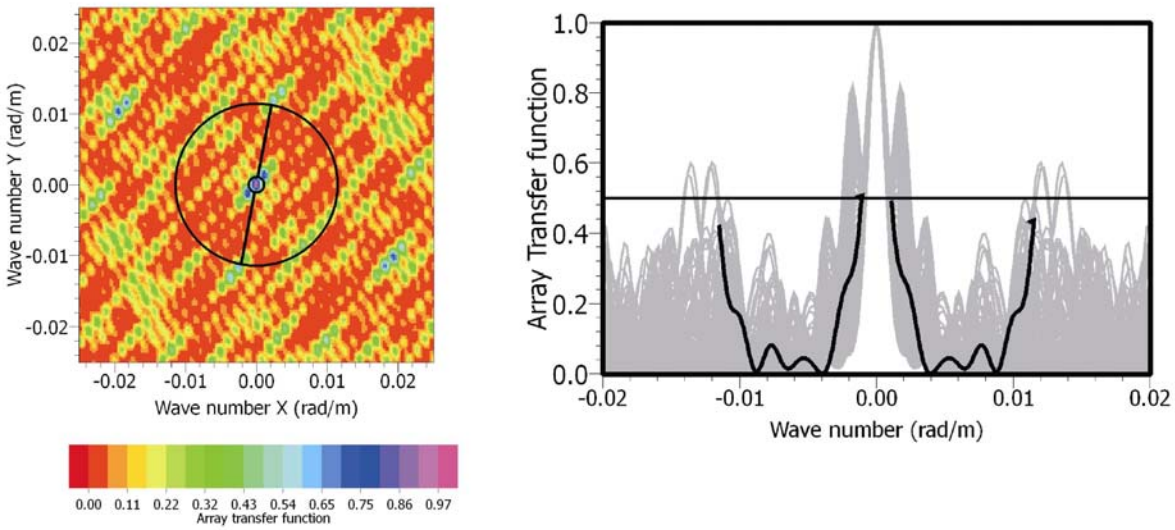

Figure 3.3.3 – Array transfer function of the array of 9 stations

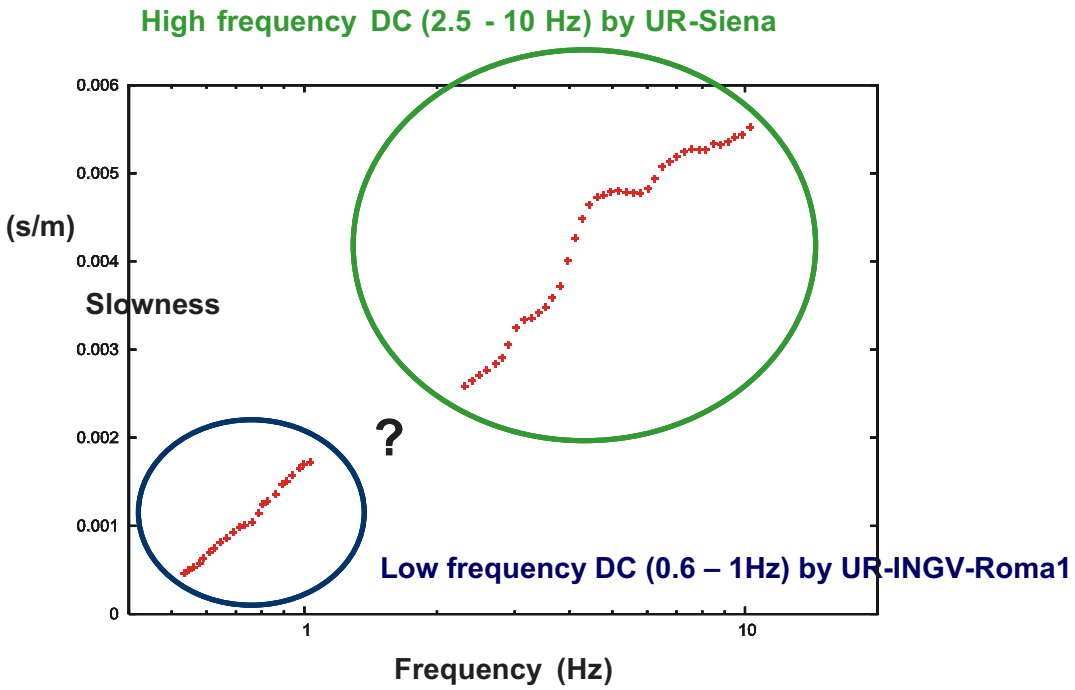

Figure 3.3.4 – Dispersion curve (DC) obtained by microtremor measurements of INGV-2D array (blue circle, between 0.6 and 1Hz) and UR-Siena linear array (green circle, between 2 and 10Hz)

3.3.1 Broad Band Inversion at S2

Starting from the dispersion curve (DC) computed from ambient noise, we retrieved one-dimensional (1D) shear velocity profiles of the subsoil by using an inversion procedure based on the neighbourhood algorithm (Wathelet, 2005).

The dispersion curve estimated in the frequency band 0.6 – 1 Hz was complemented with the phase velocities measured at higher frequencies (2-10 Hz) using the small array by UR-Siena (Fig. 3.2.2). They used a small aperture linear array deployed inside the area of the larger 2D array (Figure 3.3.1). Unfortunately, between 1 and 2 Hz there is still a lack of information of the DC. Inversion procedure generate 1D-layered models fitting the overall dispersion curve under the assumption of noise wave field mainly composed of Rayleigh waves. We performed a joint inversion of phase velocity dispersion and the average HVNSR of the target area (fundamental frequency of about 0.4 Hz). As a further constraint of the inversion we adopted the shallow P- and S-wave velocities provided by the down-hole measurements (Figg. 2.1.4 and 2.1.5).

The model classes are shown in Fig. 3.3.5 in terms of DC, Vp and Vs profiles and HVNSR. Looking at Vs profiles, they indicate a large depth of the basin (depth > 400 m) with a gradual increase with the depth of the Vs (from 500 to 1000 m/s) for the formation of the basin starting from a depth of 50 m. Among the inverted models, we selected five representative velocity profiles and we computed the 1D theoretical transfer functions. The comparison with the empirical transfer function obtained from earthquakes for station EU05 (Fig. 3.3.6), shows that the models reproduce fairly well the main resonance frequencies but they are not able to catch the whole complexity observed during earthquakes. Moreover, the level of amplification is significantly underestimated.

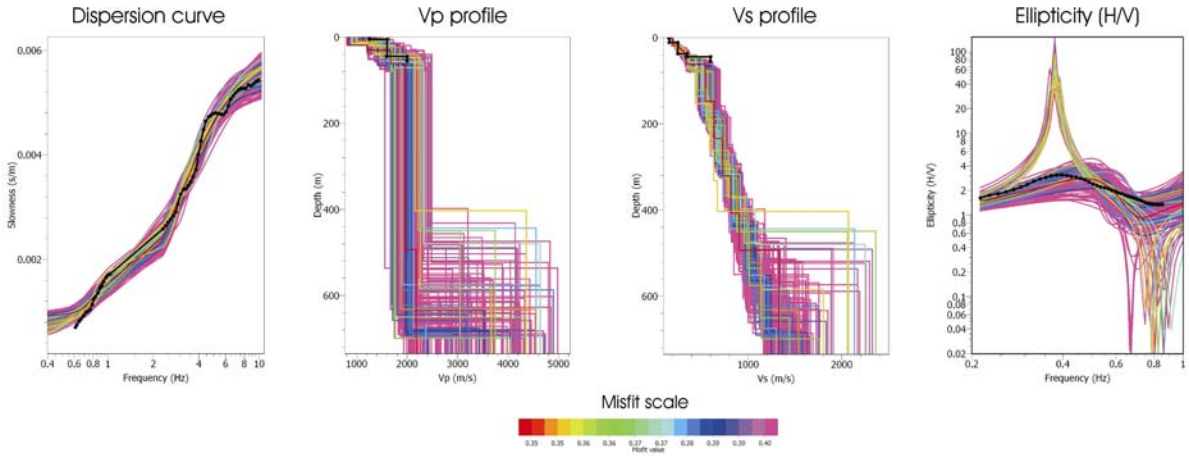

Figure 3.3.5 – Results of the joint inversion of DC: a) dispersion curves for the models compared with the experimental one; b) Vp profile; c) Vs profile; d) HVNSR (ellipticity of Rayleigh waves) for the models compared with the experimental fundamental frequency of the array.

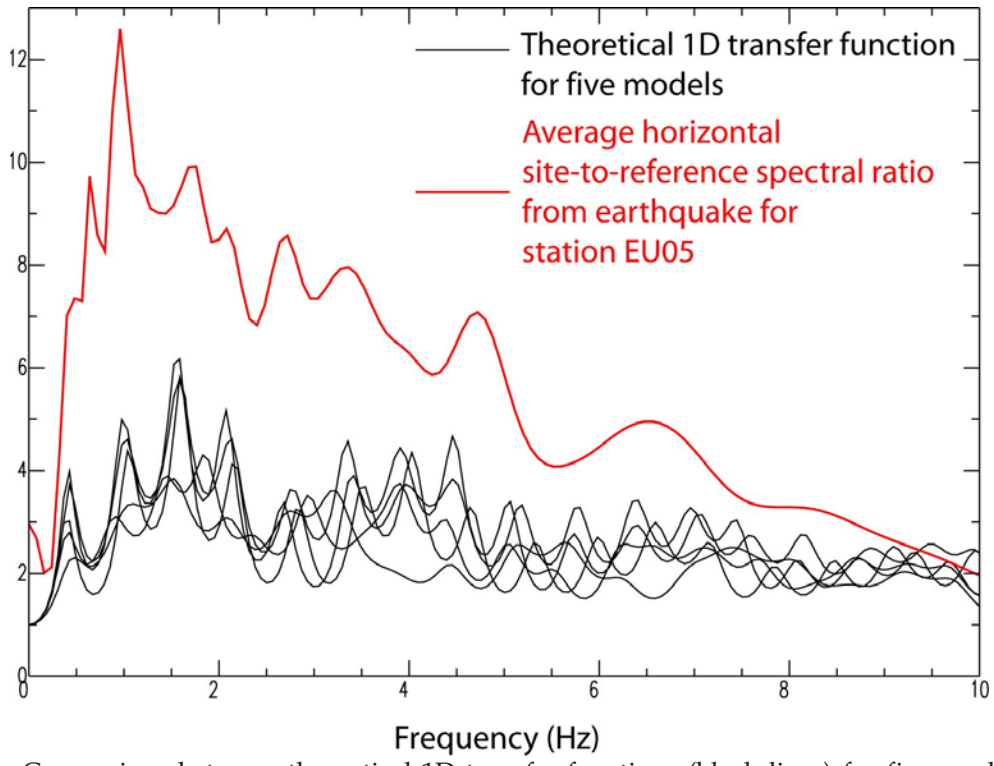

Figure 3.3.6– Comparison between theoretical 1D transfer functions (black lines) for five models obtained from inversion, horizontal site-to-reference average spectral ratio (red line) for station EU05.

4. SEISMIC REFLECTION TOMOGRAPHY

Seismic data and in particularly the travel time inversion (seismic tomography) can give us an accurate estimation of seismic velocity field and a precise depth imaging of the geological structures present in the investigated area. Within the frame of this project we provided for a 2D seismic acquisition in order to obtain an accurate depth section of the main sedimentary sequences in the Gubbio basin to be used for the reconstruction of the 3D model in the whole area.

4.1 SEISMIC DATA

The 2D seismic line was acquired in correspondence of the transversal transect of the GFZ stations, in the NNE-SSW direction (fig. 4.1). The line was acquired in two consecutive parts. In the first part we used the miniVib as sources (94 shots) and 202 geophones 20 m equally spaced (red line in fig. 4.1); in the second part, due to the absence of compacted soil, we used the minibang as sources (orange line in fig. 4.1). The total length of the line was 5300 m.

After applying seismic standard processing to the acquired data, we computed the travel time inversion of the reflected arrivals (tomography) associated to the main events interpreted on the seismic data. This method allowed us to obtain an accurate velocity model in depth and the correct reconstruction of the boundaries of the geological units (those surfaces associated to the reflected events picked on the seismic data). We singled out and picked the reflected times of three principal seismic horizons along the whole line (green, purple and blue lines in fig. 4.2); we inverted these travel times, by applying the tomographic algorithm, and we obtained a 2D velocity section in depth with the position and shape of the corresponding interpreted horizons. This result was then used as velocity input file for the pre-stack migration; we got a seismic section in depth on which we discussed and produced the final geological interpretation of this area.

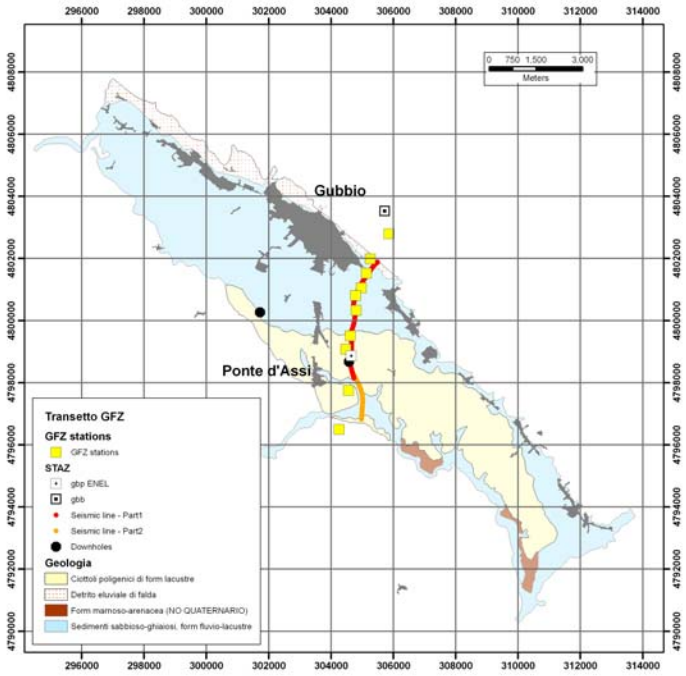

Figure 4.1 – Plan view of the position of the two seismic lines acquired.

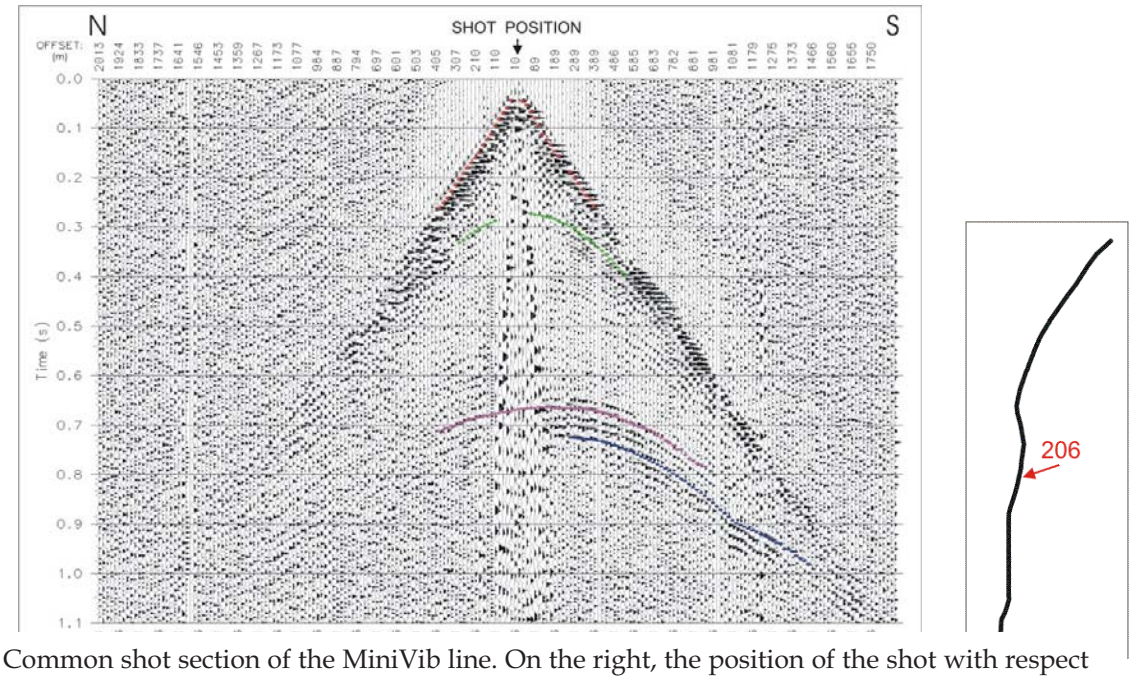

Figure 4.2 – Common shot section of the MiniVib line. On the right, the position of the shot with respect to the line. The coloured lines represent the picked events used for the travel time inversion.

The reflection tomography may be considered an iterative process, where for each iteration the velocity field and the depth of the interfaces are estimated separately (Figure 4.3 left). After picking the travel times associated to the reflector to be estimated, we choose an initial model defined by an horizontal surface and a constant velocity field. On this model, we compute the reflected travel times by using the ray tracing procedure. In a first step, the travel time residuals (the difference between the picked and the computed times) are used to update the velocity field above the reflector by the minimization methods like ART (Algebraic Reconstruction Technique), SIRT (Simultaneous Iterative Reconstruction Technique) or similar.
In a second step the new velocity field and the travel time residuals are used to update the interface by using the method of the minimum dispersion of the reflection points we describe in this work. From this new model (the update velocity and interface) new reflected travel times are computed. These two steps are repeated many times until the difference between the actual model and the model obtained by the previous iteration is less than a chosen threshold.

The method we use for the interface estimation follows the principle of minimum dispersion of the reflection points (Figure 4.3 right). The travel time residuals associated to each reflected event is transformed in depth, dz, by using the velocity field Vm updated in the first step of each iteration, and applied to the Z coordinate of the correspondent reflection. The new location of the reflection points are then used to define, through a spline interpolation, the new position and shape of the interface. The first iteration takes into account only the points associated to the near offset, being less affected by velocity errors. In the following iterations new points, with increasing offsets, are added in the interface building process, if they show the minimum dispersion, i.e. their distance from the estimated surface is less than a chosen threshold. The number of points increases during the iterations until all reflection points are included in the spline interpolation for creating the interface. The procedure stops when the mean value of the point dispersion is

minimum (less than a threshold) or when it doesn't change anymore (it oscillates on a fixed value).

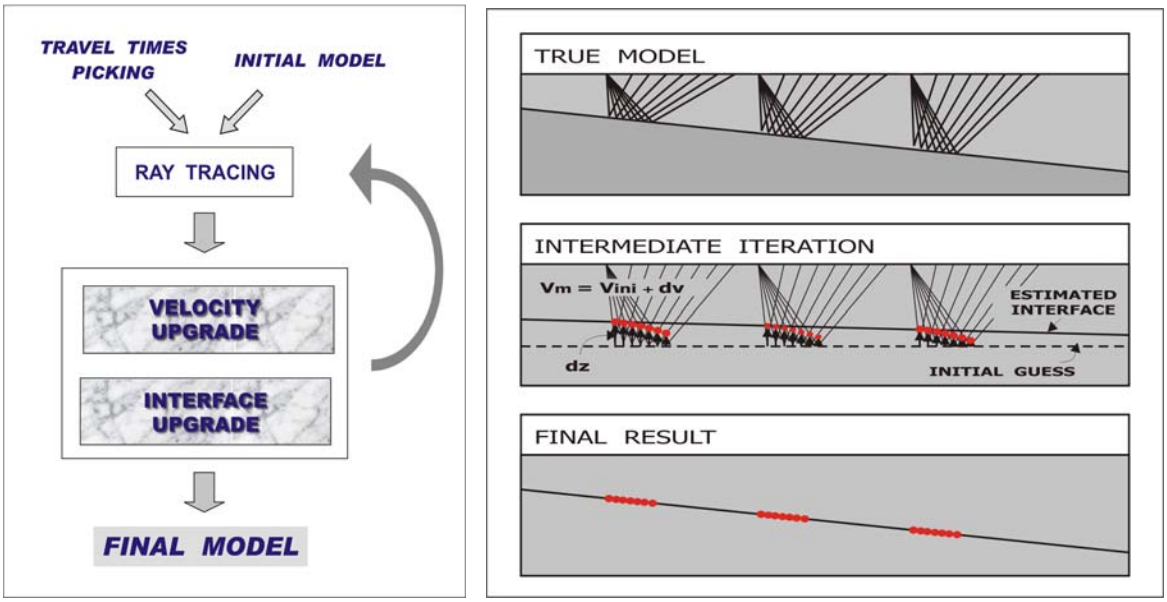

Figure 4.3 – Scheme of the whole inversion procedure (left) and the description of the method of the minimum dispersion of the reflection points applied to the interface estimate.

4.3 THE P-VELOCITY MODEL

The velocity field obtained from the tomographic inversion is displayed in the fig. 4.4. This section is obtained by the junction of the first part, acquired with the Minivib source, and the second part, acquired with the Mini Bang. The inversion also defines the position in depth and the shape of the reflectors picked in the pre-stack section.
We can observe an U-shape of the last horizon which represents the top of the bedrock (the "Marnoso-arenacea" formation). The overlaying layers (clay in prevalence) are defined by a set of structures dipping to the right part of the model. The quaternary sediments end the sequence.
The fig 4.5 shows the pre-stack depth migrated section obtained from the velocity section of fig. 4.4, on which three different lithological units are interpreted (see the coloured lines of Figure 4.5).

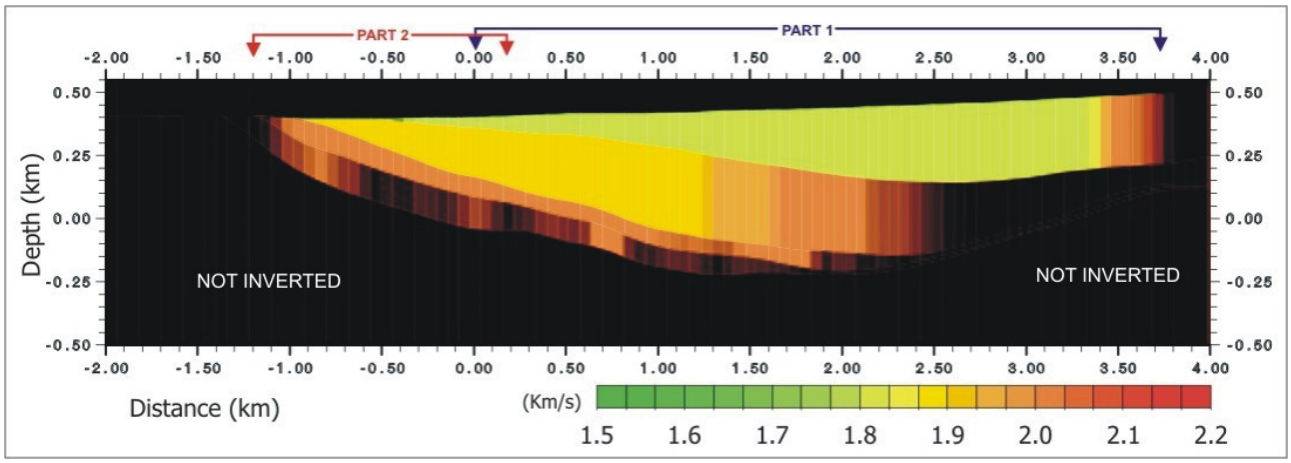

Figure 4.4 – Vertical section of the final velocity field obtained from the tomographic inversion of the reflected arrivals.

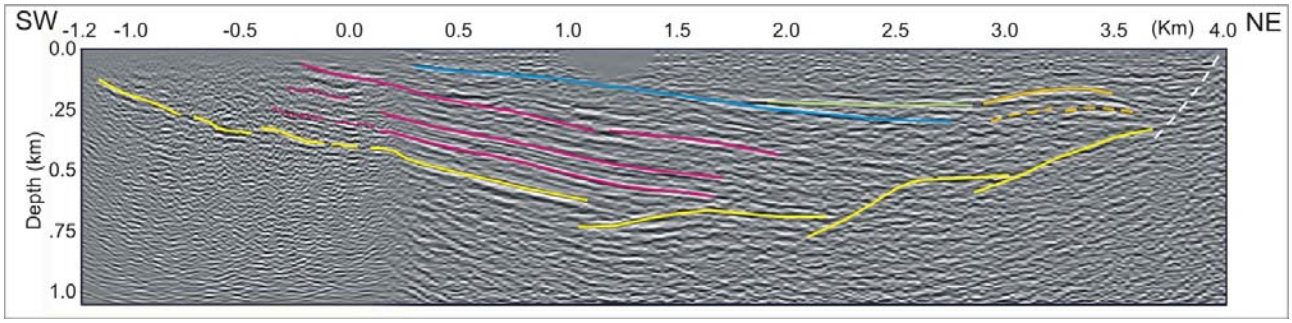

Figure 4.5 – Pre-stack depth migrated section by using the velocity field of fig. 4.4. The coloured lines represent the interpreted horizons: the yellow ones define the top of the "marnoso-arenacea" formation, the red lines are the clay-sand formations, the blue ones could be associated to the top of the fluvio-lacustrine deposits, the green ones to alluvial deposits and the orange lines to the breccias. On the right the dash white line shows a fault which separates the sedimentary basin from the calcareous outcrops.

5. BUILDING THE 3D MODEL

5.1 BEDROCK DEPTH

Information collected by considering both active and passive seismic surveys converge in the indication of an alluvial basin characterised by maximum depths of the order of 500-600 meters from the surface. The topography of the seismic bedrock results well constrained by seismic reflection data but remains unknown in the most part of the basin.
In order to constrain the bedrock profile in the whole basin, the f0 values deduced from H/V measurements have been used. In fact, by following Ibs-von Seht and Wohlenberg (1999), one can suppose that a simple relationship exists between f_0 and the depth H of the bedrock in the form $H \approx a f_0^x$ where a and x are empirical parameters to be determined by the regression analysis of experimental data. The data set used for the determination of a and x values have been obtained by considering f_0 estimates obtained close to the seismic profile described in section 4.1. The data considered for this analysis are reported in table 5.1.1

Table 5.1.1- Resonance frequency estimates obtained at the sites located along the seismic section in figure 6.1.1.

fo [Hz]	1.66	0.59	0.59	0.41	0.38	0.44	0.47	0.47	0.63	0.51	0.3	0.34	0.45	0.45	0.5	0.5
H [m]	190	338	445	506	611	649	663	626	431	338	611	663	626	532	431	420

The regression analysis reveals that f_0 and H are well related (in terms of log-log linear relationship) with a value of the correlation coefficient equal to 0.87. This implies that the simple model here considered works well in the case under study.

The resulting value for *a* and *x* are respectively 280 and -0.78. By using these values one can convert in depths the f_0 values in table 1 by obtaining the bedrock thicknesses shown in figure 5.1.1. The good agreement between the measured and computed profile suggests that the empirical relationship could be safely used to constrain the bedrock profile along the whole basin from f_0 estimates. One should note that the empirical relationship here determined between f_0 and H is not compatible with the "standard" profile determined in section 3.2. However this result is expected since the Vs profile deduced in section 3.2.1 clearly indicate a different Vs pattern near the surface (H<100 m) and at depth. In addition, results obtained above also indicate that different Vs profile characterize different parts of the plain. These considerations imply that the relationship here considered between f_0 and H is a sort of "equivalent" of the more complex pattern in figure 3.2.5 and does not correspond to any realistic Vs profile.
The results obtained by using this approach are shown in figure 5.1.2.

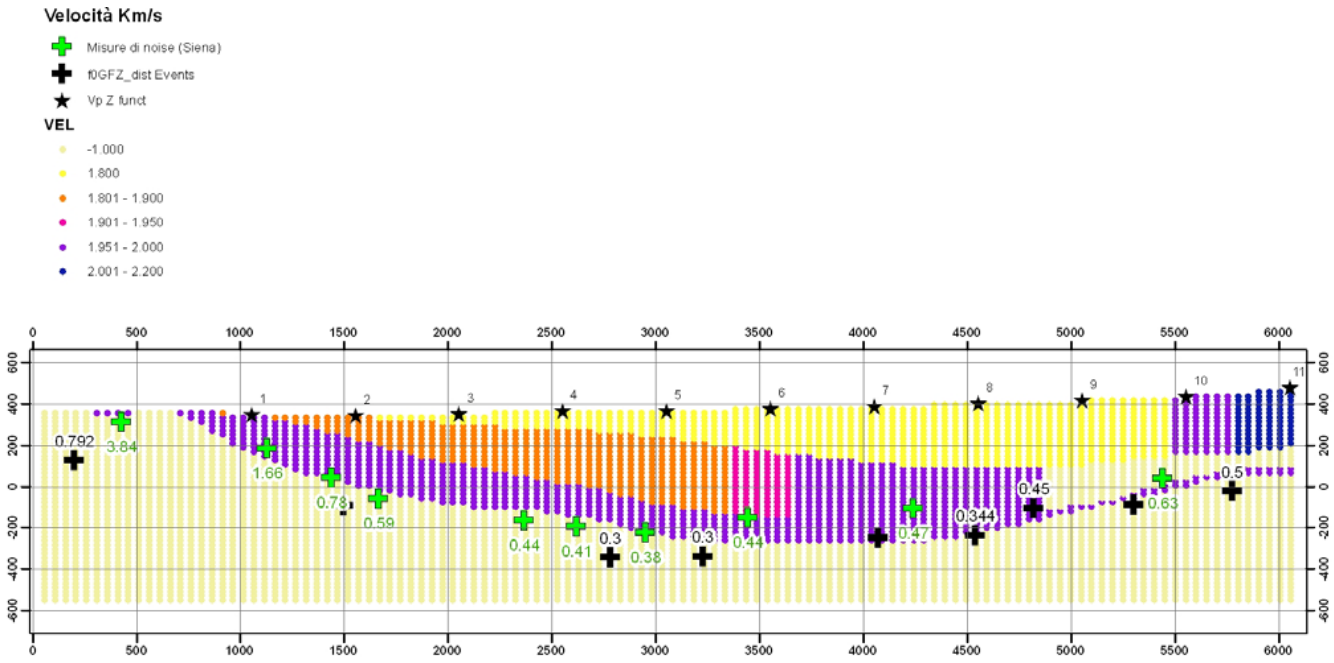

Figure 5.1.1- Depths of the seismic bedrock along the profile in figure 4.1. Stars indicate the position of sites where the resonance frequency f_0 has been measured. Crosses indicate the depth estimated for the seismic bedrock H obtained from the relevant f_0 values by using the relationship $H=280f_0^{-0.78}$

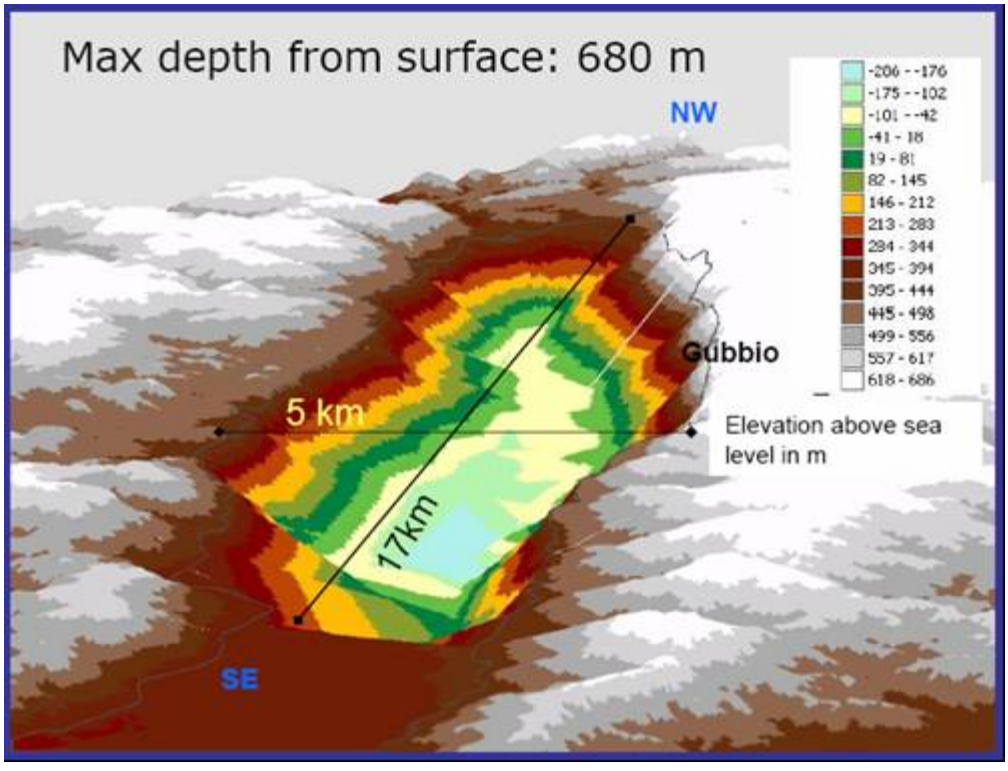

Figure 5.1.2 - Depths of the seismic bedrock (H) in the whole basin as reconstructed by interpolating the depths deduced from f_0 values by using the relationship $H=280f_0^{-0.78}$

5.2 GEOLOGICAL INTERPRETATION

The seismic section of figure 5.1.1 has been used by the geologists, together with detailed field data, to interpret the geometry and structure of the basin, firstly by defining which geological units correspond to the layers evidenced by the tomography model and then by extending this interpretation to other sections, parallel to the tomography transect, covering the whole basin .The superficial yellow zone of the seismic section (Vp = 1800m/s) is interpreted as formed by three different geological units, based on their outcrop in the field while the orange and violet layers (Vp from 1800 to 2000 m/s) are interpreted as a unique unit, since it was not possible to distinguish them on the ground. The dip of the geological units shown by the tomography (NE dipping strata in figure 4.4) was confirmed by some measures taken in the field on the stratified clay and sand. The resulting geological interpretation is shown in Figure 5.2.1, while figure 5.2.2 shows three cross sections of the interpolated model

The units identified are:
L1: breccias
L2: alluvial fan deposits
L3: fluvio-lacustrine deposits.
L4: stratified clay and sand.
The bedrock corresponds to the top of the Marnoso-arenacea (Interbedded marl and sandstone).

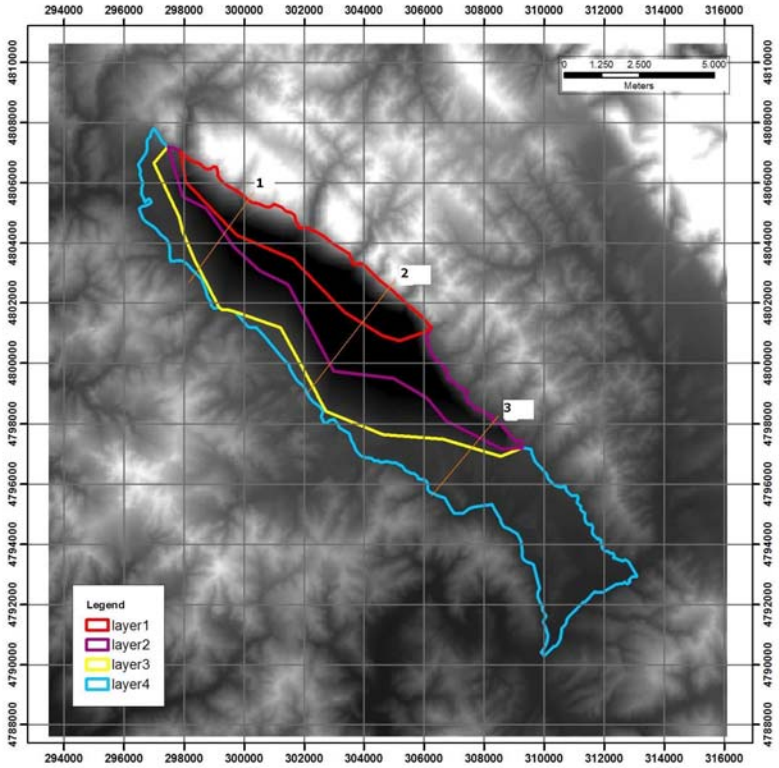

Figure 5.2.1 – Simplified geological interpretation of the Gubbio basin with the four units used in the model. Lines 1 to 3 are the trace of three cross sections of fig 6.2.2

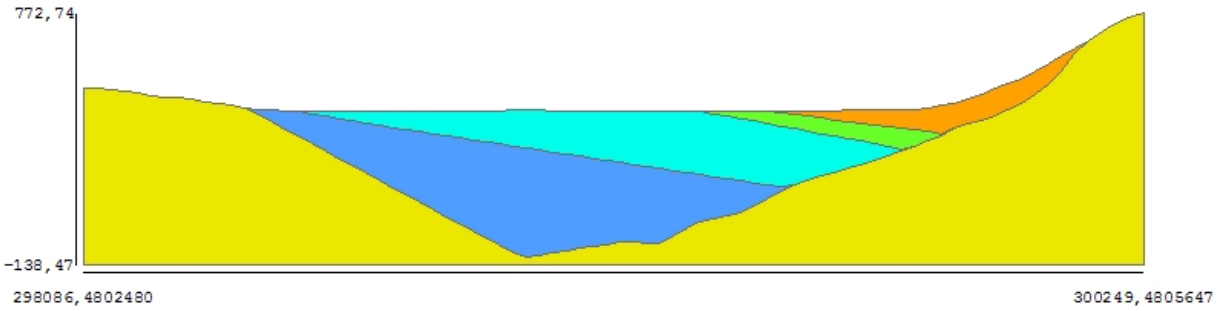

Section1 – Orientation SW_NE

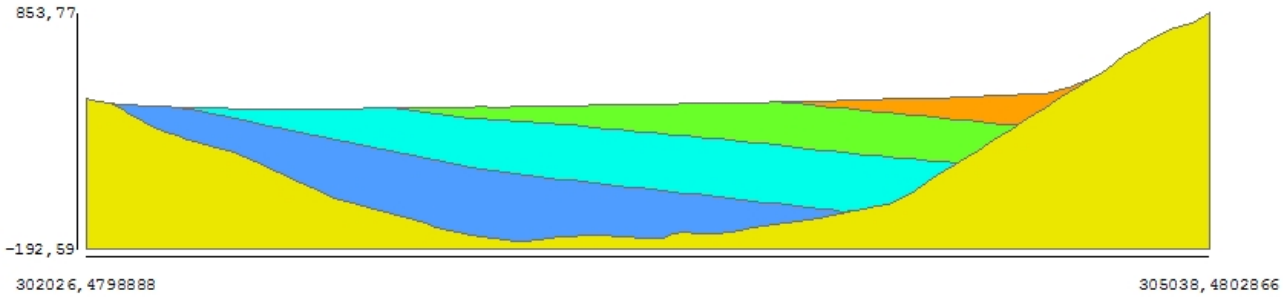

Section2 – Orientation SW_NE

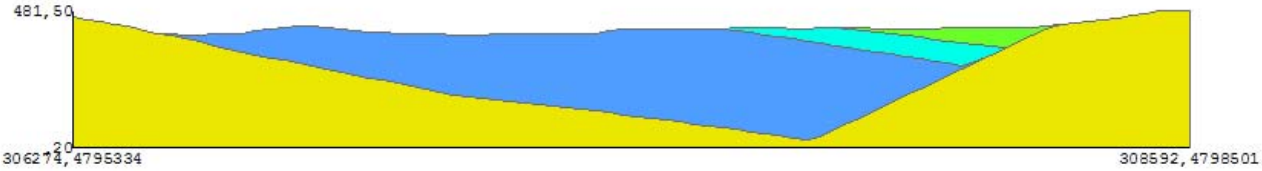

Section3 – Orientation SW_NE

Figure 5.2.2 – Cross sections 1 to 3 shown in figure 6.2.1 – Orange = L1 (Breccias), green = L2 (alluvial fan deposits), cyan = L3 (fluvio-lacustrine deposits), Blue = L4 (stratified clay and sands)

5.3 CHARACTERISATION OF THE GEOLOGICAL UNITS

The simple empirical relationship described in section 5.1, allows the estimate of the subsurface topography of the seismic bedrock from f_0 estimate provided by H/V seismic noise measurements. However, as stated in section 5.1, the parameters are not expected to correspond to a physically plausible Vs profile for the whole sedimentary cover. On the other hand, at least a rough estimate of Vs values for the main geological units present in the basin is necessary for the 3D modelling of seismic waves propagation within the basin. In order to provide this information, an hybrid approach has been attempted.
As first step, the bedrock topography provided from the interpretation of the f_0 values has been assumed as valid for the whole basin.
As a second step, a geological interpretation has been provided for the seismic section in figure 5.1.1. This interpretation has been performed by also taking into account geotechnical and geological data relative to the shallowest layers (section 2, 3 and 4) and the general interpretation of the basin evolutionary history. This resulted in the simplified geological section in figure 5.3.1.

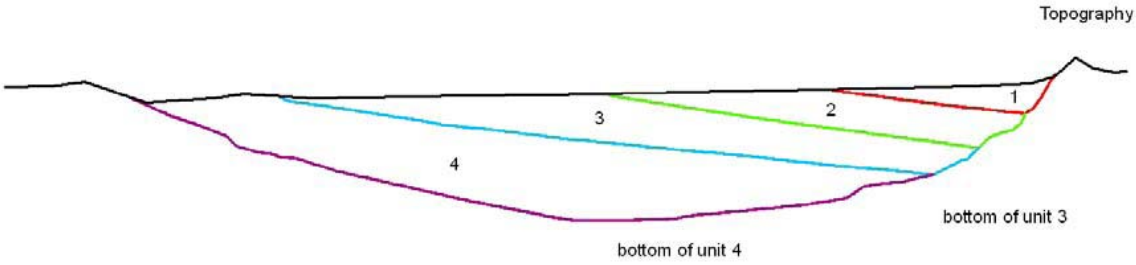

Figure 5.3.1 – General geological model of the Gubbio basin. The section is parallel to the GFZ transect (NNE-SSW). 1- breccias, 2- alluvial fan deposits), 3- fluvio-lacustrine deposits, 4- stratified clay and sands)

As a third step, uniform Vs velocity values have been attributed to each layer in figure 5.3.1. To this purpose the f_0 values have been considered as a constrain in the assumption that in correspondence of each measuring point (x) the following relationship holds at least as a first approximation

$$f_0(x) = \frac{1}{\sum_{i=1}^{4} \frac{h_i}{V_i}}$$

Here, the index i represents the corresponding geological unit (see caption of figure 5.3.1) that at the position x is characterised by a thickness h_i and a Vs value V_i. The values of h_i at each point (including the value 0 when the layer is lacking) are given by the geological section in figure 5.3.1 while the values of the relevant Vs velocities have been attributed by a trial and error procedure.
After this first order modelling, the tentative Vs values have been used to compute the complete transfer function in correspondence of the measuring points. The comparison with the experimental ones has allowed to better constraint the plausible Vs values.

The results of this analysis can be summarized as follows:

Units L1/L2 = 1100m/s
Unit L3 = 600m/s
Unit L4 = 900m/s

Actually, the comparison between H/V and the theoretical transfer function does not allow to constrain the Vs in the Units L1 and L2 since these layers influence the higher modes of the transfer function that are not present in the empirical one. If Vs in the unit L2 is set equal to 800m/s (more compatible with values deduced from direct and indirect measurements), the fundamental frequency is not altered.
In order to take into account results provided by direct Vs estimates (see section 2.1) it is possible to introduce a linear velocity gradient in the unit 3 by assuming that Vs = 300 m/s in the range 0-50m and 600 m/s below 50 m.
The mechanical characterization of the geological units have been completed by assuming for the respective P waves velocity values compatible with the ones provided by seismic reflection profiles (section 4.4). The density values are assigned on the base of the collected geothecnical data and quality factor are assumed from literature.

The resulting model is reported in the table 5.3.1

Table 5.3.1 – Geothecnical Parameters of the Gubbio Basin

Layer	Vp [m/s]	Vs [m/s]	γ [g/cm^3]	Qp	Qs
L1 (Breccias)	1900	1100	1.9	100	50
L2 (Alluvial fan)	1800	800	1.85	100	50
L3 (Fluvio_lacustrine)	600	300/600 (gradient)	1.95	100	50
L4 (clay & sand)	2000	900	2.0	100	50
Bedrock	3500	1800	2.3	200	100

5.4 GIS MODELLING

The geological and seismic data described in the previous paragraphs were input into a Geographic Information System, Arc Map 9, to build a model of the sub-surface geology of the Gubbio basin. Each unit recognised during the geological interpretation has been modelled as a raster surface layer, that is a grid of cells in which the cell values represents the elevation above sea level of the bottom of the unit considered. The topmost surface is the Digital Elevation Model, corresponding to the topography, or 'bottom' of the air layer. Below it there is layer1 (bottom of breccias), layer2 (bottom of alluvial fan deposits), layer3 (bottom of fluvio-lacustrine deposits) and layer4 (bottom of stratified clay and sands), also corresponding to the top of bedrock.
The surfaces were produced in three main steps, the data input, the surface interpolation and the surface processing.

Data input
In the first step all data needed for the interpolation were input in the GIS, converted in a suitable format and referenced to a common map system. The map projection used in the work was the Universal Transverse Mercator, zone 33N, with the European datum 1950 (called in the following ED50_UTM33). For each geological unit a file of points referenced to this system was created, storing in the attribute table the height of the surface in that location.
The file of noise measurements was used to calculate the bedrock depth by assigning to each point the elevation from a Digital Elevation Model and subtracting from it the thickness of deposits, previously calculated from the fundamental frequencies. For the other units the geological cross sections were scanned and digitised using a local reference system with X = distance (from the starting point of the section) and Z = elevation above sea level. The digitised lines were converted to points and two fields added to the attribute table, one storing the distance from the origin of the section and one storing the quote of the point. The attribute table was then used to create a new point file in map view using X = constant and Y = distance, passing in this way from a vertical, XZ reference system to an horizontal XY system. One file for each section was created and all files were then georeferenced to a common XY system, i.e. ED50_UTM33.
In the final step one point file for each geological unit was created by extracting the corresponding points from each section file and importing them in a geodatabase.

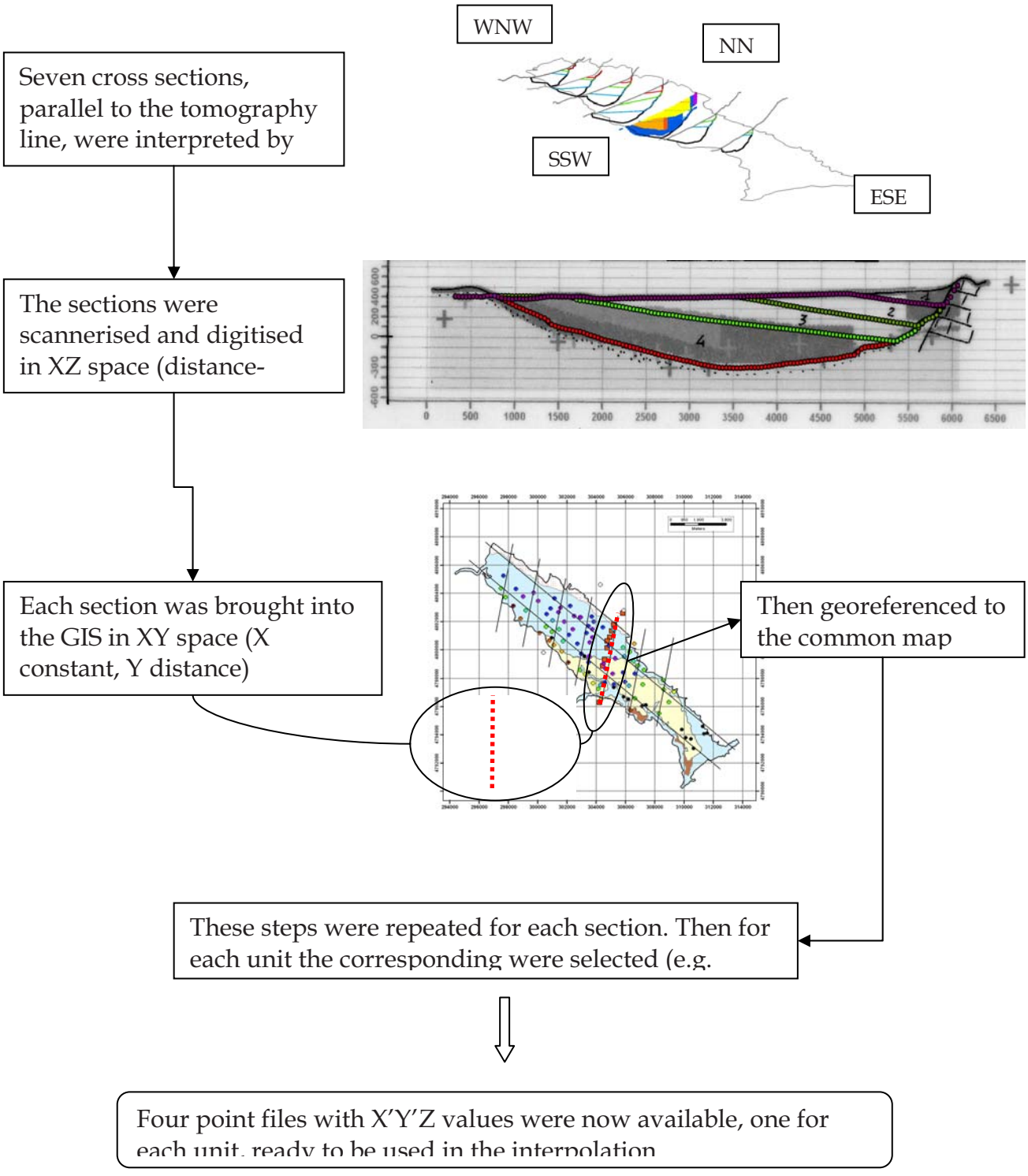

Figure 5.4.1 – Flowchart of the data input procedure for the 3D modelling

Surface interpolation

To create the final surfaces a Triangular Irregular Network (TIN) was produced first and then converted to a raster with 40 meters resolution. Triangulation was preferred over other interpolation methods as the data were not regularly spaced and distributed over the whole area but concentrated along the section lines. Also the triangulation method allows to handle different type and density of data in the interpolation.
On top of the points storing the elevation of the various surfaces other two files were used, the outcrop line and the depocentre line.
These were used as 'hard lines', which is lines across which the triangulation is not permitted. In this way the outcrop lines set the extent of the subsurface layers while the depocentre lines avoided the triangulation of points on opposite side of the valley, thus preserving the geometry of the basin. For the layer4 (bottom of clay and sand/top of bedrock) the points of bedrock depth from noise measurements were also used in the triangulation.

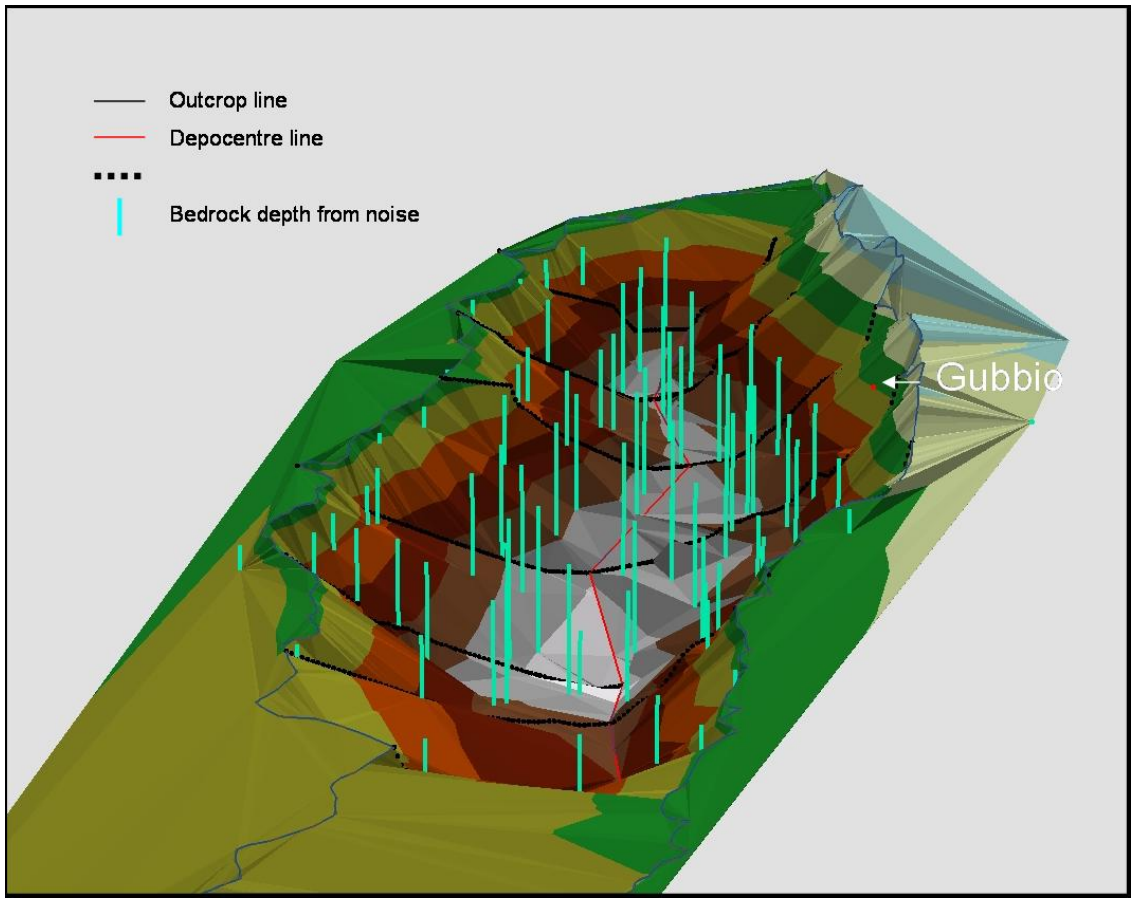

Figure 5.4.2 – The TIN model for the bedrock layer with the data used in the interpolation: bedrock depth form noise measurements, bedrock depth from geological sections, depocentre line, outcrop line.

Surface processing

All surfaces which were to be used for the 3D modelling of the seismic waves (see section 6.3.3) needed to have the same extent and be perfectly coincident where the different layers were overlapping. For example the bottom of layers 1, 2, and 3 were to be coincident with that of layer 4 where these three deposits hit the bedrock (see fig 5.4.1 above). The processing was done with 'Map Algebra', which allows to use logical statements and mathematical operators to perform calculations on multiple raster and store the results in a new one.
It was decided that the raster layers should have an extent larger than the limits of the basin by 2 km, so the DEM was cut to the proper size and its extent used in all the following processing. Each TIN layer was converted to raster using as mask a polygon created from the outcrop line of the layer and with extent equal to the DEM cut to size. The resulting rasters had all the same extent, with value equal to 'No Data' outside of the outcrop line and with the interpolated surface values within it. A conditional statement was then used to assign the DEM values to all 'No Data' cell by using 'CON (ISNULL ([GRID4]), [DEM], [GRID4]), which translates as 'if the value of GRID4 is null, then assign to it the value of the DEM in that point, otherwise assign the value of GRID4. Other statements of this kind where used to correct the surfaces as needed, obtaining in the end the 4 layers which were used in the 3D modelling, and the thickness of each geological unit to be used in the 1D models (see section 6.2).

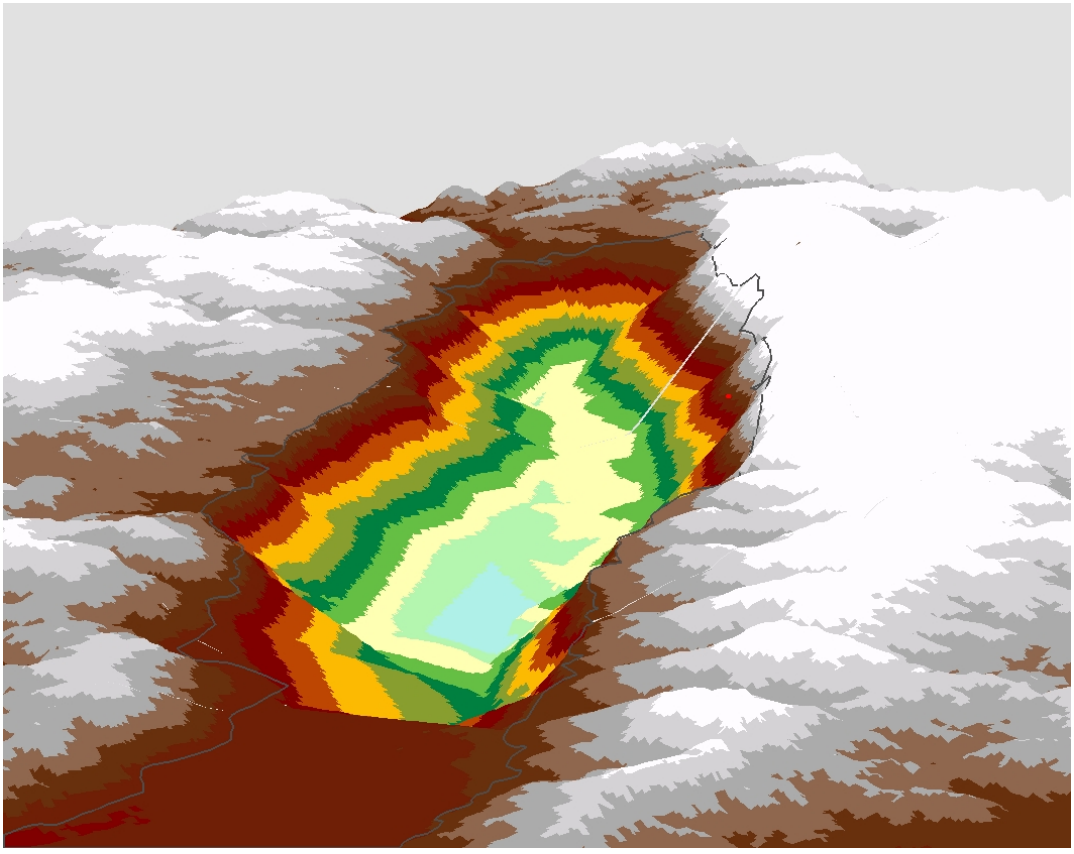

Figure 5.4.3 – The final raster surface of the top of bedrock.

6. RESULTS

6.1 ENGINEERING GEOLOGICAL MODEL UP TO 30M

The engineering geological sections defined in chapter 2 were used for 1D seismic response analysis through the ProShake software, with the aim of defining the shear strain induced in the ground within the first 50 m b.g.l.. The seismic input is the one already used for the 3D analysis done within the project by the other UURR, by considering the wave forms given by the two stations closest to the considered sites (GBP for S1 and S3 and EU04 for S2). Assessment of earthquake-induced shear strain on the three considered soil columns were performed for each site by considering three different PGA values (0.05, 0.15, 025g) according to the national seismic codes, and assuming the soils degradation curves from three distinct formulations (Vucetic & Dobry 1991), hereinafter labelled as VD; Ishibashi & Zhang 1993, IZ; Zhang 2005, ZH) as for the silty-clayey units, while for the gravelly and sandy units, use was made of curves proposed in the literature for similar lithologies. The decision of using different degradation curves was taken to assess the influence of the different parameters that are considered by the 3 formulation:

- plasticity interval (domain) in VD (1991);
- plasticity domain and confining pressure in IZ (1993);
- plasticity domain, confining pressure and deposit age in ZH (2005).

Here in after are presented the Gmax –γ curves for the three different approaches in relation to the three analysed columns (labelled S1, S2 and S3) which stress the stiffness of the single soil layers and the stiffness profile of each column as a whole versus depth. As for site S1 (fig. 6.1.1) is well evident the stiffness contrast among the three superficial layers and the bottom forth, typical of a soil profile with marked contrasting bedrock; in addition, is significant the stiffness inversion between the first and the second layer, once the linearity threshold has been trespassed, even though only in VD and ZH hypotheses it is clear. In sites S2 (fig.6.1.2) and S3 (fig. 6.1.3), on the contrary, it is not present a marked stiffness contrast at depth, especially for S3 where the gravels are abundant. In S2 there is a clear stiffness inversion between the third and second layer of the soil column in all of the adopted approaches, even if for IZ and VD it is less significant, while in S3 the inversion is between the first and the third stratum (gravel) showing the same stiffness of the second one (silty clay). All these findings show the lack of a linear incf rease of the stiffness along depth in all the three investigated columns.

In general, it can be deduced that using different approaches the main influence in defining the soil stiffness and its trend along each soil column is represented by the plasticity interval. This is well evident by observing fig. 6.1.1 for the case VD and IZ which show similar trends, notwithstanding in the ZH hypothesis also the confining pressure and the deposit age are considered.

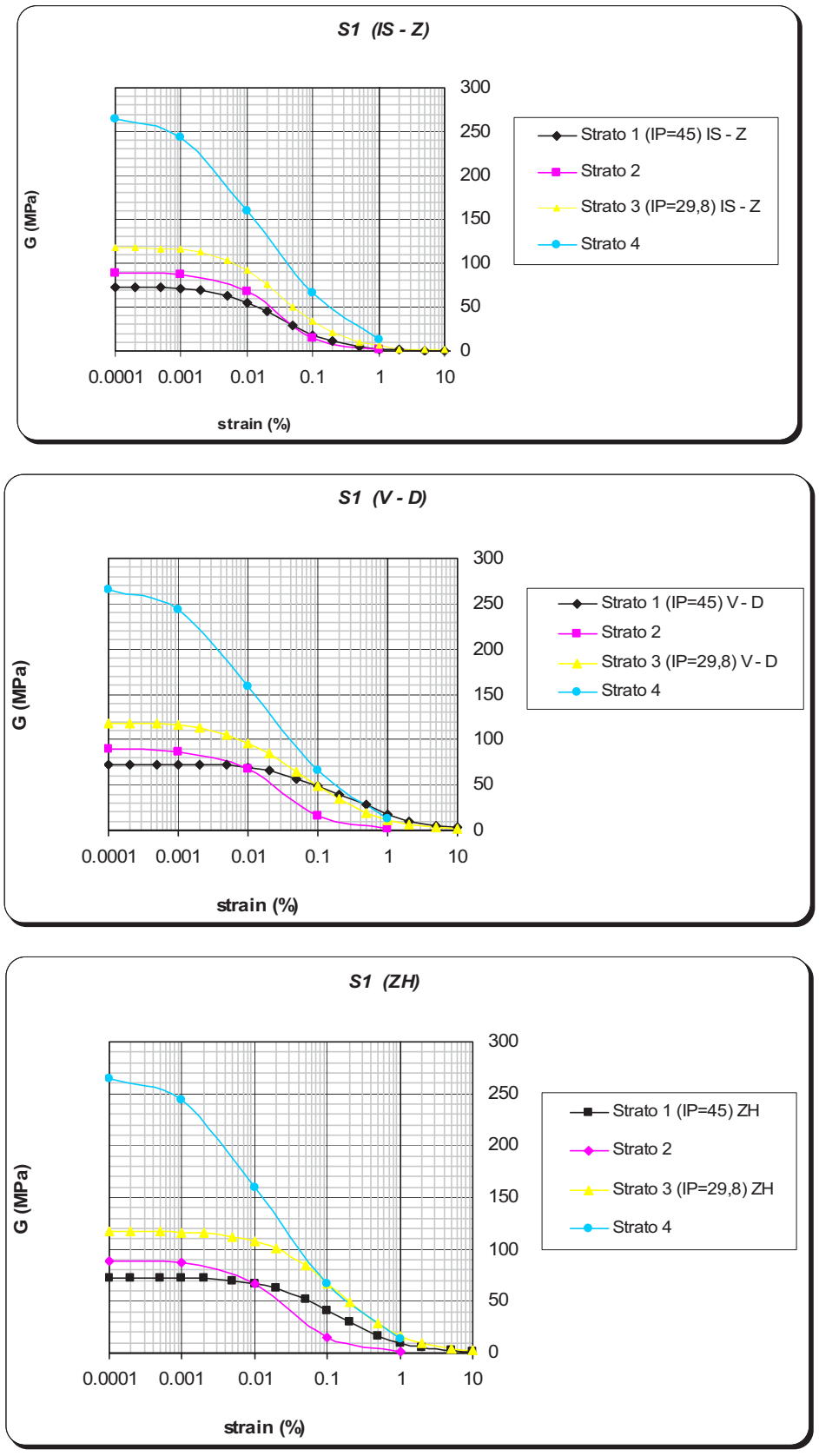

Fig. 6.1.1 –Gmax- γ diagram for S1 site (Cabina Enel Gubbio Piana).

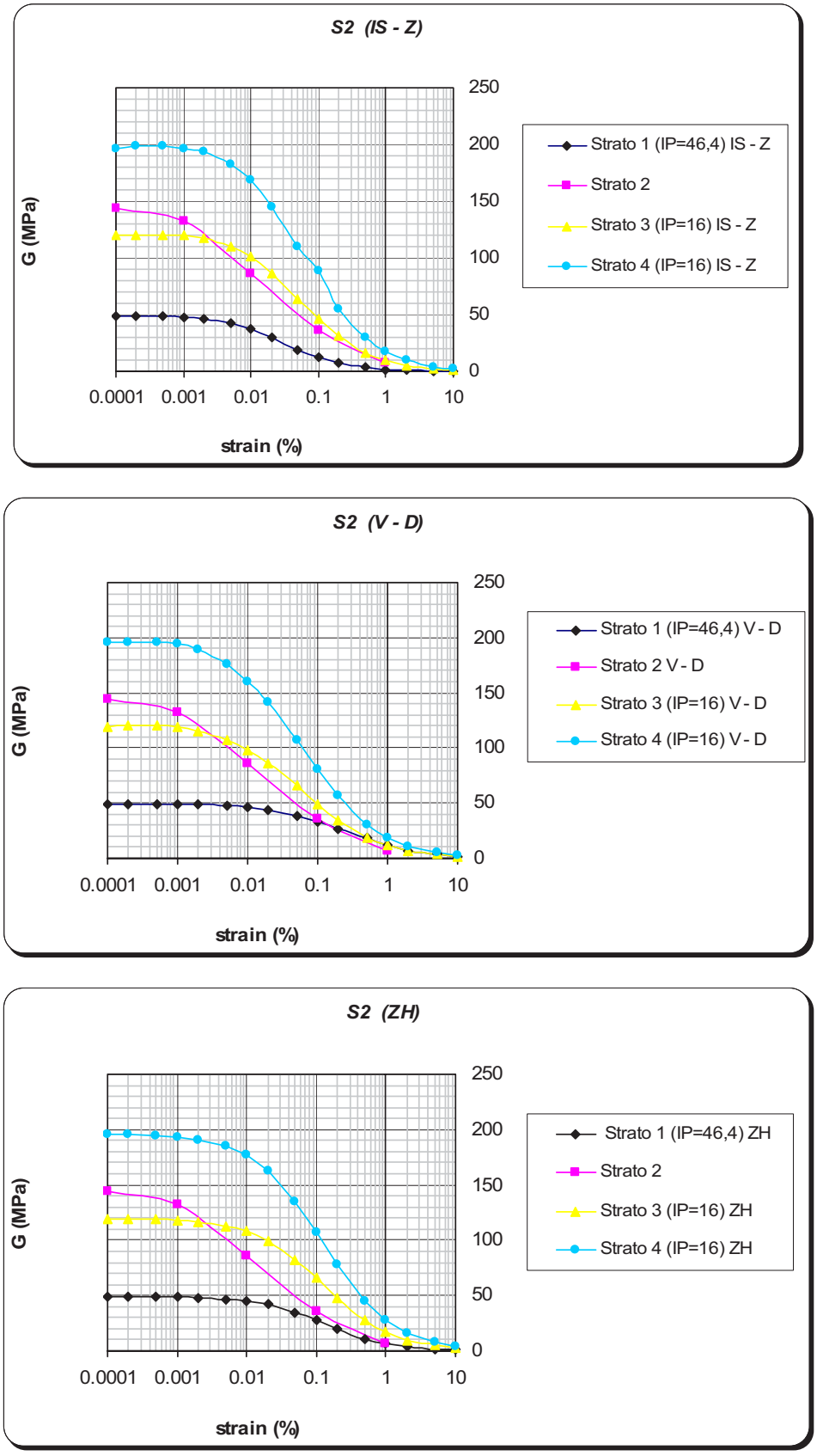

Fig. 6.1.2 – Gmax-γ diagram for S2 site (Vivaio La Torraccia).

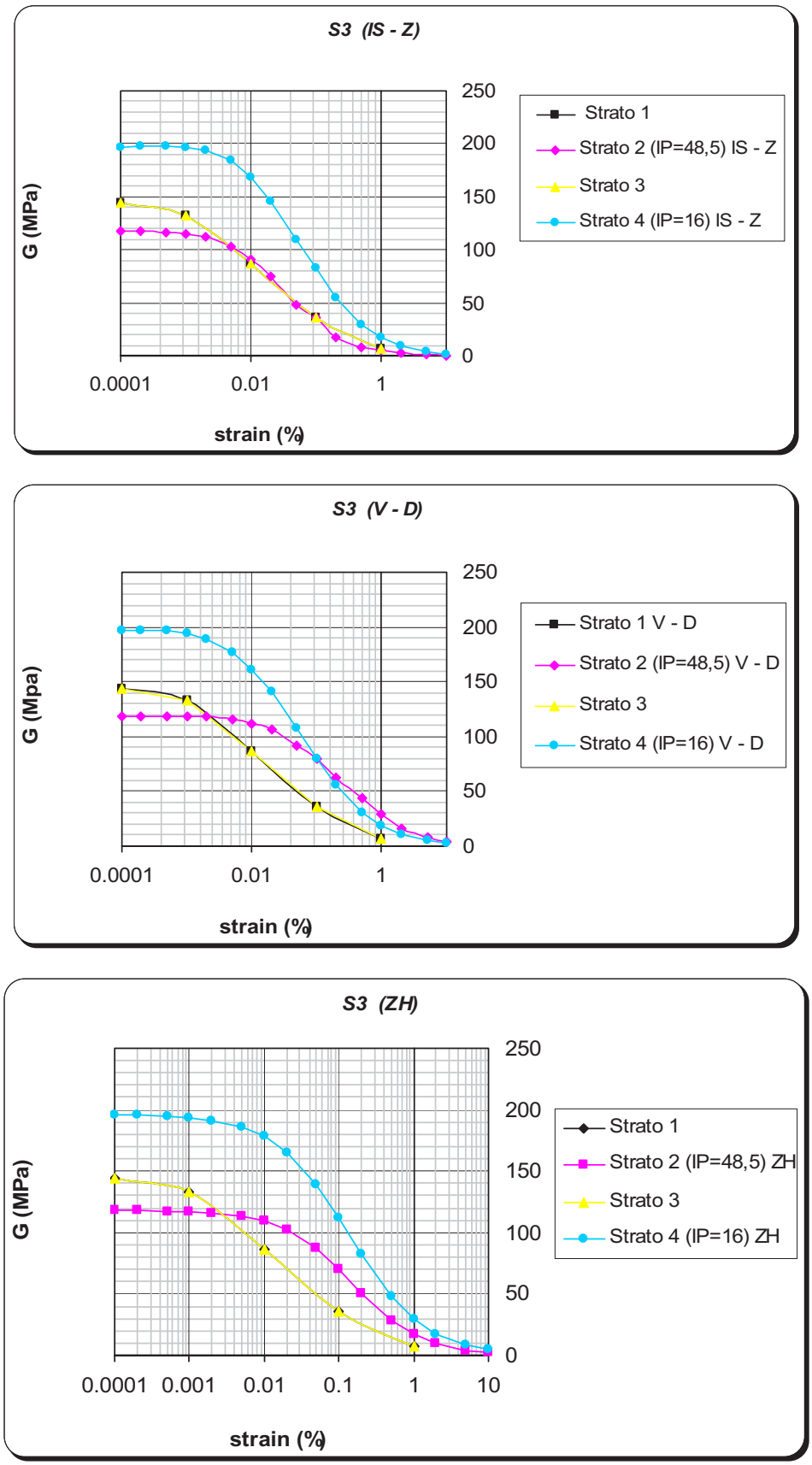

Fig. 6.1.3 – Gmax-γ diagram for S3 site (Gubbio Vittorina).

The trend of the earthquake induced shear strains in site S1 (fig. 6.1.4a, b and c) shows a peak at about 15 b.g.l., increasing with higher assumed PGA values. However, significant differences can be observed along the soil column as a function of the selected degradation curves. In particular, by considering those ones by VD and Z instead of that one by IZ for PGA values equal to 0.15 and 0.25 (fig. 6.1.4b, c) it can be observed a sharp decrease of the shear strain magnitude at depths between 28 and 40m b.g.l., differently from what recorded between 10 and 20 m. In fig. 6.1.4 c it has been considered the shear strain in comparison with previously assumed conditions of linearity along the soil column; it can be inferred the sharp difference involved in the change of behaviour form linear to the non-linear domain. This especially occurs in the first 20m and it can be explained by considering the typical stiffness profile of a soil column (fig. 6.1.1) showing a highly contrasting bedrock at the soil bottom which produces the greatest shear strains in the top layers. The shear strain gradients (fig. 6.1.5) are particularly high in the first 20m in agreement with the connected shear strain profiles, with a significant variation in the trend when considering the VD curves

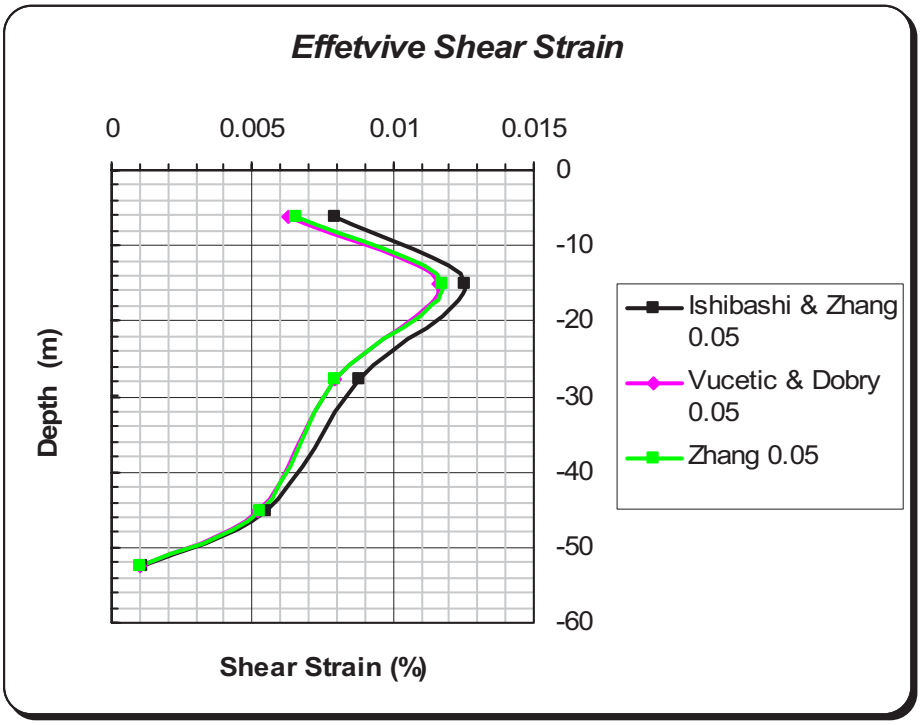

a)

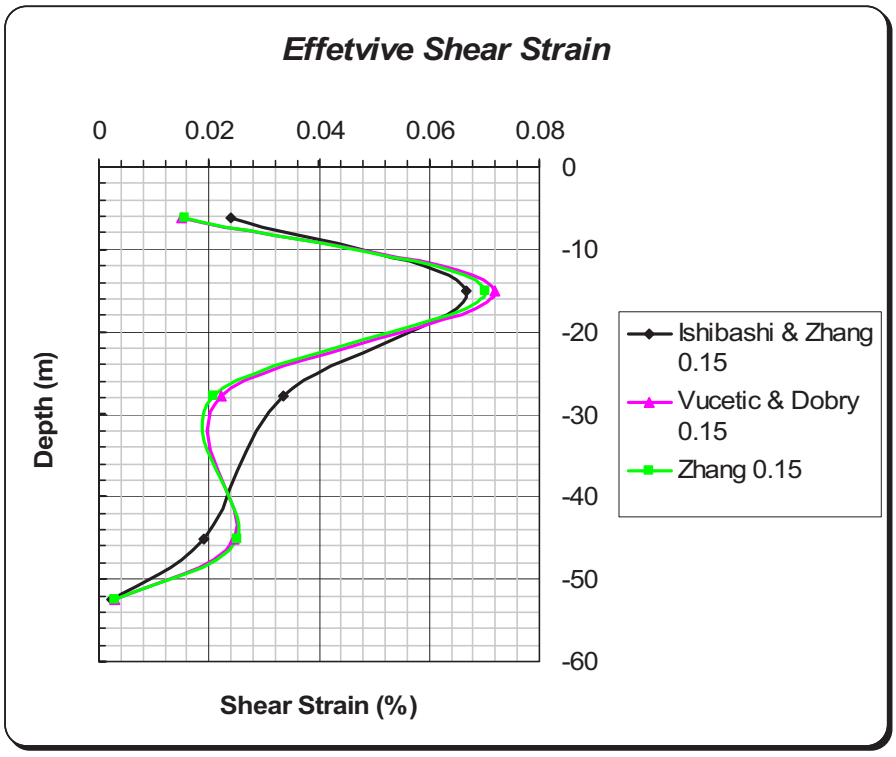

b)

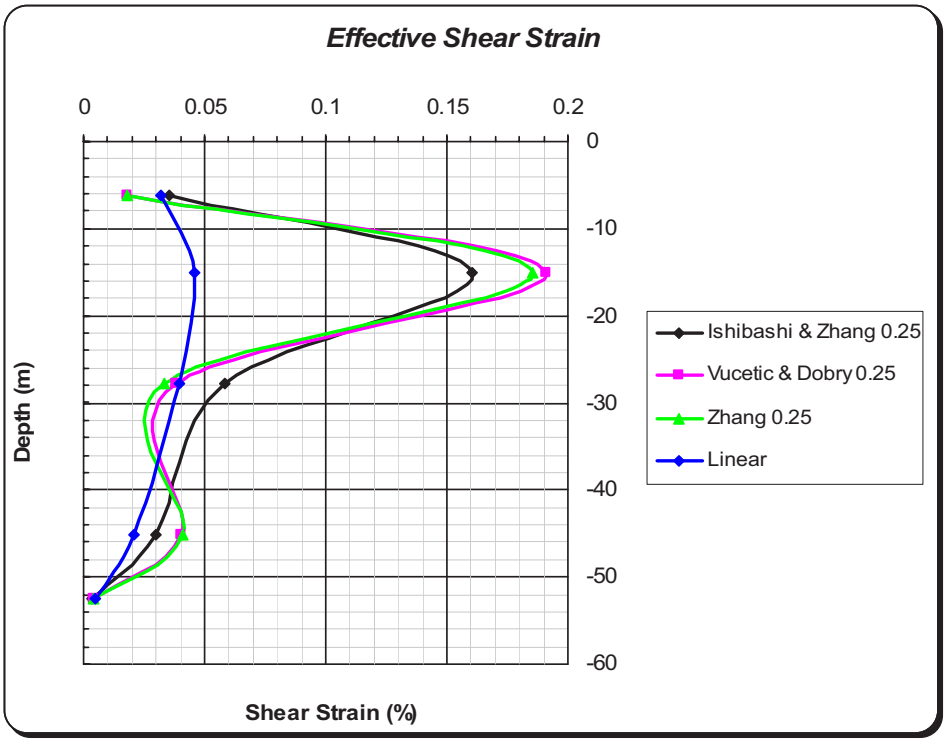

c)

Fig. 6.1.4 – Shear strain vs depth for site S1 for three PGA level 0.05 a), 0.15 b), 0.25 c).

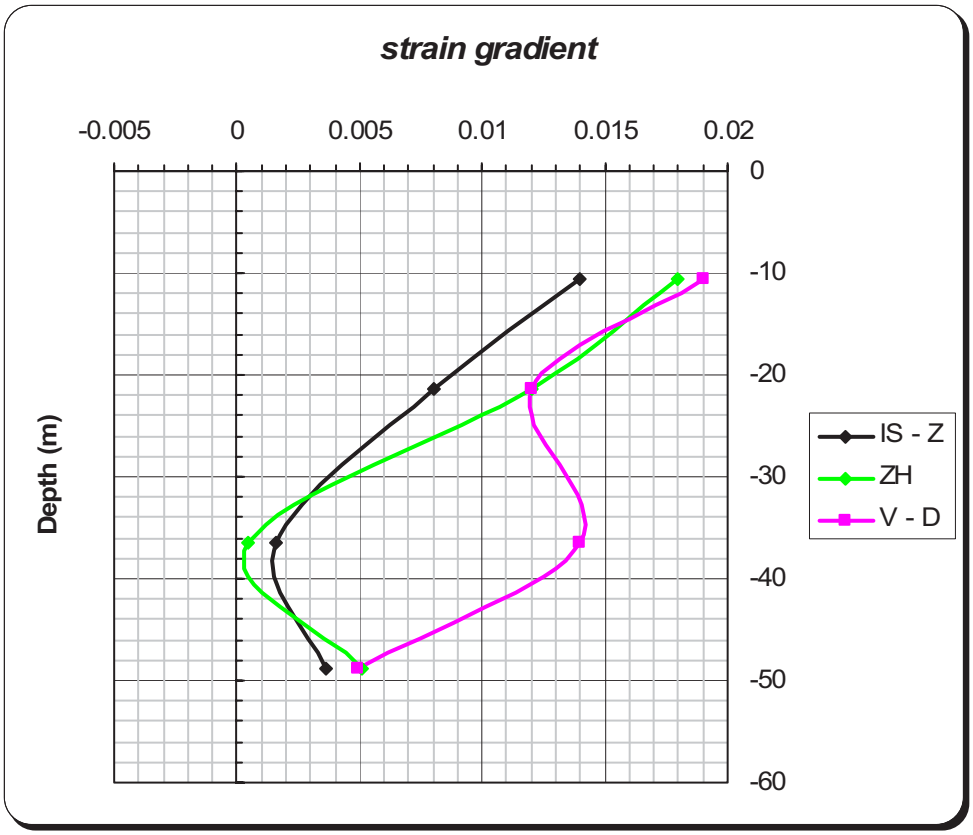

Fig. 6.1.5 – Strain gradient for site S1 (PGA 0.25).

In site S2 (fig. 6.1.6 a, b and c) the shear strain profiles are more homogeneous for all the three PGA assumed values and without significant influences due to the considered degradation curve. In addition, in this case the influence of non-linear behaviour has a minor influence on the induced shear strain profiles (fig. 6.1.6c). This is consistent with the absence of marked stiffness contrast with depth because of the lack of a bedrock constraining the soil column and, as a consequence, with a uniform strain of the soil column itself.

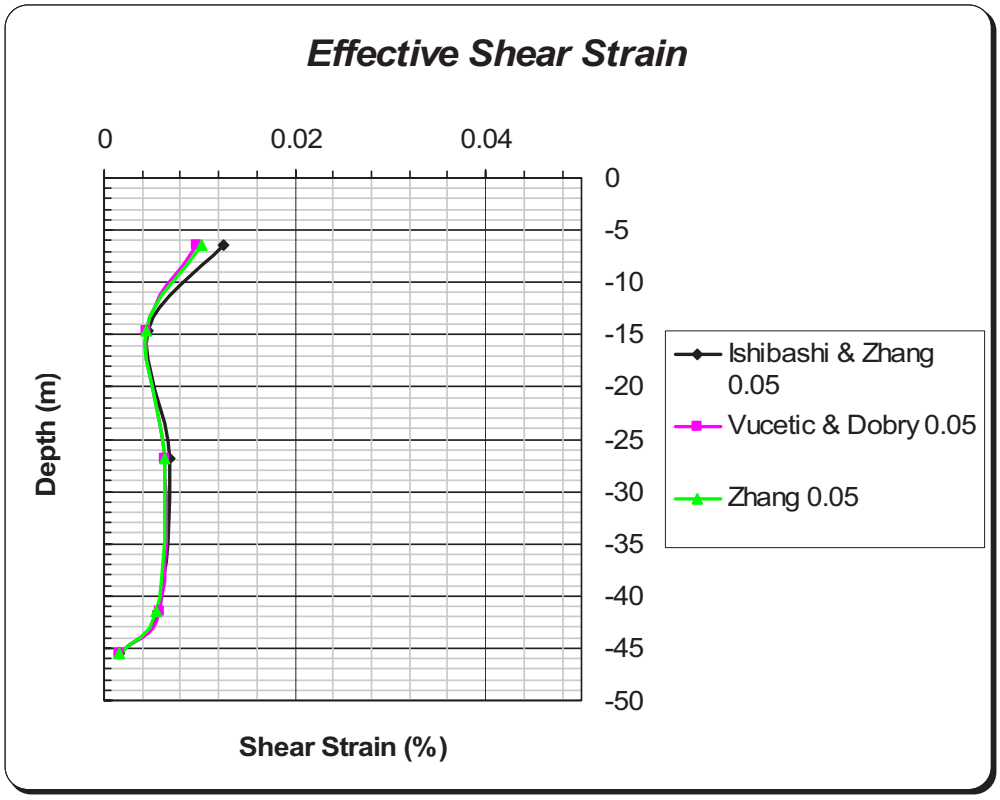
Effective Shear Strain
0
0.02
0.04
0
-5
-10
-15
-20
-25
-30
-35
-40
-45
-50
Depth (m)
Shear Strain (%)
Ishibashi & Zhang 0.05
Vucetic & Dobry 0.05
Zhang 0.05

a)

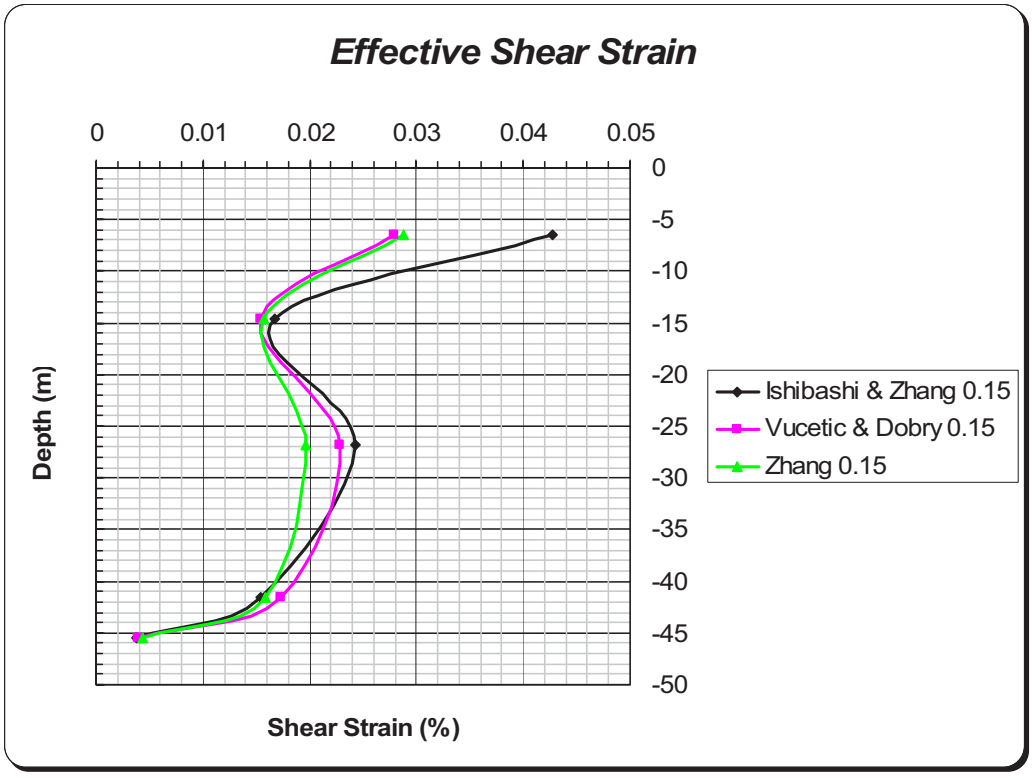
Effective Shear Strain
0
0.01
0.02
0.03
0.04
0.05
0
-5
-10
-15
-20
-25
-30
-35
-40
-45
-50
Depth (m)
Shear Strain (%)
Ishibashi & Zhang 0.15
Vucetic & Dobry 0.15
Zhang 0.15

b)

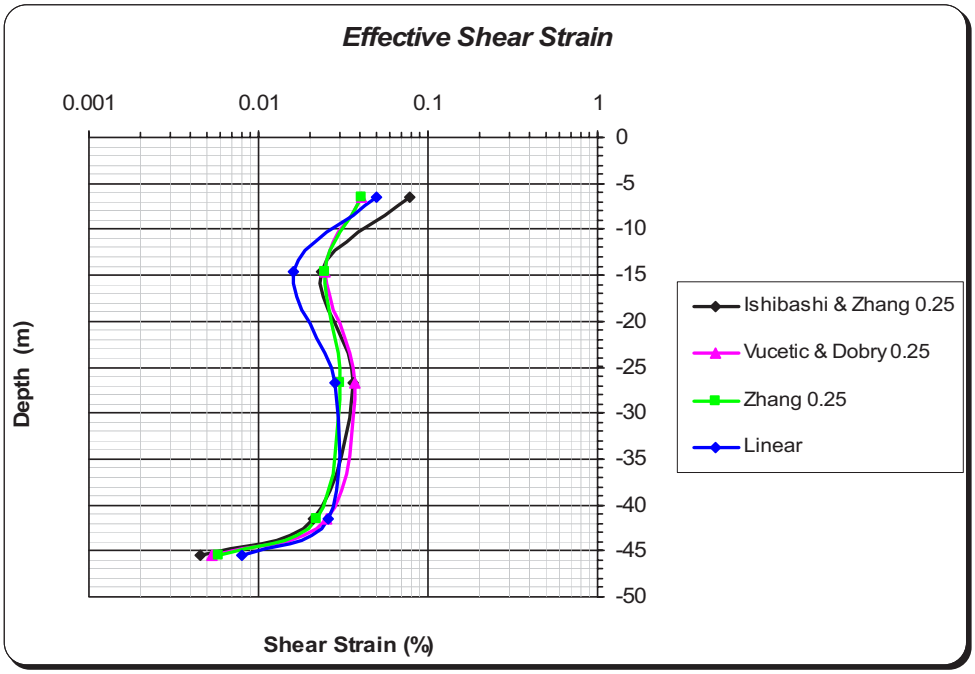

c)

Fig. 6.1.6 – Shear strain vs depth for site S2 for three PGA level 0.05 a), 0.15 b), 0.25 c).

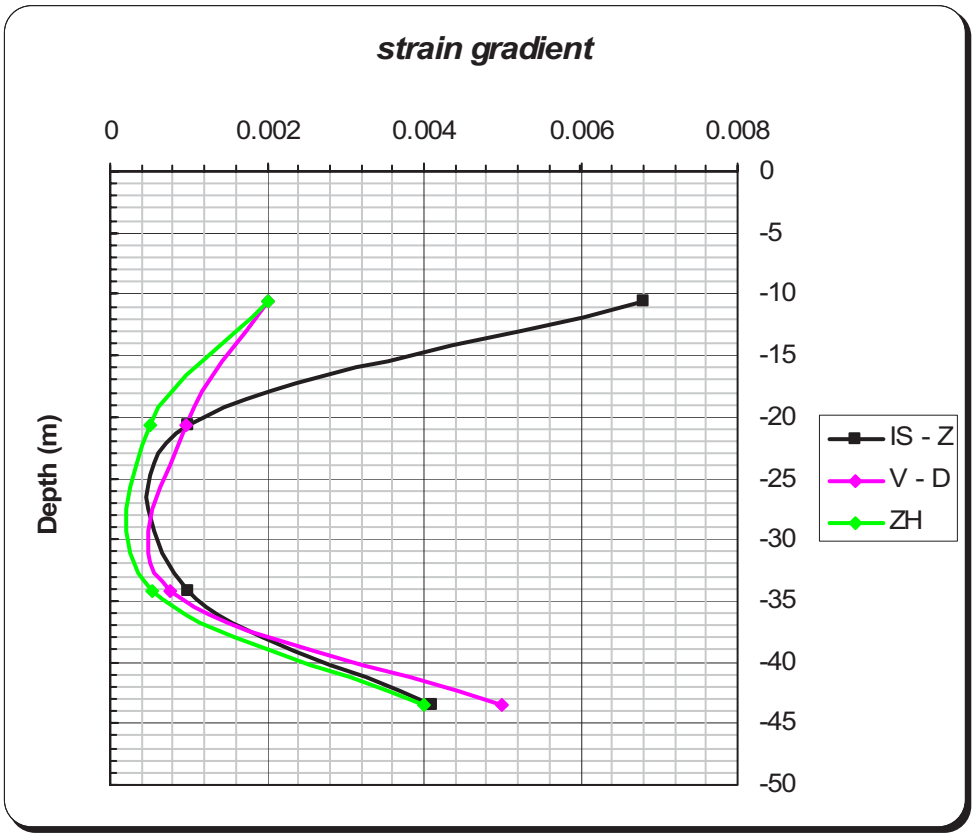

Fig. 6.1.7– Strain gradient for site S2 (PGA 0.25).

In site 3 the results of the simulations (fig. 6.1.8 a, b and c) show a shear strain trend similar to the one of site S1, with a peak at about 25m in coincidence with the second gravel bed. The effect induced by the non-linear behaviour appear well observable especially when considering the degradation curves by IZ.

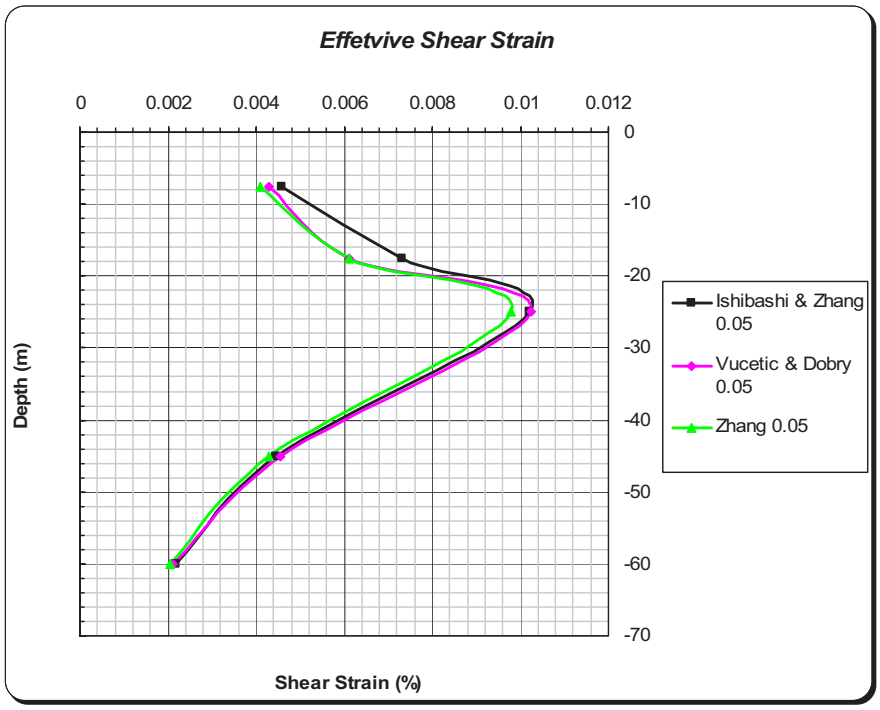

a)

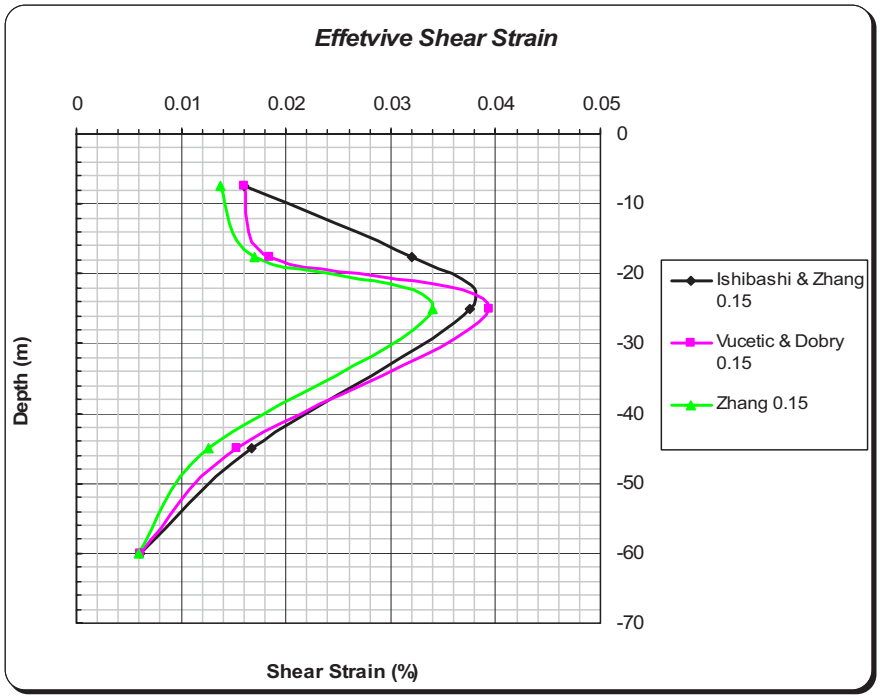

b)

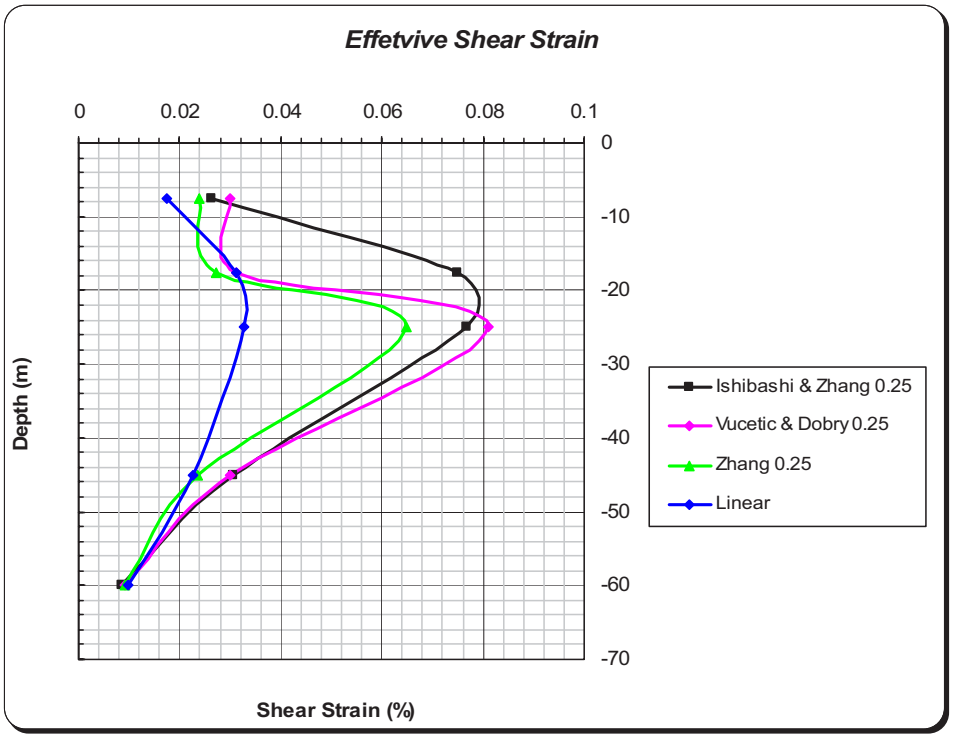

c)

Fig. 6.1.8 – Shear strain vs depth for site S3 for three PGA level 0.05 a), 0.15 b), 0.25 c).

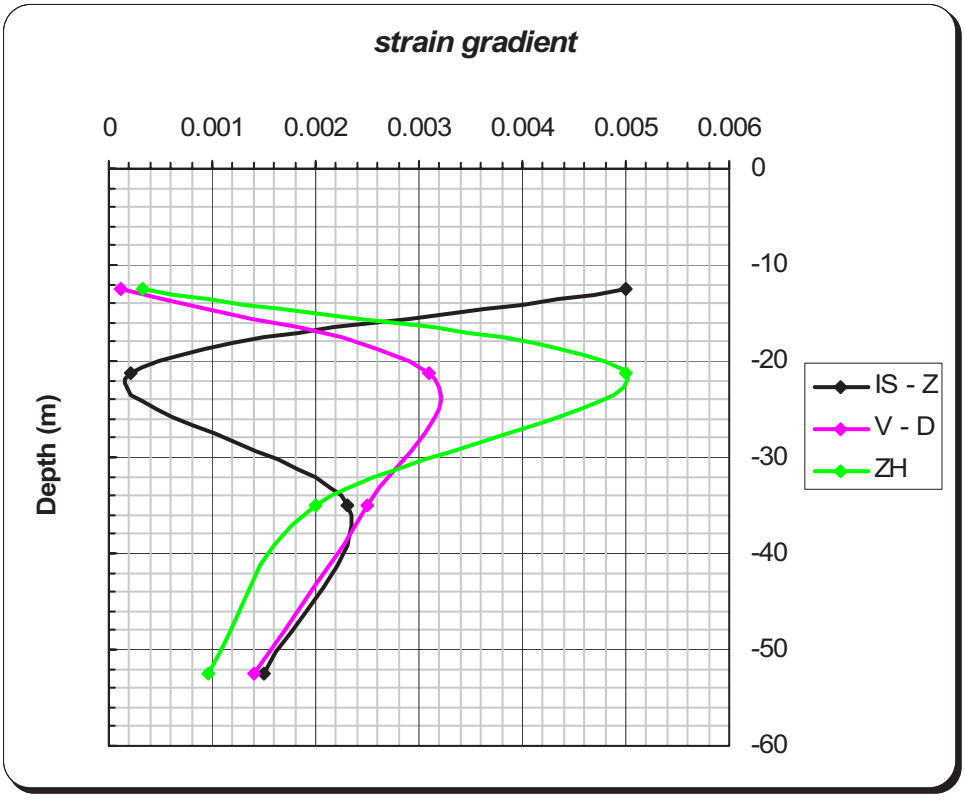

Fig. 6.1.9 – Strain gradient for site S3 (PGA 0.25).

The obtained amplification functions in all the three sites for PGA 0.25, by considering the three degradation curves proposed by VD, Z and IZ, show a good agreement in terms of resonance frequencies, close to 1 Hz (fig. 6.1.10), with the results obtained through the geophysical measurements performed .

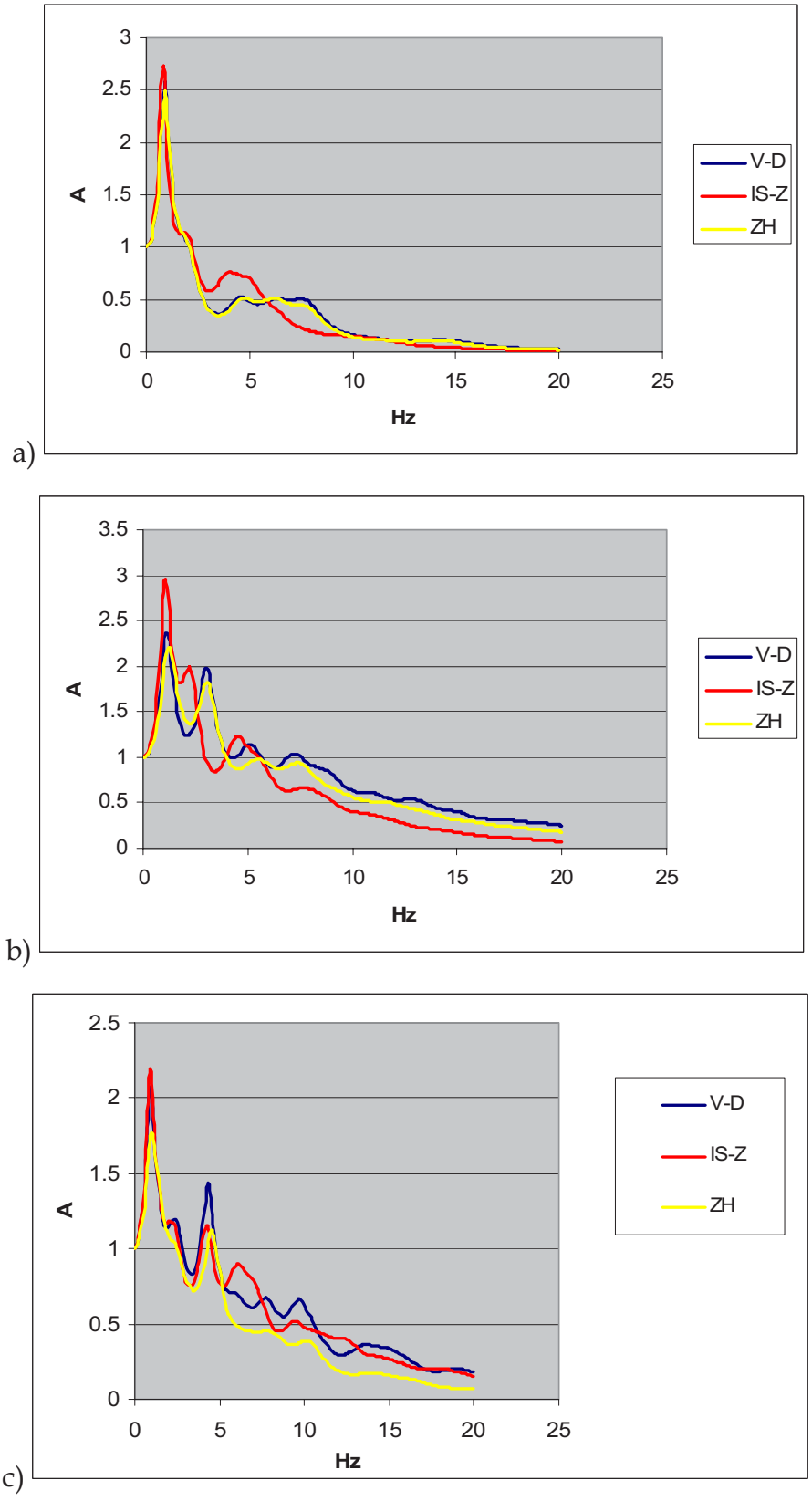

Fig. 6.1.10 – Amplification function for 0,25 PGA for the three studied sites: S1 a), S2 b) e S3 c).

As regards possible permanent site effects an assessment of liquefaction potential was performed for site S1. In fact, in this soil column is present a layer of silty sand, below groundwater level, 5.5 m thick below 12.3 m b.l.g. which could be susceptible of liquefaction.
For this assessment Seed and Idriss (1971) method was used which relates "maximum shear stress" induced from earthquake ($\tau = 0.65\ \gamma_n\ h\ a_{max}\ r_d$) and "cyclic shear resistance" of soil $(\tau/\sigma'_0)_{DR} = (\sigma_{dc}/2\sigma_0)_{50}\ c_r\ Dr\% / 50$), along all the studied column.
From the obtained data, it was realized the diagram of fig. 6.1.11 from which it is possible to note that maximum shear stress (black line) is always less than cyclic shear resistance (red line); for this reason the sandy layer would not undergo liquefaction also for the maximum expected PGA of 0.25g.

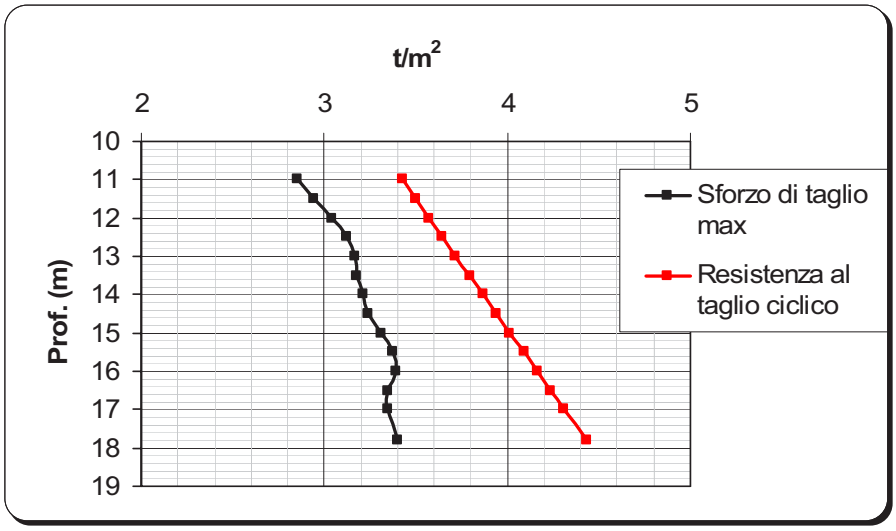

Fig. 6.1.11 – Assessment of liquefaction potential for the sandy layer in site S1.

In conclusion, on the basis of the engineering geological model of the Gubbio basin and the related boundaries of the lithotecnical units, as well as the 1D numerical simulations, a zonation of the Gubbio plain area has been proposed. Three main zones have been introduced in relation to the strain behaviour of the first 50 m soil depth. For the three different zones, the earthquake induced shear strain correspond to the ones simulated for the soil columns adopted as representative for each zone.
Zone A (characterized by gravels with clayey layers) even though showing a bedrock 300 m deep, has a shear strain behaviour consistent with a basal bedrock. This zone is located on the north-eastern border of the plain.
Zone B (silty-sandy layers resting on a gravelly bedrock), shows a marked stiffness contrast which determines significant shear strains in the upper 20 m. This zone is located in the centre of the plain (Cipolleto borough).
Zone C (characterized by a bedrock 100m deep overlain by silty clay) shows a shear strain trend along the soil column which can be considered homogeneous without strain peak. This zone is located in the SW border of the plain with the exception of the Ponte d'Assi area, where the marly-arenaceous bedrock is close to the groundsurface.
The zonation map in reported in ANNEX A.

6.2 1D MODELLING

The 3D geological model was used to extract 1D profiles of Vs and geotechnical characteristics in correspondence of the velocimetric stations of the GFZ, Genoa and INGV transects (Deliverable D22-23). We then used these profiles to simulate one-dimensional response site with the Haskell Thompson method (HASKELL, 1953; THOMSON, 1950)
The 3D model proposed in this study is a model of a more complex real world, obtained through interpretation and interpolation of a wide set of data. The characteristics of the final model are shown in table 6.3.1 (see figure 6.4.1 for the geological structure).

To verify the quality of it we compared the theoretical fundamental frequency *fo*, estimated from 1D transfer function with the experimental horizontal to vertical spectral ratio H/V obtained from the earthquakes recorded at the transects (a description of the methodology followed to calculate the H/V is given in D22, section 3.2).

Figure 6.2.1 shows the position of the velocimetric stations along the transects and highlights four sites, located in characteristic points of the basin, for which the 1D profiles and the comparison between 1D model and H/V curves are shown in figure 6.2.2.

- Station 'STAA' is on the northern edge of the basin, in an area characterised by a small thickness of deposits (38 m) and by the presence of the only high velocity layer L1;
- Station 'GU07' is at the centre of the basin, where the thickness of deposits is about 660 m; Station 'EU08' is at the centre on the NW end of the valley, with bedrock depth at about 470m;
- Station 'STAD' is on the southern edge of the basin, where the deposits are getting thinner (around 350 m here).

It can be seen that there is a quite good agreement between the modelled and the experimental resonance frequency *fo* (obtained respectively from the 1D model and the H/V curves) for all stations shown here.
Generally a very good match between the *fo* is found in stations located at the centre of the basin, while some problem can occur for the stations located on the edges.
This is not very evident for the stations located on the high velocity layer since here the 1D response is nearly flat (see STAA), while the mismatch is at times more evident for the stations on the southern edge of the basin, which are on soft layers of deposits and show a larger amplification.

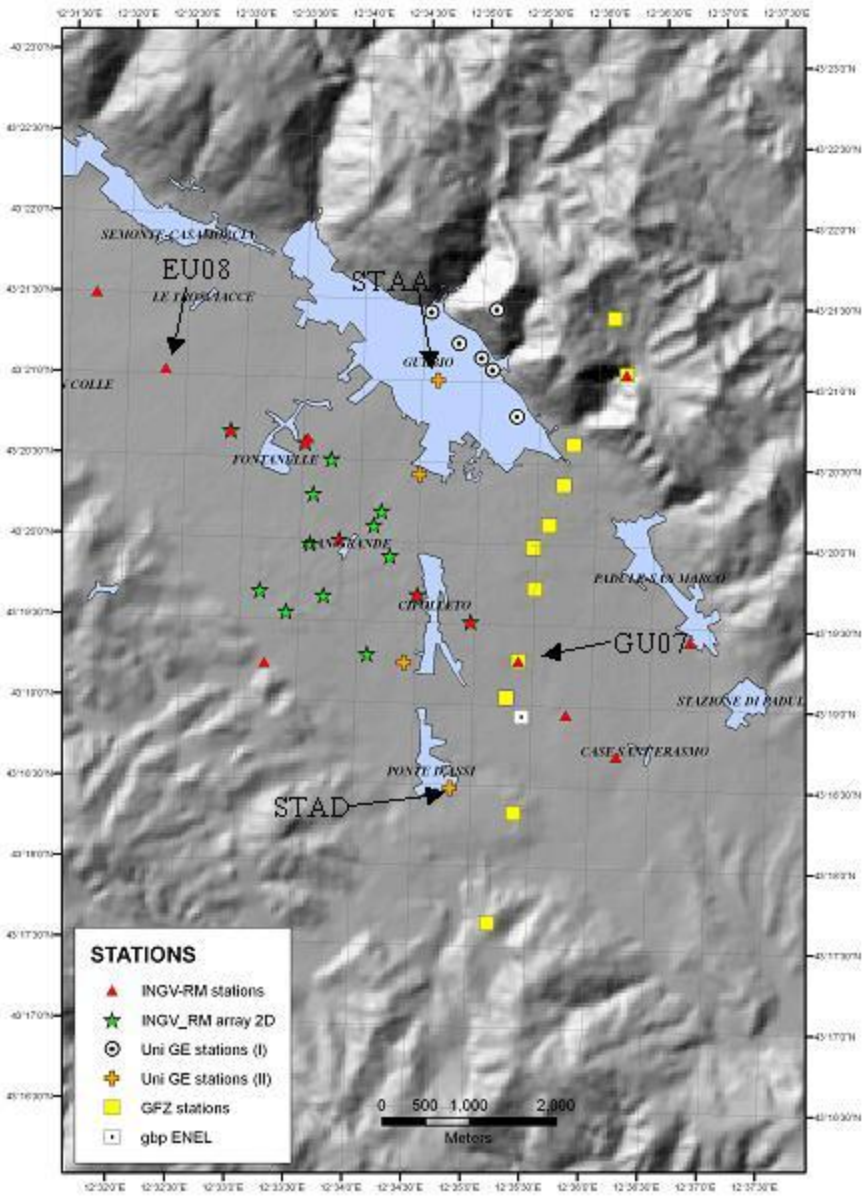

Figure 6.2.1 - Station map with location of 1D profiles shown in fig 7.2.2

Figure 62.2 also shows the comparison with the empirical response site computed by the generalized inversion technique (GIT) curve and described in detail in Deliverable 22-23, which can evidence the difference between a model that takes into accounts only the 1D effects, and the real world where 2D and 3D effects occur. The 2D and 3D effects are dominant almost everywhere in the basin, with very large amplifications occurring on thick deposits of soft sediments (e.g. GU07).

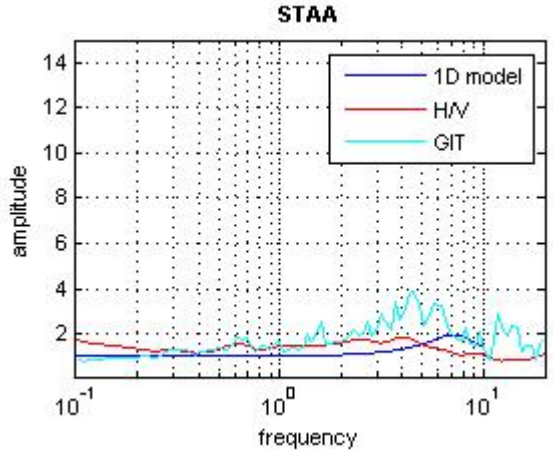

Laye	Thick(m)	Vs′	density	Q
L1	38	1100	1.9	100
BR		1800	2.3	100

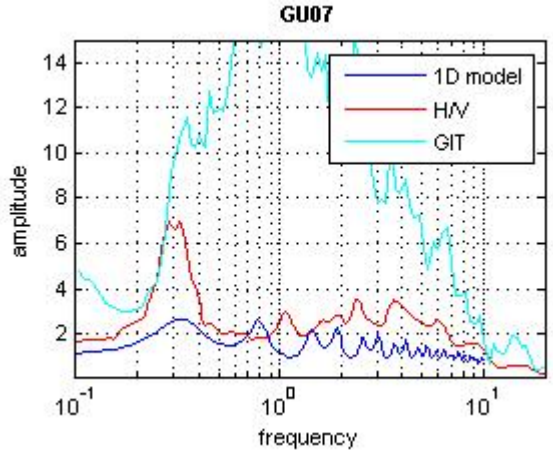

Laye	Thick(m)	Vs′	density	Q
L3	257	600	1.9	30
L4	420	900	1.95	50
BR		1800	2.3	100

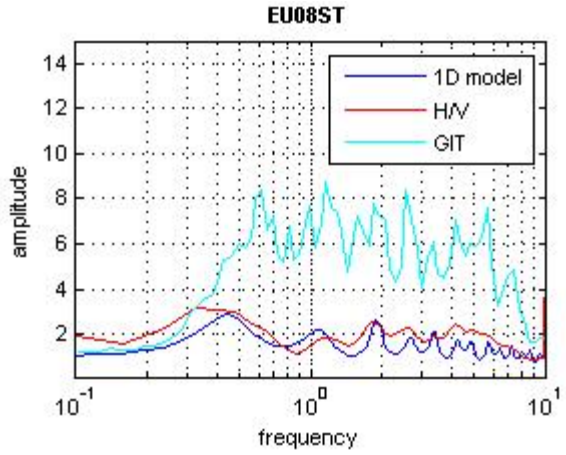

Laye	Thick(m)	Vs′	density	Q
L3	229	600	1.9	30
L4	249	900	1.95	50
BR		1800	2.3	100

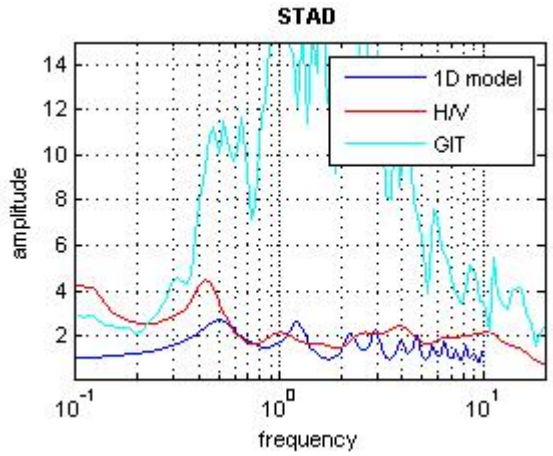

Laye	Thick(m)	Vs′	density	Q
L3	164	600	1.9	30
L4	276	900	1.95	50
BR		1800	2.3	100

Figure 6.2.2 – On the left the curves of the 1D model, H/V and GIT. On the right the 1D profiles at the corresponding stations.

6.3 3D modelling

The availability of a detailed 3D geological and geophysical model (Chaper 5) allowed attempting the calculation of synthetic seismograms, considering the propagation of the wavefield in a 3D structure using a hybrid Finite-Difference formulation (Oprsal and Zahradnik, 2002).
In order to carry out the calculation the model had to be simplified considering only 4 geological units within the basin plus a bedrock. The body wave velocities, density and quality factors assumed for each unit are reported in Table 5.3.1

Since we were interested in simulating synthetic seismogram with frequency content up to 5 Hz, a very small grid spacing was required. Therefore, in order to limit to a feasible amount the computation time, the calculation was limited to a very narrow area around the basin. The input motion was 1-sided S-wave pulse polarized consistently with the incoming S-wave given by the crustal structure, focal mechanism, and position of the mainshock of the Umbria-Marche 1997 seismic sequence (point source). Such a pulse response is analogous to one component of a Green's tensor and thus can be convolved with direct-S-wave record (borehole od de-convolved) of the respective earthquake to obtain the realistic response.

For that reason the pulse (here in in velocities) has the integral normalized to 1:

f(t)=(4/(3*t))* ((0.75-cos(2*PI*t/T)+.25*cos(2*PI*t/T)).

where PI=3.14159, t is time, and T is a time constant given by the highest frequency (f_hi) that corresponds to 1% of the spectral maximum of this function; that is here T=3.1/f_hi.

For our computation, f_hi is 4.7 Hz and its duration T is 0.492 sec.

Example of synthetic pulse responses at positions consistent with those of the linear array installed by GFZ, for the vertical (Z) component and the x component (approximately NE-SW) are shown in Figure 6.3.1 and Figure 6.3.2 respectively. Position of stations GU00 and GU10 is only indicative.
The synthetic impulse response named as GU00 corresponds to a site much closer to the basin than the station GU00, that is located outside of the model.
The scale amplitude scale is different between the two different plots.

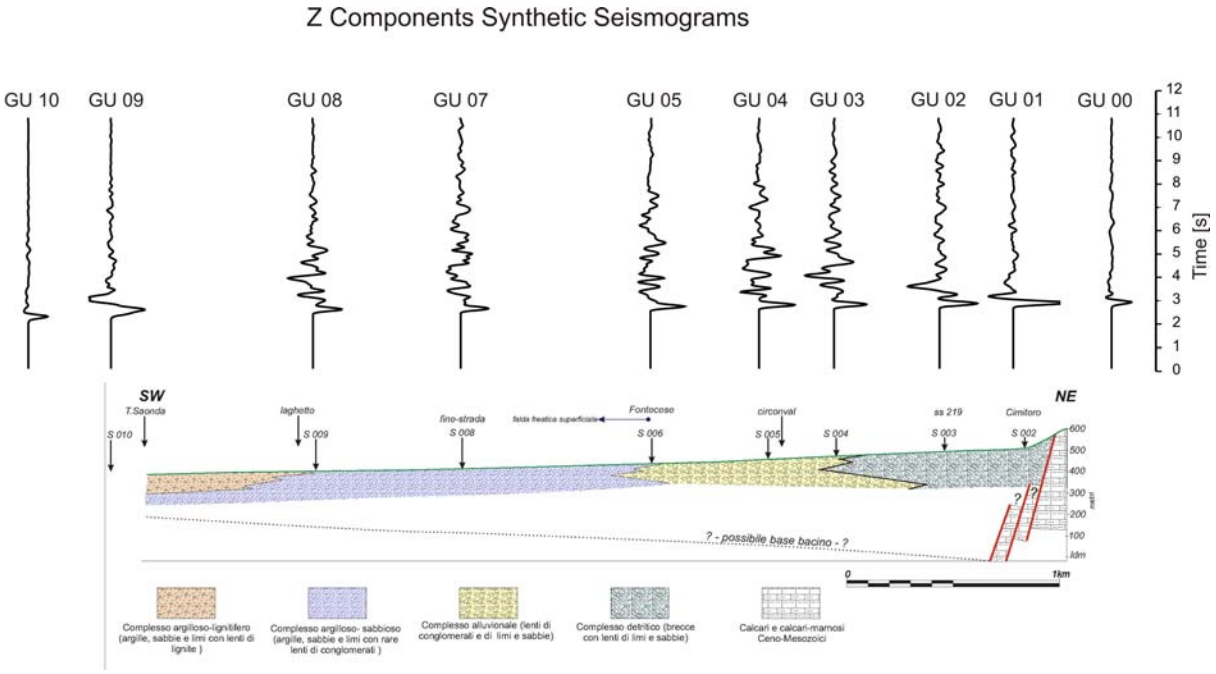

Figure 6.3.1 – Vertical component of synthetics computed along the velocimetric transects of the GFZ.

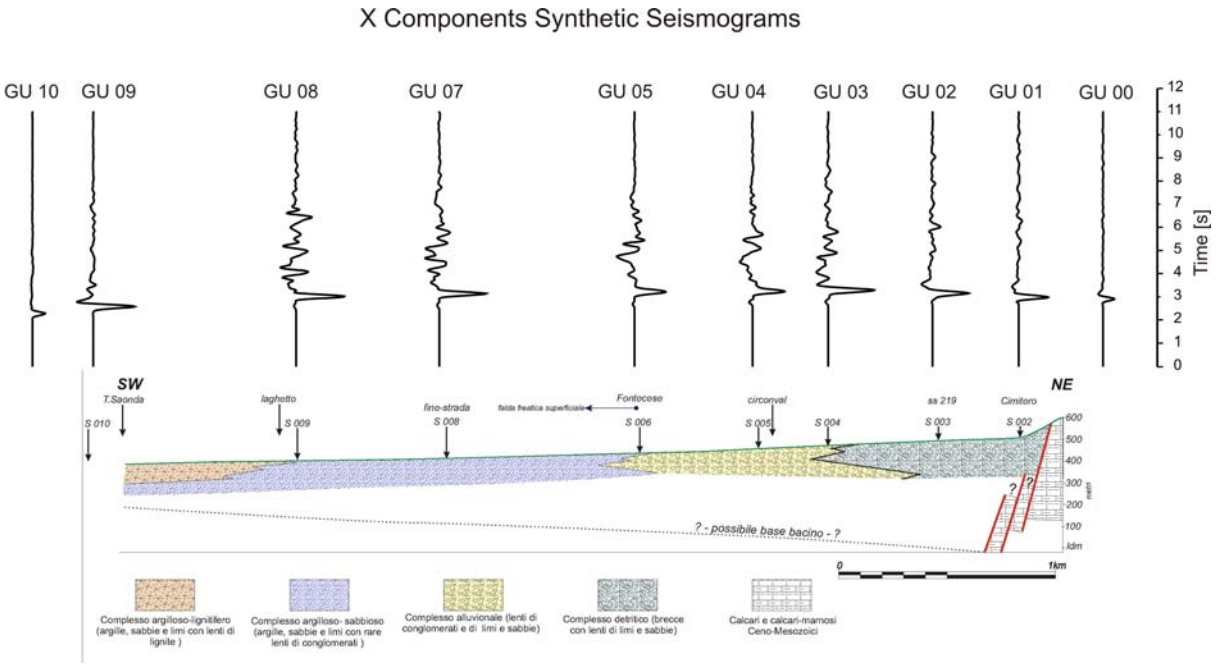

Figure 6.3.2 – Horizontal component of synthetics computed along the velocimetric transects of the GFZ.

The amplitude of the S-wave ground motion is clearly amplified and the ground motion duration is significantly larger at the stations within the basin. For instance the pulse response being ~0.5sec long is about 7 sec long in the GU02 station, which contributes also to prolongation of the incoming signal seismogram. These characteristics are similar to those shown on observed seismograms (see Progetto S3

Deliverable D22-D23).
Figure 6.3.3 and Figure 6.3.4 show the response spectra ratios of the synthetic seismograms (using the station named GU00 as reference) compared with those obtained by real data analysis (See deliverables D22-D23).

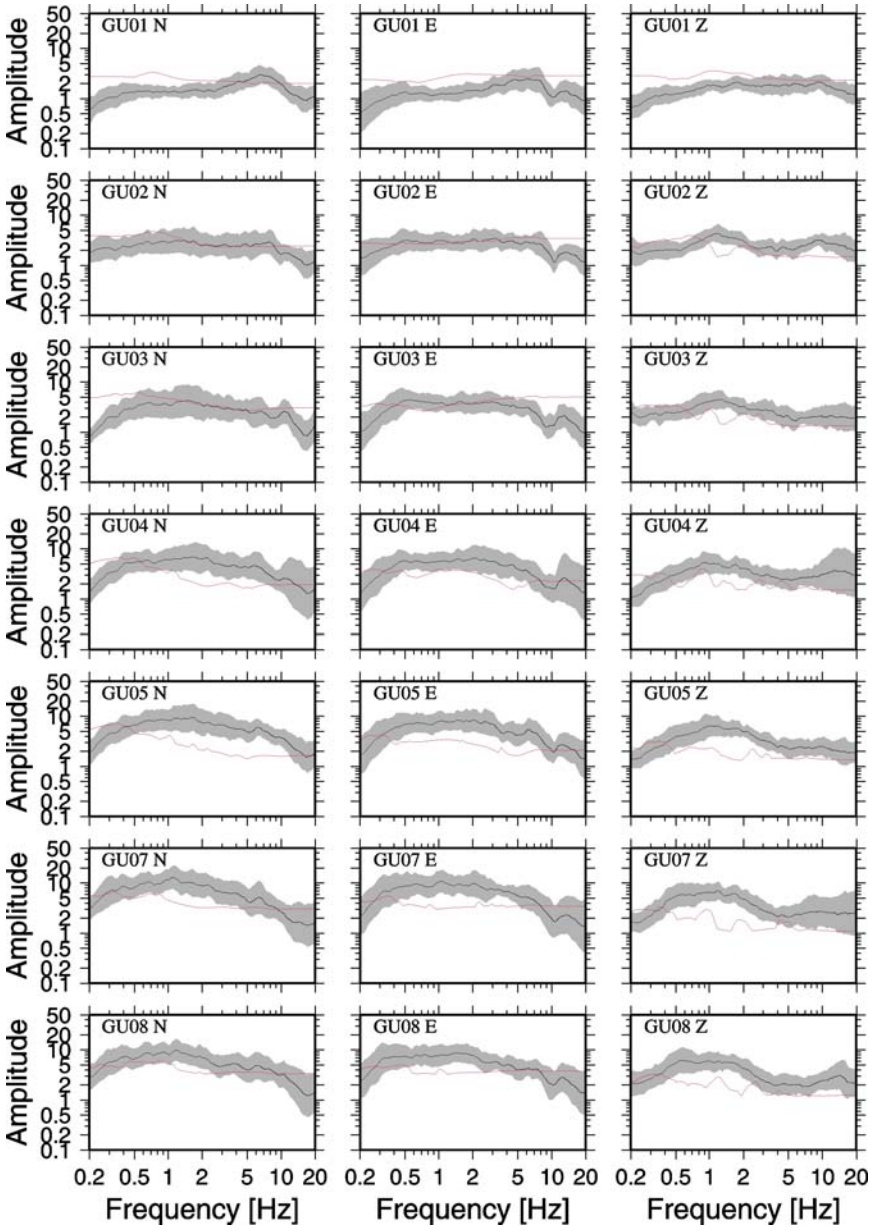

Figure 6.3.3 – Ratios between response spectra in correspondence of some velocimetric stations of the GFZ transect. GU00 is used as reference station. Black line represents the observed ratio, red line the synthetic ratio.Vertical component of synthetics computed along the velocimetric transects of the GFZ.

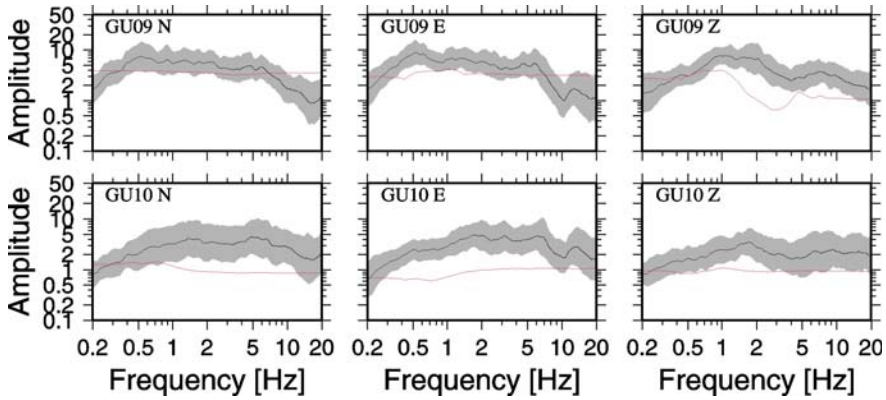

Figure 6.3.4 – Ratios between response spectra in correspondence of velocimetric stations GU09 and GU10 of the GFZ transect. GU00 is used as reference station. Black line represents the observed ratio, red line the synthetic ratio.

Although the general level of amplification is in fairly reasonable agreement for the stations inside the basin, large differences exists especially for the stations located at the edge of the basin.
For these stations greater approximation in the velocity structure below the site were done (see chapter 5). Differences might also depend on the choice of the reference station that does not correspond with the real GU00.
Finally, for the stations well within the basin (GU04-GU09) a tendency in underestimating the high frequency amplification, consistently with the above analysis of the synthetic seismograms, is shown.
Although the numerical simulations allow to reproduce, qualitatively, the mechanisms determining the large increase of ground motion amplitude and of shaking duration within the Gubbio basin, more work is necessary in order to perform a quantitative comparison between synthetic and observed data.

7. CONCLUSION

The main goal of this study was the reconstruction of the subsurface model of Gubbio basin in order to understand the origin of the strong seismic amplification observed in this site. The reconstruction of the model has been done at different scales using data coming from various active and passive measurement surveys, also favoured by the intense seismic activity typical of the area.
An engineering geological characterization was done for the deposits filling the basin of Gubbio within 30-50 meters from the ground surface using data from pre-existing investigations and from two boreholes drilled during the project. These data allow to reproduce a realistic spatial distribution and thickness of soils in the basin, classified as gravels, sands and silts or clays. Moreover the basin was subdivided in three zones in relation to the strain behaviour of the first 50 m soil depth.

The geometry of the basin below 500 m of depth was investigated through the acquisition of a 2D active seismic line 4.5 km long, located in correspondence of one of the transversal transects of velocimetric stations. The seismic data were used to perform a tomography of arrival times which allowed to recognize the position and shape of the reflecting horizons. The top of the bedrock, having U-shape, is characterised by maximum depths of the order of 500-600 meters from the surface and it is identified with the "Marnoso-arenacea" formation. The overlaying sequence, mainly constituted by Quaternary clay and sand deposits, forms roughly a moclinal structure dipping to the Northeast.

Using velocimetric and noise measurements we were able to measure the fundamental frequency fo at more than 90 points inside the basin. These data, together with the results from the seismic line were used, applying an empirical relation, to evaluate the depth of the bedrock for the entire basin. The results indicate an a-symmetric geometry of the basin, excluding a cylindrical shape.
The tomography data and the estimates of the bedrock depths, together with data from field work, were then interpreted by the geologists and the 3D model of the subsurface geology of the Gubbio basin was built with a Geographic Information System. The shear velocity of the main geological units present in the basin were determined in a least squares sense by minimizing the discrepancy between the fundamental frequency of resonance predicted by the model and the one estimated from the H/V spectral ratios of the earthquake and noise records. The S-wave velocity profiles of soft sediments estimated from seismic arrays were also used.

The simulation of theoretical transfer functions showed that the observed amplification in the Gubbio basin cannot absolutely be reproduced with a 1D model. In fact the 2D and 3D effects are dominant almost everywhere in the basin, with very large amplifications occurring on thick deposits of soft sediments. However, although the 3D numerical simulations allow to reproduce, qualitatively, the mechanisms determining the large increase of ground motion amplitude and of shaking duration, more work is necessary in order to perform a quantitative comparison between synthetic and observed data.

REFERENCE

Arai, H., and K. Tokimatsu (2004). S-wave velocity profiling by inversion of microtremor H/V spectrum, *Bull. Seism. Soc. Am*. **94**, 53-63.

Barnaba P. F. (1958) – Geologia dei Monti di Gubbio, Boll. Soc. Geol. It. 77 (3), 39-70.

Böhm, G., G.Rossi, e A. Vesnaver, 1999. *Minimum time ray-tracing for 3-D irregular grids*, J. of Seism. Expl., 8: 117-131

Böhm, G., Galuppo, P. and Vesnaver, A. 2000. *3D adaptive tomography by delaunay triangles and Voronoi polygons.* Geophysical Prospecting 48, 723-744.

Cardarelli, E. (2007) Technical report – Indagini sismiche in foro in località Gubbio (PG), in Italian, 10 pp.

Carrion, P., Böhm, G., Marchetti, A., Pettenati, F. e Vesnaver, A.; 1993: *Reconstruction of lateral gradients from reflection tomography.* Journal of Seismic Exploration **2,** 55-67.

Coltorti M., (1994) - The Pleistocene basin of Gubbio (central Italy); geomorphology, genesis and evolution. Editor: Malone Caroline, Stoddart Simon. Cambridge University Press, Cambridge, UnitedKingdom (GBR) 17-25

Crespellani T. & Garzonio C. A. (1997) - Seismic risk assessment for the preservation of historical buildings in the City of Gubbio. Editor: Viggiani Carlo. Balkema, Rotterdam, Netherlands (NLD) p.129-138.

Crespellani T. & Garzonio C. A., (1988) – Seismic risk analysis in the historical and monumental city of Gubbio (Italy). Editor: Marinos, Paul G., Koukis, George C. A. A. Balkema, Rotterdam, Netherlands (NLD) p.1225-1231.

D'Amico, V., M. Picozzi, D. Albarello, G. Naso, and S. Tropenscovino (2004). Quick estimates of soft sediment thicknesses from ambient noise horizontal to vertical spectral ratios: a case study in southern Italy, *J. Earthquake Eng*. **8**, 895-908.

Fäh, D., F. Kind,. and D. Giardini (2001). A theoretical investigation of average H/V ratios, *Geophys. J. Int*. **145**, 535-549.

GE.MI.NA. (1963) – Ligniti e torbe dell'Italia centrale, GE.MI.NA., Geomineraria Nazionale, Roma p.319.

Herrmann, R. B. (2002). *Computer Programs in Seismology*, Version 3.2, Saint Louis University.

Ibs-von Seht, M., and J. Wohlenberg (1999). Microtremor measurements used to map thickness of soft sediments, *Bull. Seism. Soc. Am*. **89**, 250-259.

Ishibashi I. and Zhang X. (1993) - Unified dynamic shear moduli and damping ratios of sand and clay", Soils and Foundations, 33(1), 182-191.

Lachet, C., and P.-Y. Bard (1994). Numerical and theoretical investigations on the possibilities and limitations of Nakamura's technique, *J. Phys. Earth* **42**, 377-397.

Lavecchia G., Barchi M. & Brozzetti F., (1994) - Recent tectonics and active stress field in the Umbria-Marche Apennines. Memorie della Società Geologica Italiana vol. 48, part. 2 pp. 535-537, 1994.

Menichetti M. & Minelli G. (1991) - Extensional tectonics and seismogenesis in Umbria (central Italy) the Gubbio area. Boll. Soc. Geol. It. Vol. 110, n. 3-4 pp. 857-880.

Menichetti M. & Pialli G. (1986) – Geologia strutturale del Preappennino Umbro tra i Monti di Gubbio e la catena del M. Petrano - M. Cucco. Mem. Soc. Geol. It., 35 (1986), 371-388.

Menichetti M., (1992) - Evoluzione tettonico-sedimentaria della valle di Gubbio. Studi Geologici Camerti Vol. Spec. 1992/1, 155-163.

Mirabella F., Ciaccio M. G., Barchi M. R., Merlini S., (2004) - The Gubbio normal fault (Central Italy): geometry, displacement distribution and tectonic evolution. Journal of Structural Geology, v. 26, iss. 12, p. 2233-2249 12/2004

Nakamura, Y. (2000). Clear identification of fundamental idea of Nakamura's technique and its applications, *Proc. XII World Conf. Earthquake Engineering, New Zealand*, Paper n. 2656.

Nelder, J.A., and Mead, R. (1965) A simplex method for function minimization. *Comp. J.* **7**, 308-313

Ohori, M., A. Nobata, and K. Wakamatsu (2002). A comparison of ESAC and FK methods of estimating phase velocity using arbitrarily shaped microtremor analysis, *Bull. Seism. Soc. Am.* **92**, 2323-2332.

Okada, H. (2003). *The Microtremor Survey Method*. Geophys. Monograph Series, SEG, 129 pp.

Parolai, S., M. Picozzi, S.M. Richwalski, and C. Milkereit (2005). Joint inversion of phase velocity dispersion and H/V ratio curves from seismic noise recordings using a genetic algorithm, considering higher modes, *Geoph. Res. Lett*. **32**, doi: 10.1029/2004GL021115

Pauselli C., Marchesi R. & Barchi M. R. (2002) – Seismic image of the compressional and extensional structures in the Gubbio area (Umbrian-Pre Apennines). Boll. Soc. Geol. It., Volume speciale n. 1 (2002), 263-272.

Picozzi, M., and D. Albarello (2007). Genetic and linearized algorithms for the joint inversion of Rayleigh wave dispersion curves and H/V spectral ratios from environmental noise recordings: a case study in the Po river valley (Northern Italy), submitted to *Geophys. J. Int*.

Picozzi, M., S. Parolai, and S.M. Richwalski (2005). Joint inversion of H/V ratios and dispersion curves from seismic noise: Estimating the S-wave velocity of bedrock, *Geoph. Res. Lett*. **32**, No.11 doi: 10.1029/2005GL022878

PS3-Deliverables D20 (2007). Task6 – GUBBIO - Deliverables D20 – Bedrock Shaking scenarios, July 2007.

PS3-Deliverables D22-D23 (2007). Task6 – GUBBIO - Deliverables D22-D23 - Shaking scenarios including site effects, July 2007.

Pucci S., De Martini P.M., Pantosti D., Valensise G. (2003) – Geomorphology of the Gubbio Basin (Central Italy): understanding the active tectonics and earthquake potential. Annals of Geophysics N. 5 October 2003 Vol. 46, 837-864.

Seed H.B. & Idriss I.M. (1971) – Simplified procedure for evaluating soil liquefaction potential. ASCE J. of Soil Mech. & Found. Division, Vol. 97 (9), 1249-1273.

Selvaggi G. & Sylos Labini S. (1989) - Analisi sismotettonica del bacino di Gubbio. Atti 8° Convegno Annuale G.N.G.T.S., Roma 7-9 novembre 1989, Volume 1, 67-72.

SESAME European project, 2005. *Guidelines for the implementation of the H/V spectral ratio technique on ambient vibrations - Measurements, processing and interpretation*. Deliverable D23.12. http://sesame-fp5.obs.ujf-grenoble.fr/SES_TechnicalDoc.htm

Tokimatsu, K. (1997). Geotechnical site characterization using surface waves, *Earthquake Geotech. Eng.* 1333-1368.

Vesnaver, A., Böhm, G., 2000: *Staggered or adapted grids for seismic tomography?* The Leading Edge, 9, 944-950.

Vesnaver, A., Böhm, G., Madrussani, G., Rossi, G., Granser, H., 2000: *Depth imaging and velocity calibration by 3D adaptive tomography,* First Break, 18, 303-312.

Vesnaver, A., G. Böhm, G. Madrussani , S. Petersen, e G. Rossi, 1999. *Tomographic imaging by reflected and refracted arrivals at the North-Sea*, Geophysics, 64,6 1852-1862.

Vucetic, M. and Dobry, R. (1991) -"Effect of soil plasticity on cyclic response", Journal of Geotechnical Engineering, ASCE, 117(1), 89-107.

Wathelet, M. (2005). Array recordings of ambient vibrations: surface waves inversion, *PhD Thesis*, University of Liege, Belgium, 177 pp.

Yamanaka, H., and H. Ishida (1996). Application of genetic algorithms to an inversion of surface-wave dispersion data, *Bull. Seism. Soc. Am*. **86**, 436-444.

Yamanaka, H., M. Takemura, H. Ishida, and M. Niwa (1994). Characteristics of long period microtremors and their applicability in the exploration of deep sedimentary layers, *Bull. Seism. Soc. Am*. **84**, 1831-1841.

Zhang, J., Andrus, R.D., and Juang, C.H. (2005) - "Normalized Shear Modulus and Material Damping Ratio Relationships". Journal of Geotechnical and Geoenvironmental Engineering, ASCE, 131(4),453-464.

ANNEX A – ZONATION MAP